

UNIVERSITÀ DEGLI STUDI DI MILANO

PhD in Experimental, Clinical and Pharmacological Sciences

Department of Pharmacological and Biomolecular Sciences

XXXIII° Cycle

BIO/14



IMPACT OF PCSK9 ON EXTRAHEPATIC TISSUES

Main Supervisor: Chiar.mo Prof. Giuseppe Danilo Norata

Thesis of:

Lorenzo Da Dalt

N°. R11919

Academic Year 2019/2020

ITALIAN ABSTRACT	1
ENGLISH ABSTRACT	3
INTRODUCTION	5
1. PROPROTEIN CONVERTASE SUBTILISIN/KEXIN TYPE 9 (PCSK9).....	6
1.1 PCSK9 BIOLOGY AND REGULATION	6
1.2 CARDIOVASCULAR IMPACT OF PCSK9 DISCOVERY	8
1.3 PHARMACOLOGICAL PCSK9 THERAPIES:	9
1.3.1 MAB	9
1.3.2 GENE SILENCING (INCLISIRAN).....	10
1.3.3 ADNECTINES	10
1.3.4 VACCINE.....	11
1.3.5 ORAL INHIBITORS.....	11
2. LIPID METABOLISM.....	12
2.1 LIPIDS AND LIPOPROTEIN METABOLISM.....	12
2.1.1 LOW-DENSITY LIPOPROTEIN RECEPTOR (LDLR)	13
2.1.2 VERY LOW-DENSITY LIPOPROTEIN RECEPTOR (VLDLR).....	15
2.1.3 CLUSTER OF DIFFERENTIATION 36 (CD36).....	15
2.2 INTRACELLULAR LIPID METABOLISM	16
2.2.1 FATTY ACIDS β -OXIDATION	16
2.2.2 KREBS CYCLE - TRICARBOXYLIC ACID CYCLE (TCA)	17
2.2.3 ELECTRON TRANSPORT CHAIN (ETC)	18
2.2.4 CHOLESTEROL HOMEOSTASIS.....	19
3. LIPOTOXICITY.....	20
3.1 PANCREATIC β -CELLS LIPOTOXICITY	22
3.1.1 TYPE 2 DIABETES (T2D).....	23
3.2 CARDIAC LIPOTOXICITY.....	23
3.2.1 HEART FAILURE	24
AIM OF THE STUDY	27
MATERIALS AND METHODS	29
1. MICE MODEL.....	30
1.1 DIETS	30
1.2 DNA ISOLATION AND GENOTYPING	31
1.2.1 MOUSE EAR BIOPSY DIGEST PROTOCOL.....	31
1.2.2 DNA EXTRACTION AND PRECIPITATION.....	31
1.2.3 PCR PROTOCOL	32
1.2.4 AGAROSE GEL ELECTROPHORESIS PROTOCOL.....	33
2. GENE EXPRESSION.....	33
2.1 RNA EXTRACTION.....	33
2.2 RNA REVERSE TRANSCRIPTION	34
2.3 REAL-TIME PCR	34
3. PROTEIN EXPRESSION	35
3.1 PROTEIN EXTRACTION	35
3.2 PROTEIN QUANTIFICATION (LOWRY)	36
3.3 WESTERN BLOT.....	36
4. GLUCOSE TOLERANCE (GTT) AND INSULIN TOLERANCE TESTS (ITT)	37
5. CHOLESTEROL, TRIGLYCERIDES, INSULIN, C-PEPTIDE AND PCSK9 MEASUREMENT.	38
6. METABOLOMICS ANALYSIS.....	38

7.	OXYGEN CONSUMPTION RATE (OCR).....	39
8.	MITOCHONDRIAL DNA QUANTIFICATION.....	39
9.	EXHAUSTION TEST.....	40
10.	FORELIMB GRIP TEST	40
11.	PROTEOMICS	41
11.1	SAMPLE PREPARATION AND PROTEIN EXTRACTION.....	41
11.2	PEPTIDE PREPARATION AND PURIFICATION IN SOLUTION DIGESTION	41
11.3	LC-MS/MS	41
11.4	ANALYSIS OF PROTEOMIC DATA	42
12.	ECHOCARDIOGRAPHIC.....	43
13.	PLIC STUDY.....	44
14.	STATISTICAL ANALYSIS	45
	RESULTS.....	46
	PCSK9 KO MICE DISPLAY AN IMPAIRED GLUCOSE TOLERANCE EXCLUDING INSULIN RESISTANCE	47
	PCSK9 DEFICIENCY AFFECT PANCREATIC ISLET MORPHOLOGY AND INSULIN SECRETION. .	47
	THE REDUCED LDLR DEGRADATION MEDIATES CHOLESTEROL ACCUMULATION AND PANCREATIC ISLET DYSFUNCTION	48
	BETA CELL FUNCTIONALITY IS NOT AFFECTED IN PCSK9 LIVER SELECTIVE KO MICE.....	48
	IMPACT OF GENETIC POLYMORPHISM OF PCSK9 IN SYSTEMIC METABOLISM AND CARDIAC PHENOTYPE.....	49
	MICE MODEL KO FOR PCSK9 DISPLAY A HEART FAILURE WITH PRESERVED EJECTION FRACTION	49
	MITOCHONDRIAL IMPAIRMENT AND ALTERED CARDIAC METABOLISM IN PCSK9 DEFICIENT MICE.....	50
	PCSK9 DEFICIENCY LEADS TO LIPID ACCUMULATION THROUGH LDLR AND CD36.....	51
	CIRCULATING PCSK9 DOES NOT IMPACT HEART METABOLISM.	52
	DISCUSSION.....	54
	FIGURES.....	59
	REFERENCES	83
	ACTIVITY REPORT	91

Abstract

Introduzione e scopo: la proproteina convertasi subtilisina kexin tipo 9 (PCSK9) è una glicoproteina di 692 amminoacidi che appartiene alla famiglia delle proproteine convertasi. È prodotta principalmente dal fegato dal quale viene secreta nel torrente circolatorio. PCSK9 interagisce con diversi recettori della famiglia dell'LDLr, inclusi VLDLr, LRP1 ma anche con CD36, e guida la loro degradazione lisosomiale. La mancanza di PCSK9 determina quindi una maggiore espressione dei recettori della famiglia LDLr e favorisce l'accumulo di lipidi nei tessuti extraepatici. L'eccesso di lipidi cellulari è associato a disfunzione mitocondriale e danni tissutali in diversi organi, tra cui il pancreas e il cuore. Per questo motivo ci siamo chiesti se la mancanza di PCSK9 circolante e localmente prodotto possa influenzare l'accumulo di lipidi nei tessuti extraepatici come il pancreas e il cuore influenzandone la funzionalità.

Metodi: Animali *WT*, *Pcsk9* KO, albumin CRE PCSK9LoxP / LoxP KO condizionali (privi di PCSK9 selettivamente nel fegato e quindi non presentando proteina PCSK9 rilevabile in circolazione) e topi maschi Doppo KO *LDLr-Pcsk9* di 2 mesi sono stati nutriti per 20 settimane con SFD o HFD. I livelli plasmatici di GTT, ITT, insulina e peptide C, morfologia del pancreas e accumulo di colesterolo nelle isole pancreatiche sono stati studiati nei diversi modelli animali. Inoltre su questi topi sono state eseguite analisi ecocardiografiche del cuore e test funzionali. La respirazione mitocondriale è stata studiata in condizioni di riposo e in seguito a condizioni massime di accoppiamento e disaccoppiamento in tutti i modelli di topo, seguite da caratterizzazione delle proteine mitocondriali mediante western blot e analisi di metabolomica approfondita.

Risultati: Il metabolismo glucidico è significativamente ridotto nei topi *Pcsk9* KO alimentati sia con una dieta standard che con una dieta ricca di grassi per 20 settimane rispetto agli animali WT; la sensibilità all'insulina, tuttavia, non viene alterata. Un'analisi dettagliata della morfologia del pancreas dei topi *Pcsk9* KO rispetto ai controlli ha rivelato isole più grandi con un maggiore accumulo di esteri del colesterolo, che si associa ad aumentati livelli intracellulari di insulina e alla diminuzione dei livelli plasmatici di insulina e C-peptide. Questo fenotipo è stato completamente ripristinato nei topi *Pcsk9 / Ldlr* DKO, il che implica che l'aumentata espressione di LDLr potrebbe spiegare il fenotipo osservato. Da notare che i topi privi di PCSK9 circolante non presentavano un fenotipo alterato, indicando così che PCSK9 circolante e di origine epatica non influisce sulla funzione delle cellule beta e sulla secrezione di insulina. In parallelo, una caratterizzazione dettagliata della funzionalità cardiaca, ha rivelato che i topi *Pcsk9* KO mostrano un fenotipo caratteristico dello

scompenso cardiaco con frazione di eiezione conservata. Inoltre, i topi *Pcsk9* KO presentano una ridotta resistenza alla corsa senza difetti muscolari accoppiata a importanti adattamenti nel metabolismo cardiaco e nella funzionalità mitocondriale dovuti all'accumulo di colesterolo cardiaco. Un fenotipo simile è stato osservato negli *LDLr* Doppi KO confermando un effetto indipendente dall'espressione dell'*LDLr*. Il fenotipo cardiaco risulta completamente ristabilito nel modello KO selettivo del fegato escludendo così il coinvolgimento del PCSK9 circolante nello sviluppo dell'insufficienza cardiaca con frazione di eiezione conservata. Studi traslazionali hanno mostrato che i soggetti umani portatori del polimorfismo di perdita di funzione R46L mostravano un aumento della massa ventricolare sinistra senza alterazioni nella frazione di eiezione rispetto ai controlli con BMI R46R abbinati.

Conclusione / Discussione: PCSK9 prodotto localmente nel pancreas e nel cuore limita l'accumulo di lipidi in modo dipendente da *LDLr* nel pancreas e in modo *LDLr* indipendente nel cuore contribuendo così a mantenere l'omeostasi dei tessuti. La carenza genetica di PCSK9 porta allo sviluppo di intolleranza al glucosio e insufficienza cardiaca con frazione di eiezione conservata nei modelli murini e nell'uomo.

Abstract

Background and Aim: Proprotein convertase subtilisin Kexin type 9 (PCSK9) is a 692-amino acid glycoprotein that belongs to the family of proprotein convertases. It is produced mainly by the liver and secreted into the circulation. PCSK9 interacts with several receptors of the LDLr family, including VLDLr, LRP1 but also with CD36, and drives their degradation in the lysosome. As a consequence, PCSK9 deficiency results in increased expression of LDLr family receptors and favors lipid accumulation in extrahepatic tissues. Lipids overload is associated with mitochondrial dysfunction and tissue damage in different organs including the pancreas and the heart. We wondered whether the lack of both circulating and locally produced PCSK9 may affect lipid accumulation on extrahepatic tissues such as the pancreas and the heart those affecting their functionality.

Methods: 2-months old WT, Pcsk9 KO, Albumin CRE PCSK9LoxP/LoxP conditional KO (lacking PCSK9 production selectively in the liver and thus presenting undetectable PCSK9 protein in the circulation) and Double KO LDLr-Pcsk9 male mice were fed for 20 weeks with SFD or HFD. GTT, ITT, insulin and C-peptide plasma levels, pancreas morphology, and cholesterol accumulation in pancreatic islets were studied in the different animal models. Moreover, echocardiographic analysis of the heart and functional tests were performed on these mice. Mitochondrial respiration was investigated under resting conditions and following maximal coupling and uncoupling conditions in all mice models followed by mitochondrial protein profiling by western blotting and extensive metabolomic analysis.

Results: Glucose clearance was significantly reduced in Pcsk9 KO mice fed with a standard or a high-fat diet for 20 weeks compared with WT animals; insulin sensitivity, however, was not affected. A detailed analysis of pancreas morphology of Pcsk9 KO mice vs. controls revealed larger islets with increased accumulation of cholesteryl esters, paralleled by increased insulin intracellular levels and decreased plasma insulin, and C-peptide levels. This phenotype was completely reverted in Pcsk9/Ldlr DKO mice implying that increased LDLR could explain the phenotype observed. Of note mice lacking circulating PCSK9 did not present an impaired phenotype, thus indicating that circulating, liver-derived PCSK9 does not impact beta-cell function and insulin secretion. In parallel, a detailed characterization of heart function revealed that Pcsk9 KO displays a phenotype characteristic of heart failure with preserved ejection fraction. Moreover, PCSK9 KO mice present a reduced running resistance without muscular defects coupled to major adaptations in cardiac metabolism and mitochondrial functionality due to heart cholesterol accumulation. A similar phenotype was observed in LDLr Double KO confirming an effect independent of LDLr

expression. The cardiac phenotype is completely reverted in the liver selective KO model thus excluding the involvement of circulating PCSK9 in the development of Heart Failure with preserved Ejection Fraction. Translational studies showed that human subjects carrying the R46L loss of function polymorphism displayed increased left ventricular mass without alterations in ejection fraction compared to R46R BMI-matched controls.

Conclusion/Discussion: PCSK9 locally produced in the pancreas and the heart affects lipid accumulation in an LDLr dependent manner in the pancreas and an LDLr independent manner in the heart thus contributing to maintaining tissue homeostasis. Genetic PCSK9 deficiency leads to the development of glucose intolerance and heart failure with preserved ejection fraction in mice models and humans.

Introduction

1. Proprotein Convertase Subtilisin/Kexin Type 9 (PCSK9)

1.1 PCSK9 Biology and Regulation

Proprotein Convertase Subtilisin/Kexin Type 9 (PCSK9) is a protein with a molecular weight of 62 kDa and is mainly produced by the liver. The liver is not the only producer of PCSK9 that is also produced in the small intestine, the kidneys, the pancreas, and the central nervous system. PCSK9 was discovered in 2003 as neural apoptosis-regulated convertase 1 (NARC-1) in the brain. PCSK9 is a member of a group of serine proteases that catalyze the hydrolyzation of peptide bonds mediating the activation of target proteins. PCSK9 is synthesized as a 75 kDa proPCSK9, which is composed of a signal peptide, a prodomain, a catalytic domain, an exposed hinge region, and a C-terminal domain enriched in cysteine and histidine (Seidah et al., 2003).

The signal peptide drives PCSK9 to the endoplasmic reticulum and the proPCSK9 undergoes an autocatalytic cleavage required for its folding and secretion. The cleaved signal peptide remains close to the catalytic domain of PCSK9 thanks to hydrogen bond inhibiting side interaction with other substrates on cell cytoplasm. The secretion of PCSK9 is mediated by vesicles produced in the Golgi apparatus in a common mechanism with Low-Density Lipoprotein Receptor (LDLr) secretion. The protein release is common between PCSK9 and LDLr but differs for cellular localization on the cell membrane. While the LDLr remains attached to the cellular membrane PCSK9 is rapidly release in the extracellular matrix (Seidah et al., 2003).

Upon secretion, the catalytic domain of PCSK9 binds to the Epidermal growth factor A (EGF-A) domain on the receptors that belong to the LDLr-Family, localized on the plasmatic membrane. Once PCSK9 is bounded to the EGF-A domain are both internalized in clathrin-mediated endocytosis (Poirier et al., 2009). The low pH characteristic of the late endosome strengthens the bind between PCSK9 and EGFA and this strong interaction prevents the dissociation and the recycling of the receptor to the cell membrane. In this way, PCSK9 enhances LDLr lysosomal degradation within the cell cytoplasm reducing the recycling of the receptor on the cell membrane (Figure 1)(Wang et al., 2012). As a consequence, we observe a reduced LDLr expression, decreased LDL metabolism on hepatic cells, and augmented plasma levels of LDL-cholesterol (Lipari et al., 2012). PCSK9 can also target other receptors, including other members of the LDLr family as Very Low-Density Lipoprotein Receptor (VLDLr) and ApoER2. PCSK9 can also interact with CD36,

promoting its degradation both through an intracellular and extracellular pathway, reducing CD36 levels at the cell surface and, similarly to LDLr, preventing its recycling or translocation at the plasma membrane. As happened with the LDLr family receptor, PCSK9 mediates CD36 degradation driving the receptor directly to the lysosomes. It has been demonstrated that CD36 expression is increased both in vitro and in vivo models of PCSK9 deletion. In *Pcsk9* knockout mice, increased hepatic CD36 is associated with augmented fatty acids uptake and triglycerides accumulation in lipid droplets (Demers et al., 2015).

PCSK9 has also an intracellular role in regulating cholesterol metabolism but the relevance requires further investigations. PCSK9 is an important cholesterol metabolism regulator and in turn, it is regulated at different levels. Once released in the circulation PCSK9 might undergo post-transcriptional modifications: for instance, furin cleaves mature PCSK9 producing a truncated protein of about 55 KDa that is less able to bound the LDLr to compare to the full form (Benjannet et al., 2006). The furin cleaved form is less active (less able to bound the EGFA), but still maintains a valid residual ability to bind LDLr. In line with this observation, circulating PCSK9 can be free, and more susceptible to furin cleavage, or bind to LDL particles, maintaining its uncut form with the highest ability to bind its target (Kosenko et al., 2013).

PCSK9 is almost entirely produced and released by the liver and goes against several intracellular modulations in addition to the extracellular furin cleavage. Indeed, its expression is regulated at different levels and by several factors, including diurnal rhythm, hormones, diet, exercise and cholesterol levels, and hypocholesterolemic drugs.

The genetic expression of PCSK9 is finely regulated and its promoter contains different elements, including the sterol-regulatory element (SRE), the highly conserved hepatocyte nuclear factor 1 (HNF-1) (Dong et al., 2017) binding site, and the transcription factor 1 (SP1). PCSK9 expression regulation is extremely complex and its production is sensible to intracellular cholesterol level variations and endogen cholesterol biosynthesis. The most known regulating factor that increases the transcription of PCSK9 is the reduction of intracellular cholesterol levels. Sterol-regulatory element-binding protein-2 (SREBP2) and SREBP-1c are transcriptional factors responsive to cholesterol levels and with their bind to the Sterol Regulatory Elements (SRE) sequence on PCSK9 and LDLr promoter can up-regulate protein transcription. Particularly, PCSK9 expression is upregulated in the specific condition of intracellular cholesterol depletion and as a consequence of hypocholesterolemic drug treatment to compensate and attenuate the reduction of circulating LDL-C levels. Further confirming the strange co-stimulation of LDLr and PCSK9, cholesterol-lowering

drugs, especially statins, inhibiting HMG-CoA Reductase and reducing intracellular cholesterol levels, increase PCSK9 gene expression in vitro and in vivo. A group of patients treated with atorvastatin, showed a 34% enhance in plasma PCSK9 levels (Careskey et al., 2008). The second key regulator of PCSK9 expression is HNF1 whose sequence is also located at the level of the PCSK9 promoter close to the SRE sequence. Collaborating with SREBP2, HNF1 activation up-regulates PCSK9 expression in situations of low intracellular cholesterol levels. Close to the promoter sequence of PCSK9, there are also many binding sites for co-activator that can increase the gene transcription. One of those is the binding site for histone nuclear factor P (HINFP) that promoting the acetylation of the histones H4 in a complex with the histone acetyltransferase cofactor transformation/transcription domain-associated protein (TRRAP) and the cofactor nuclear protein of the ATM locus (NPAT) favorites PCSK9 production. Being acetylation of histone H4 a positive regulator of PCSK9 expression, the lack of histone deacetylases Sirtuin 6 (SIRT6) and Sirtuin 1 (SIRT1) was also associated with increased production of PCSK9. The transcriptional factor forkhead-box protein O3 (FOX3), plays the opposite role and leading to the deacetylation of histone H3 and promoting the activity of SIRT6 leads to the inactivation of SREBP2 and HNF1 and the consequent inhibition of PCSK9 transcription (Li et al., 2012; Tao et al., 2013).

1.2 Cardiovascular Impact of PCSK9 discovery

PCSK9 became very interesting from a cardiovascular point of view in 2003 when two gain of function (GOF) mutations related to the PCSK9 gene were discovered in French families with autosomal dominant hypercholesterolemia (Abifadel et al., 2003). Another gain of function mutation was discovered in the next years but the one that had the greatest impact in the cardiovascular world was the discovery, in 2005, of a loss of function (LOF) PCSK9 mutations including two nonsense mutations (Y142X and C679X). The LOF was associated with reduced LDL-C and was protective for coronary artery disease (Cohen et al., 2006; Norata et al., 2010). For this reason, PCSK9 GOF leads to a reduced expression of LDLr in the liver and the classical familial hypercholesterolemia phenotype (Abifadel et al., 2003).

1.3 Pharmacological PCSK9 therapies:

The discoveries of genetic variants associate with higher and lower PCSK9 circulating levels were the first brick in investigating the pharmacological modulation of PCSK9 as a tool to reduce plasmatic levels of LDL-C (Figure 2) (Chaudhary et al., 2017).

1.3.1 mAb

Monoclonal antibodies (mAbs) that target PCSK9 (alirocumab and evolocumab) are the first and most advanced pharmacological approach that has been developed and approved to inhibit the activity of the protein and reducing hepatic LDLr expression. One of the first two mAbs approved for patient's treatment is Alirocumab (Praluent) that was approved by the Food and Drug Administration (FDA) in July 2015 for patients affected by heterozygous familial hypercholesterolemia and severe atherosclerotic CVD. The second was Evolocumab (Repatha) which was also approved by the FDA in August 2015 for patients affected by either heterozygous or homozygous familial hypercholesterolemia and those affected by atherosclerotic CVD requiring an additional decrease in LDL-cholesterol. The phase III clinical program to test the adverse effect, long-term safety, and efficacy of Evolocumab and Alirocumab were respectively PROFICIO and ODYSSEY trials. Both the clinical program supports the efficacy and the safety of PCSK9 mAbs treatment confirming the use of mAbs as monotherapy or in combination with the maximum tolerated dose of statin with approximately a ~ 60% LDL-C levels reduction (Sabatine et al., 2017; Schwartz et al., 2018). The efficacy of LDL-C reduction and cardiovascular events reduction has also been confirmed by two outcomes studied (FOURIER and ODYSSEY OUTCOME). The first show that evolocumab on top of statin treatment on subject with LDL-C more than 70 mg/dL and CVD can reduce by 15% the risk of Cardiovascular Death, Myocardial Infarct and stroke. The second shows a 15% reduction of primary endpoint with alirocumab treatment on subject in secondary prevention with a recent coronary syndrome (Figure 2).

1.3.2 Gene silencing (Inclisiran)

Genetic silencing is another therapeutic approach for lowering cholesterol levels targeting PCSK9. Small interfering RNA (siRNA) acting as a post-transcriptional mechanism selectively silences the translation of their target mRNA. This process happens in the cytoplasm, the siRNA, produced as double-strand RNA, (around 20/25 nucleotides length) is incorporated in the RNA-induced silencing complex (RISC), in the presence of target mRNA the siRNA is reduced to a single strand and the target is then processed from RISC complex (Watts et al., 2012). Specific modifications on siRNA structure, such as the addition of 2-fluoride, 2-O-methyl groups, and phosphorothioate allow the siRNA to survive the action of nucleases. Moreover, to make the siRNA more selective for the circulating PCSK9, produced by the liver, the addition of 3 molecules of N-acetylglucosamine (GalNAc) allows the siRNA to be picked-up selectively in the liver by specific receptors for GalNAc such as the receptor for asialoglycoproteins (ASGPR) (Peters et al., 2016).

In phase 1 study PCSK9 inhibitor. Inclisiran showed a significant reduction in both PCSK9 (up to 84%) and LDL-C plasma levels (up to 60%) (Fitzgerald et al., 2017; Ray et al., 2017). ORION-1 is a dose-ranging trial in 501 patients for the assessment of different starting doses (single doses of 200, 300, or 500 mg, and two-dose regimens of 100, 200, or 300 mg administered 90 days apart). Measurement of LDL cholesterol was continued for 12 months. The study showed that Inclisiran has similar LDL-C lowering efficacy as the PCSK9 mAbs. Moreover, Inclisiran has been shown to produce a robust reduction also in VLDL-C and triglycerides (Ray et al., 2018). However, because Inclisiran inhibits the translation of PCSK9 mRNA to protein, it alters PCSK9 intracellular levels. Instead mAbs only affect PCSK9 circulating levels. Moreover, compares to mAbs, Inclisiran showed a longer duration of action with sustained effect, suggesting an improved safety and tolerability profile (Figure 2) (Ray et al., 2018).

1.3.3 Adnectines

Adnectines have been developed as an alternative to mAbs. Adnectines are a non-antibody binding protein that containing the fibronectin type III domain. BMS-962476 is generated to specifically recognize and bind PCSK9 inhibiting its interaction with the EGF-A domain on the receptor of the LDLr family. A single injection of BMS-962476

has been shown to reduce free PCSK9 (up to 90%) and LDL-C levels (up to 48%). Another Adnectins that have been developed is LIB003. In comparison to the previous one LIB003 is an adnectine that specifically recognizes PCSK9 with a linkage with Human Serum Albumin. This has been performed to increase the half-life of the treatment up to 15 days (Figure 2) (Dadu et al., 2014).

1.3.4 Vaccine

Vaccination represents another strategy for PCSK9 inhibition. The vaccine AT04A targets PCSK9 inducing an antibody response to PCSK9 and leading in mice to a strong and stable immune response against PCSK9. In the mice model, the reduction was followed by a significant reduction in LDL-C plasmatic levels and atherosclerotic development. The significant trend observed in the mice model was much less in the human subject where the reduction in LDL-C levels was lower (Figure 2) (Pan et al., 2017).

1.3.5 Oral Inhibitors

Another possibility to target PCSK9 is an oral inhibitor. PCSK9 to binds the LDLr at hepatic levels need the heparan sulfate structures (heparan sulfate proteoglycans, HSPG). The generation of these new compounds originates from the observation that heparin competing with HSPG prevents binding with PCSK9 and therefore its reduced interaction with LDLr. For this reason, DRP molecules have been generated and tested in mice model where display a reduction in LDL-C levels and atherosclerotic plaque size (Figure 2) (Shapiro et al., 2018).

2. Lipid metabolism

2.1 Lipids and lipoprotein metabolism

Lipids are hydrophobic molecules insoluble in a polar solvent and for this reason, can be transported in the bloodstream as free fatty acid conjugated to albumin or packed in lipoproteins. Lipids in the human body can be used as a source of energy or as a building block to create cellular structures (i.e. cellular membrane). Lipoproteins are water-soluble particles with a hydrophobic core mainly composed of cholesterol esters and triglycerides that are surrounded by a hydrophilic membrane consisting of phospholipids, free cholesterol, and apolipoproteins. Lipoprotein differs in size, shape, and lipid composition. Their purpose is to transport water-insoluble lipids such as cholesterol and triglycerides and can differ for both the lipidic and proteic parts. The biggest lipoprotein and most rich in lipids are the Chylomicrons. In comparison to other lipoproteins, the most abundant protein is apolipoproteins ApoB-48 and are mainly composed of triglycerides that make them the fewer dens lipoprotein (Figure 3). Contrary to other lipoproteins, chylomicrons are packed in the small intestine in a postprandial phase, and then immediately secreted into intestinal lymph. Subsequently, they reach the blood through the thoracic duct where, binding specific receptors on the wall of capillaries, can deliver fatty acids to peripheral tissues (Feingold et al., 2000). Chylomicrons and in general triglycerides-rich lipoproteins (TGRLs) once reached their destination are hydrolyzed by the lipoprotein lipase (LPL) into fatty acids and glycerol. Once released from the lipoprotein Free Fatty Acids (FFA) can pass through the endothelium and reach the peripheral cells for storage or oxidation (Olivecrona, 2016). The hydrolyses of triglycerides from chylomicrons result in the generation of smaller particles called chylomicron remnants that are denser than the previous one and richer in cholesterol. Chylomicron remnants can be removed from the circulation by the liver through the binding with different receptors including LDLr, SR-B1, and the LDL receptor-related protein (LRP)(Brown et al., 1976). The binding with the specific hepatic receptor allows the lipoproteins to be internalized and metabolized through lysosomal pathways. This process leads to the release of intracellular cholesterol, which is then either converted into bile acids, excreted in bile, or incorporated into new lipoproteins originated in the liver the Very-Low Density Lipoprotein (VLDL) (Figure 3). VLDLs are the second class of triglycerides-rich lipoproteins together with Chylomicrons from which they differ in the protein component. VLDLs are produced in the liver and possess ApoB-100 instead of the truncated form ApoB-

48 that is produced in the intestine. Once released into circulation VLDLs can reach their tissue target as happening for chylomicron the LPL hydrolyzes triglycerides with the generation of VLDL remnant formation and the release of free fatty acids. The smaller remnant VLDL, called IDL, are removed from the circulation by the liver through the binding with LDLr (Feingold et al., 2000). By the time almost all of the cholesterol is removed, VLDL are transformed into Low-Density Lipoprotein (LDL). LDLs are the richest in cholesterol and contain a single copy of ApoB-100 (Figure 3). LDL core included triglyceride and cholesteryl ester molecules while the surface monolayer comprised phospholipid molecules and ApoB-100. LDL contains unesterified cholesterol, located both in the core and in the phospholipid layer. LDL delivers cholesterol to all the organism through the binding with LDLr. The cholesterol excess is removed from the tissue by HDL. HDL particles, synthesized by the liver, are involved in the cholesterol reverse transport by extracting cholesterol from peripheral tissues and delivering it back to the liver (Marques et al., 2018). Their main protein constitute is ApoA1 that serves as a recognition molecule for proteins that interact with HDL, such as lecithin-cholesterol acyltransferase (LCAT), ATP binding cassette 1 (ABCA1), and the scavenger receptor B1 (SR-B1). The efflux process is mediated by the binding between ApoA1 to ABCA1 on the surface of cells at peripheral tissue. After that, discoidal HDL are internalized inside the cells and targeted into endocytic vesicles where ApoA1 picks up lipids to form the apolipoprotein-lipid complexes that are expelled from the cells by exocytosis. Discoidal HDL then develop into mature spherical HDL through interaction with LCAT, which mediates the conversion of discoidal into spherical HDL by catalyzing the transfer of the 2-acyl group of lecithin to the hydroxyl group of cholesterol and so promoting the conversion of cholesterol into cholesteryl esters (Ossoli et al., 2016). Cholesterol esters are more hydrophobic than free cholesterol. They accumulate in the center of HDL particles inducing a change in the shape from discoidal to spherical. Mature HDL return cholesterol to the liver through interaction with SR-B1, which mediates the elimination of cholesterol esters from HDL, driving them to the liver where cholesterol is eliminated as bile or used for VLDL production (Pagler et al., 2006).

2.1.1 Low-Density Lipoprotein Receptor (LDLr)

The low-density lipoprotein receptor (LDLr) is one of the members of the LDLr family that is composed of a group of a cell-surface glycoprotein involved in the homeostasis of cholesterol, triglycerides, and fatty acids. The mature LDLr is a modular, single-pass

transmembrane glycoprotein of 839 amino acids. The receptor presents three different regions in the extracellular protein domain. The N-terminal domain of the protein is composed of seven repeats characterized by a Cysteine-rich sequence. The first module is called LDL receptor type-A (LA) repeats and is responsible for binding lipoproteins (Russell et al., 1989). The LA is followed by a region of 400-residue, the epidermal growth factor precursor (EGFP), which consists of two epidermal growth factor-like (EGF) modules, EGFA and EGFB, followed by a β -propeller (YWTD, tyrosine, tryptophan, threonine, and aspartate) that separate the first two domain from the third EGF module, the EGFC. This part of the LDLr is implicated in the release of bound lipoproteins at low pH (Davis, Goldstein, et al., 1987). The EGFP domain is then followed by a region rich in serine and threonine residues that undergoes O-linked glycosylation. This part is a spacer that separates the LDLr functional domains from the cell surface (Davis et al., 1986). After the O-glycosylated domain, there is a transmembrane segment and the sequence that is needed to drive the LDLr to the clathrin-coated region of the plasmatic membrane and the sequence important for receptor endocytosis (Davis, van Driel, et al., 1987).

The main role of LDLr is to specifically bind apoB100 and internalize LDL particles supplying cholesterol to the cells. After the binding, the complex between lipoprotein and LDLr is internalized in the cells by endocytosis via clathrin-coated vesicle (Tall, 1998). The vesicles are then fused with the lysosome, where the low pH causes the separation of lipoprotein from LDLr and the release of lipoprotein consequently. The receptor then goes back to the cell surface in a process called receptor recycling. At this point, LDLr can be recycled and exposed on the cell membrane, or, the bind of PCSK9 in the EGFA domain keeps the receptor locked in the lysosome and leads to it being degraded with the rest of the lipoprotein (Lagace, 2014). Of note, LDLr production is finely regulated by the intracellular cholesterol levels through the activation of a sterol-regulated binding protein (SREBP). SREBPs is present in the cells as membrane-bound proteins attached to the endoplasmic reticulum. As a sensor of cholesterol levels, when cholesterol decreases SREBPs are transported to the Golgi, where are processed by two proteases to release a soluble fragment that enters the nucleus and activates transcription of the genes encoding for HMG-CoA reductase. On the contrary, when cellular cholesterol levels increase, the production of LDLr is reduced because cholesterol blocks the mobilization of SREBPs from the Golgi inhibiting the proteolytic release of the active fragment SREBPs from membranes (Horton et al., 2002). The increase in cholesterol levels also leads to increased production of oxysterols that in turns can activate another key regulator of LDLr expression, the liver X receptor (LXR)

which in turns initiate the transcription of a series of genes, including inducible degrader of the LDL receptor (IDOL), an E3 ubiquitin-ligase (Zelcer et al., 2009).

2.1.2 Very Low-Density Lipoprotein Receptor (VLDLr)

The LDLr family has a wide range of physiologic functions, particularly mediating the recognition and the uptake in the liver and peripheral tissue of lipoprotein (Argraves, 2001). Very low-density lipoprotein receptor (VLDLr) is a member of the LDL receptor family and it is expressed at a high level in the heart, adipose tissue, brain, and muscle. The receptor has the same structure as the LDLr with an extra repeat sequence in the binding domain (Takahashi et al., 1992). VLDLr can bind the ApoE-rich particles such as VLDL and IDL, but not the LDL (Yamamoto et al., 1993). Indeed, the most closely related family member is the ApoE receptor 2 (ApoER2), which shares half of its structure with the LDLr and has an almost identical spatial organization (Dlugosz et al., 2018). VLDLr expression is important in fatty acids metabolism particularly in the heart as shown in Balb/c mice heart where, in fasting condition, the VLDLr production, together with the expression of other genes implied in FA oxidation, is upregulated, indicating a role of the receptor in the TGs intake as a substrate for ATP generation (Kwok et al., 1997). The importance of VLDLr in cardiac Fatty acids supply is supported by different studies in which the receptor expression is modulated to reduce fatty acids overload in hypertrophic heart or upregulated in hypoxic conditions (Perman et al., 2011).

2.1.3 Cluster of Differentiation 36 (CD36)

Another receptor involved in the homeostasis of fatty acids is the cluster of differentiation (CD36). CD36 was discovered as a platelet integral membrane glycoprotein (glycoprotein IV) and is recognized as a multi-ligand scavenger receptor because it interacts with different ligands (Silverstein et al., 2009). CD36 is a Fatty Acids Translocase (FAT) and is almost ubiquitous express from many cells, such as endothelial cells, macrophages, dendritic cells, microglia, retinal pigment epithelium cells, hepatocytes, adipocytes, cardiac and skeletal myocytes; and in specialized epithelial cells of the breast, kidney, and gut (Febbraio et al., 2001). The family of CD36 includes other two members, the lysosomal integral membrane protein-2 (LIMP-2) and the scavenger receptor B-1 (SRB-1) (Calvo et al., 1995). CD36 is

formed from one large extracellular domain with six conserved cysteines linked in three disulfide bridges, important for the attachment at the cellular membranes, two transmembrane domains, and a short intracellular fragment (Febbraio et al., 2001). The extracellular part of CD36 is has a highly glycosylated domain, in which glycosylation mediates the correct receptor trafficking and targeting to the plasma membrane. CD36 was initially discovered as signal molecules in innate immunity (Hoosdally et al., 2009) and was associated with the phage ability of immune innate cells and thanks to this ability is involved in different functions and biological processes (Silverstein et al., 2009). Together with different proteins, such as fatty acid-binding proteins, caveola-associated proteins, integrins, cytoskeletal proteins, and signaling molecules mediates the internalization of long-chain fatty acids and their trafficking through the membrane. CD36 is important for fatty acids uptake in different cells type, particularly in the adipocytes, where is involved in the formation of lipid droplets, but also in tissues highly dependent on fatty acids metabolisms such as heart and skeletal muscle (Ibrahimi et al., 1999). Moreover, CD36 knockout mice that have increased plasma cholesterol, triacylglycerol, and fatty acids levels showed impairment in lipids transport and uptake and the development of cardiomyopathy (Glatz et al., 2013). To further support the key role of CD36 in cardiac metabolism it has been seen that in peri-infarcted areas the reduction of CD36 expression is protective against the development of cardiac damage due to lipotoxicity (Ibrahimi et al., 1999).

2.2 Intracellular lipid metabolism

Fatty acids and cholesterol can have a double function in the cells. It can be used as a structural brick for the construction of membrane, as phospholipids, as well as a source of energy when are metabolized in different metabolic pathways (de Carvalho et al., 2018).

2.2.1 Fatty Acids β -oxidation

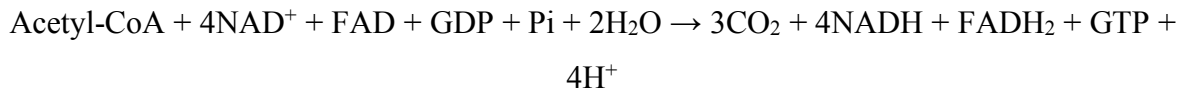
Fatty acids in the cells are principally metabolized through the β -oxidation, also known as Fatty Acid Oxidation (FAO). FAO takes place in the mitochondrial matrix and using fatty acids of different lengths leads at every cycle the dissociation of a molecule of acetyl-CoA with the production of flavin adenine dinucleotide (FADH₂) and NADH. While short-chain (SCFA) and medium-chain fatty acids (MCFA) can freely pass the organelle membrane,

long-chain fatty acids (LCFA) cannot enter the mitochondrion. For this reason, they need to use the carnitine shuttle, in which carnitine palmitoyl-transferase 1 and 2 (CTP-1 and 2), binding a molecule of acyl-CoA can mediate its internalization in the mitochondrial matrix in two steps. CTP-1 is located in the outer mitochondrial membrane and carries long-chain acylcarnitine across the membrane. While CTP-2 located on the inner mitochondrial membrane converts back long-chain acylcarnitine in long-chain acyl-CoA using mitochondrial coenzyme-A. This process is regulated by malonyl-CoA levels, which is the first intermediate of the fatty acid synthesis, in the attempt to avoid futile cycles (Kerner et al., 2000).

The β -oxidation involves 4 reactions, with specific enzymes for each step for long, medium, and short-chain length fatty intermediates. The first step is catalyzed by acyl-CoA dehydrogenase (CAD), followed by 2-enoyl-CoA hydratase (ECH), and then from the 3-hydroxyacyl-CoA dehydrogenase (HADH). The final step is catalyzed by the 3-ketoacyl-CoA thiolase (3-KAT), which regenerates acyl-CoA for another round of β -oxidation and releases acetyl-CoA for the Krebs cycle. CAD and HADH reduce a molecule of FADH₂ and NADH, respectively, and the acetyl-CoA formed from β -oxidation is then used to produce more NADH and FADH₂ in the Krebs cycle (Judge et al., 2020). An unbalance between the uptake and the use of lipids and the intracellular levels of fatty acids are elevated, the excess, especially triglycerides, are stored in lipid droplets (Figure 4) (Goldberg et al., 2012).

2.2.2 Krebs cycle - Tricarboxylic acid cycle (TCA)

The Krebs cycle also called the tricarboxylic acid cycle (TCA) occurs in the mitochondria and is finely regulated at different levels: in particular, the conversion of pyruvate into acetyl-CoA and the entry of acetyl-CoA mediated by the citrate synthase, which is one of the limiting steps of the cycle. The starting brick of the TCA is acetyl-CoA which can come from different ways. One is the β -oxidation of fatty acids from which a molecule of acetyl-CoA is generated at each cycle. Another pathway that can supply acetyl-CoA is glycolysis which from the metabolism of a molecule of glucose generates two molecules of pyruvate. Pyruvate is then converted in the mitochondria in acetyl-CoA by an enzyme called pyruvate dehydrogenase (PDH) or undergoes decarboxylation to form oxaloacetate or malate. Here, acetyl-CoA or the other intermediates enter the Krebs cycle and take part in a series of irreversible reactions. The yield of the Krebs cycle is:



The possibility of obtaining acetyl-CoA from different pathways, such as glycolysis and β -oxidation, makes the concentrations of all the intermediates of the pathway very important in the regulation of metabolic flow. The other two key enzymes in the control of the Krebs cycle are isocitrate dehydrogenase and α -ketoglutarate dehydrogenase. Glucose and fatty acid metabolisms are strictly connected: increased FAO leads to higher acetyl-CoA/free CoA and NADH/NAD⁺ ratios that inhibit PDH by the activation of PDH kinase. On the contrary, lower FAO rates increase glucose metabolism through the decrease in citrate concentration and the acetyl-CoA or NADH levels in the mitochondrial matrix. In general, increased acetyl-CoA production from pyruvate stimulates the production of malonyl-CoA, which inhibits the shuttle involved in the intake of long-chain FA into the mitochondria (Figure 4) (Judge et al., 2020).

2.2.3 Electron Transport Chain (ETC)

All aerobic metabolic pathways lead to the production of reduced forms of NADH and FADH₂ which are brought to the level of mitochondrial respiration, which is the final step in the production of ATP. The electron transport chain (ETC) is located in the Inner Mitochondrial Membrane (IMM) and consists of four complexes in which occur the transfer of electrons from donors to acceptors.

The electron transport chain is supplied mainly at the level of complex I by NADH while FADH₂ and succinate exchange their protons at the level of complex II. In the first part of the chain, NADH donates two electrons, carried away from the TCA, to complex I. These electrons are then passed to the lipid-soluble redox carrier coenzyme Q. Coenzyme Q moves freely in the membrane and is reduced by both complexes I and II to donate its electrons to the third complex of the electron transport chain, cytochrome c reductase. The protons obtained from the oxidation of coenzyme Q are carried in the intermembrane space by cytochrome c. From cytochrome c, electrons are targeted to complex IV, cytochrome c oxidase, and molecular oxygen is reduced to produce a molecule of H₂O₂. The complexes of the chain mediate redox reactions are coupled with the pump of protons through the membrane, generating a transmembrane electrochemical gradient that is used by the complex V (ATP synthase) which push H⁺ in favor of the proton gradient creating the energy necessary for the formation of ATP molecules starting from ADP plus phosphate.

Mitochondria are one of the main producers of reactive oxygen species (ROS), including superoxide (O_2^-), H_2O_2 , and hydroxyl radical (OH^\cdot), which are a by-product of this pathway and are particularly produced at the level of complex I and III (Judge et al., 2020). Even if mitochondria produce ROS themselves, they are highly susceptible to ROS-mediated damage due to the lack of histone-like proteins on mitochondrial DNA (mtDNA) that is in this way site of possible damage (Figure 4) (Sharma et al., 2019).

2.2.4 Cholesterol homeostasis

Cholesterol is the structural support for membranes and in the organism can be found in the cells as free cholesterol in the membrane or esterified in the lipid droplets. Cholesterol is transported in the circulation as lipoprotein and particularly in LDL. Low-Density lipoproteins are recognized by the cells thanks to the LDLr. After the cells have internalized the complex between LDL/LDLr, receptors are recycled to the cell surface, while LDL are hydrolyzed to release cholesterol, which is incorporated into cell membranes or used for cell metabolism, such as the synthesis of steroid hormones (Kwiterovich, 2000). Inside the cells, cholesterol triggers negative feedback to block its synthesis, inhibiting HMG-CoA reductase and LDLr synthesis. Moreover, free cholesterol activates Acyl-CoA acetyltransferase, promoting its esterification (DeBose-Boyd, 2008). Cholesterol is also produced by the cholesterol synthesis pathway in the cells, and the main producers are the liver and the intestine, even if the pathways it is expressed ubiquitously. As for PCSk9 most of the genes involved in cholesterol synthesis are regulated by the SREBPs. As free cholesterol accumulation is highly harmful to the cell, the organism develops a complex mechanism to finely regulate its levels by a negative feedback control mechanism. Indeed, cholesterol synthesis has a feedback control that inhibits the gene expression of enzymes involved in the pathway of cholesterol synthesis (Figure 4) (Fears, 1981).

3. Lipotoxicity

Lipotoxicity is the deleterious events that include several toxic effects occurring particularly on tissues that depend on fatty acid metabolism for energy production including the liver, heart, kidneys, and skeletal muscles. Lipotoxicity is caused by the alteration of lipid metabolism and by the accumulation of lipid intermediates, resulting in metabolic impairment of damaged organs. The term was used for the first time in the 1990s by Roger Unger, who first hypothesized that the excess of lipids was connected with the development of diabetes and cardiomyopathy (Nishi et al., 2019). Even if many studies have been made, this toxicity mediated by lipid accumulation remains poorly understood and it is not clear whether lipotoxicity is mediated by an excessive lipid production, in a reduced FA oxidation, inadequate clearance of toxic lipid intermediates, or partially in all of them.

Neutral lipids are usually stored in Lipid droplets. Lipids enter the cell via specific receptors including lipoprotein receptor and Fatty Acids Transport Protein. Once reach the cytosol FA are catabolized in the mitochondria, stored as triglycerides (TGs), or converted into complex lipids via various pathways that take place in the ER. TGs in an energy-depleted status may be used to generate energy, membrane components, and signaling lipids. Lipid droplets also play a protective role, because they allow the cell to sequester otherwise toxic lipids (Onal et al., 2017).

Lipid droplets are composed of a core of hydrophobic lipid surrounded by a single layer of amphipathic lipids and proteins. TGs are accumulated in the core of lipid droplets by the action of acyl-CoA-diacylglycerol acyltransferases 1 and 2 (DGAT1 and 2) that conjugating a molecule of diacylglycerol (DAG) with a molecule of acyl-CoA create the lipophilic core of Lipid droplets. These enzymes are located close to the endoplasmic reticulum, where TGs accumulate and lipid droplets are created (Kassan et al., 2013).

Fatty acids are released from TGs by the action of cytoplasmic TG lipases, such as adipose triglyceride lipase (ATGL) that are bind to the surface of lipid droplets. Lipid droplets can also be metabolized using structures that are normally used by the autophagic process.

The generation of TGs is a mechanism that cells use to detoxify a high concentration of Fatty Acids. During this process, many intermediates are generated and can be harmful to the cells. One of these intermediates are the diacylglycerol (DAG) and ceramides that can be the potential culprits for lipotoxicity.

DAGs are generated in three different ways: The most prominent pathway is mediated by the ATGL that hydrolyze Fatty Acids from the TG. The second one is from the esterification of fatty acids to phosphoglycerol, and from hydrolysis of phospholipids (Moro et al., 2008). To further support the principal role of lipase on Lipid droplets metabolism the lack of the hormone-sensitive lipase (HSL), the main lipase in DAGs metabolism, leads to the accumulation of DAG (Haemmerle et al., 2002). Lipotoxicity is a metabolic disorder and can be associated with metabolic changes in different cells, particularly DAG leading to the activation of protein kinase C (PKC) ϵ and θ , and the consequent phosphorylation of insulin receptor substrate 1 can induce insulin resistance in peripheral tissues (Hur et al., 2016).

The second main lipotoxic mediator are Ceramides. Ceramides are generated in the ER and then carried to the Golgi, where they are converted into complex sphingolipids used from the cells as structural support for membrane formation. The addition of phosphocholine leads to the formation of sphingomyelin, while the addition of a glucidic headgroup generates glucosylceramides, cerebroside, and gangliosides. Sphingolipids are one of the structural components of the cell membrane and are not absorbed through dietary sources, for this reason, the cells obtain it from the metabolism of saturated fats (palmitate) or proteins (serine) (Morales et al., 2007). Initially, the first observation that ceramides might have deleterious effects was consequent to the fact that the inhibition of ceramide biosynthesis prevented lipotoxic effects on pancreatic β -cells (Shimabukuro et al., 1998). Ceramide are generated in energy surplus status and the synthesis is increased in overnutrition states, as a consequence of Fatty acids abundance (Chaurasia et al., 2015). Ceramides can also be generated from sphingomyelin by the action of sphingomyelinases and this pathway has been involved in apoptosis caused by death ligands, including TNF α and Fas (Summers, 2006).

Ceramides as DAGs are implicated in several metabolic disorders. For instance, they are involved in the development of different pathologies through the inhibition of mitochondrial function. Indeed, inhibiting the ceramides synthesis in mice, the mitochondrial dysfunctionality mediated by lipotoxic events is restored and the oxygen consumption is increased (Ussher et al., 2010).

Lipotoxicity is particularly relevant in cardiac tissue and has been observed that ceramides can affect cardiac functionality promoting apoptosis, ER stress, and inhibition of insulin signaling.

3.1 Pancreatic β -cells lipotoxicity

Lipid metabolism is relevant for pancreatic β -cells functionality. Lipotoxicity is one of the main causes of β -cells dysfunction and the development of metabolic disorders, including Type 2 Diabetes. Different lipids are involved in pancreatic beta-cell degeneration including ceramides, sphingolipids, and cholesterol. The classic pathways of lipotoxicity are one of the main drivers of β -cells dysfunction indeed ceramides have been found to accumulate in Zucker Diabetic Fatty (ZDF) rats and the increased ceramides biosynthesis in vitro leads to β -cells apoptosis. As fatty acids, cholesterol is important in β -cells metabolism and contributes to the control of the structural properties of the membranes, thus affecting the localization and function of membrane proteins as well as insulin vesicle formation and fusion. Cholesterol accumulation can affect β -cells homeostasis in different ways and can occur both for an increased uptake via LDLR (Da Dalt et al., 2019) or reduced ABCA1 mediated efflux. Cholesterol overload can impact several steps of the metabolic organization of pathways involved in insulin release localized at the endoplasmic reticulum, mitochondria, and the cell membrane. Particularly cholesterol accumulating on the endoplasmic reticulum can alter calcium homeostasis leading to the depletion of cellular storage necessary for insulin release (Cnop et al., 2002; Lu et al., 2011). As a key component of lipid rafts, microdomains of the plasma membrane present in all cells, cholesterol accumulating may lead to dysfunctional SNARE proteins syntaxin and SNAP25, as well as of K^+ ATP and voltage-gated Ca^{2+} channel thus leading to an alteration in insulin vesicles trafficking (Xia et al., 2004).

It's important to notice that cholesterol accumulation not only affects structural alteration in pancreatic β -cells but also modulates cellular energetic metabolism. Cholesterol can maintain a dimeric form of nNOS thus preventing the activation of Glucokinase and the consequent inhibition of glycolytic flux (Perego et al., 2019). Moreover, cholesterol increasing the rigidity of the mitochondrial membrane may lead to alteration of the electron transport chain (ETC) and a reduced proton efflux; this impacts the ability of mitochondria in β -cells to produce ATP with the consequent inability to promote vesicles trafficking (Figure 5) (Brand et al., 2011).

3.1.1 Type 2 Diabetes (T2D)

Type 2 Diabetes is a chronic metabolic disorder characterized by alteration in insulin production, caused by pancreatic β -cells dysfunction and insulin resistance in peripheral organs. T2D is affecting the 90-95% of a subject that develop diabetes. Initially, T2D was considered as an adult pathology but recently more children are affected by this pathology. This increases the interest in other factors than the age that can affect this disease. Indeed, the pathology can be a consequence of different lifestyles and genetics. A sedentary lifestyle, cigarette smoking, alcohol consumption, and the development of obesity have been found to have relevance in the development of this disease, and obesity itself contributes to 55% of T2D cases. T2D is therefore characterized by a peripheral reduced insulin sensitivity that is followed by a reduced insulin production as a consequence of pancreatic β -cells degeneration. To further point the role of lipid metabolism β -cells are highly susceptible to lipid accumulation that together with other factors can be one of the causes of pancreatic degeneration and β -cells loss (Pinti et al., 2019).

3.2 *Cardiac Lipotoxicity*

Lipotoxicity may occur in different tissue. The heart as a great consumer of Fatty Acids for energy production is highly sensitive to Cardiac lipotoxicity. This toxic effect is characterized by the accumulation in the cytoplasmic storage of neutral lipids, triglycerides, and ceramides which are associated with increased apoptosis and myocyte dysfunction (Finck et al., 2003). Lipotoxicity shows as organelle dysfunction that at the end can cause myocytes degeneration (Goldberg et al., 2018). The prolongation of cardiac lipotoxicity over time leads to the development of different cardiomyopathies that at the end of pathology progression leads to the development of heart failure. Lipids may damage the cells in two different ways; the first hypothesis is that fatty acids as substrate for oxidation are increasing mitochondrial activity and the consequent mitochondrial damage mediated from oxidative side products as H_2O_2 . The second hypothesis is that the unused fatty acids accumulating in the cytoplasm are damaging cells as a source of ceramides, DAG, and TAGs (Goldberg et al., 2012). Lipid accumulation, and consequently lipotoxicity, can occur as a consequence of a reduction in fatty acids oxidation or as increased uptake of fatty acids. PPAR α knockout animal models are useful to understand this complicated link between fatty acids utilization and storage; indeed these mice develop cardiac dysfunction when fatty acids oxidation is reduced and lipotoxicity occurs because no difference in lipid uptake is observed

(Nohammer et al., 2003). Moreover, to confirm the deleterious effect of lipid accumulation on cardiac tissue Adipose Triglyceride Lipase (ATGL) knockout mice show reduced fatty acids oxidation and massive cardiac lipid accumulation that is associated with severe cardiac dysfunction (Haemmerle et al., 2006). All these data suggest that lipid accumulation, rather than an excess of fatty acids oxidation, is responsible for cardiac lipotoxicity that causes cardiomyopathy and heart failure. Not all lipids are toxic to the cells. Anyways, several lipids are implicated in the process that then leads to lipotoxic cardiomyopathy and heart failure. Fatty acyl CoA, acylcarnitine, unesterified cholesterol, lysolecithin, ceramide, and diacylglycerol are thought to cause apoptosis, inflammation, mitochondrial dysfunction, and defective intracellular signaling that are involved in the development of lipotoxicity (Drosatos et al., 2013). Saturated long-chain fatty acids, particularly acids palmitic, are more toxic than unsaturated long-chain fatty acids, such as oleic acid (Figure 6).

3.2.1 Heart Failure

Heart failure (HF) is a pathological condition in which the heart is no longer able to pump enough blood to sustain the organism's requests. This disease is characterized by energy depletion due to increased oxidative stress and metabolic changes in the substrate utilized for energy production (Neubauer, 2007).

Heart failure (HF) is one of the major public health issues and it can be classified as Acute or Chronic. To further characterized this condition, it can also be subdivided into Systolic HF for the patients with reduced Ejection Fraction (HFrEF) or Diastolic HF for those with preserved Ejection Fraction (HFpEF) (Cilia et al., 2019). An increasing number of persons are affected by chronic heart failure, and 50% of it is heart failure with preserved ejection fraction (HFpEF). This syndrome is particularly affecting patients with comorbidities such as obesity, hypertension, atrial fibrillation, diabetes, and aging (Seferovic et al., 2015). During the development of the disease, cardiac myocytes are prone to become hypertrophic and fibrotic. Subject with HF is exercise intolerant with LV stiffness and changes in extracellular matrix composition, especially in fibrillar collagen (Kasner et al., 2011). In HFpEF with EF of more than 50-55%, the pathology seems to be mainly driven by a systemic inflammatory state. Subject with HF has increased reactive oxygen species (ROS) production in the microvascular endothelial cells, limiting Nitrogen Oxide (NO). To further support the comorbidity of HF with other metabolic disorder, HF has been associated with systemic insulin resistance that together with the lack of oxygen forces the myocyte to switch

to metabolic pathways for energy production that do not require oxygen as a final electron acceptor (Doehner et al., 2008). The observation is further supported by studies on HF patients, with both idiopathic dilated cardiomyopathy or ischemic heart disease, which is highlighted a reduction in the functionality of ETC's complex III comparing to healthy individuals, thus confirming an impairment in oxidative metabolic pathways and therefore a shift towards those that utilize a less extent of oxygen (Stanley et al., 2005). Failing heart shows energy deficit and general oxidation impairment, probably due to defecting ETC's complexes. In particular, it is well known that during this condition fatty acid oxidation is reduced, supposedly due to a drop in the synthesis of catalytic enzymes of the process. Besides, the switch toward another metabolism, such as the glucose one, is perhaps an attempt of the heart to achieve the ATP request of the organism. Indeed, glucose metabolism is more efficient in energy production compared to FA oxidation, as the latter requires a higher quantity of oxygen to produce the same amount of ATP (Abozguia et al., 2009).

For what concerns glucose metabolism, it has been demonstrated that there is an increase of this pathway, attributable to an intensification of anaerobic glycolysis, with a consequent reduction in the aerobic pathway (Lei et al., 2004). The impairment between the two metabolic pathways has been associated with a deficiency in cardiac function and a rise in lactate and proton production. The increased glucose metabolism is associated with dysfunction in cardiomyocytes contractility, as a result of acidification of the pH that provokes troponin I insensitivity to calcium and impedes the L-type calcium channel's current. Moreover, the cell uses ATP to eliminate protons, thus depleting even more myocyte's energy (Lopaschuk et al., 2010).

Glucose utilization is also associated with cell mass augmentation, and indeed glucose is found to increase in hypertrophic hearts and lead to the development of HF. Besides, glucose can go through the PPP producing Nicotinamide Adenine Dinucleotide Phosphate (NADPH), metabolites that are found to increase during cell growth entry and important as a reducing equivalent (Ussher et al., 2012). Normally, a limited portion of glucose fuels this pathway, but in hypertrophy heart, it is found incremented. Besides, high levels of NADPH are associated with an increase in ROS, which is also responsible for heart dysfunctions.

As said above, ROS production is involved in the progression of the disease, even though small amounts of these substances seem to be beneficial in the activation of signals from the myocardium, such as the sympathetic drive, and this is called hormesis. Pathological conditions can be due to an unbalance between the ROS overproduction and the removal ability of the scavenging system (Rosca et al., 2013). The latter can be stimulated thanks to

physical exercise, which can also be improved symptoms and quality of life of HFpEF and HFrEF subjects. Moreover, elevated levels of ROS can diminish or make fall the membrane potential and the NADPH reservoir. The leakage of ROS from the mitochondrial matrix can be due to ETC's complex defects (Maranzana et al., 2013). These can derive from an unconventional phospholipids' composition in the inner mitochondrial membrane. Indeed, Cardiolipin, a particular phospholipid containing four acyl-chains and crucial for the integrity of the functionality of the ETC, is found decreased in failing hearts (Saini-Chohan et al., 2009). Cardiolipin seems to work sticking together the subunits of which the complexes are composed, and thus its absence leads to the loss of structural integrity of the ETC (Pfeiffer et al., 2003).

Aim of the study

Several trials showed that PCSK9 inhibition reduces LDL-C levels and CVD, by a mechanism involving increased hepatic LDLr expression. Mendelian randomization studies have confirmed that PCSK9 loss of function variants associate with lower LDL-C but also with higher plasma glucose levels and increased risk of developing type 2 diabetes. The latter observation suggests that PCSK9 might affect the physiology of other pathways other than those involved in LDL uptake in the liver. However, the increased expression of PCSK9 targets, such as LDLR and CD36, leads to intracellular accumulation of fatty acid and cholesterol that is mainly affecting cellular functionality in different tissues beyond the liver. The liver is the major producer of PCSK9 and its main target but PCSK9 is also produced by other tissues and therefore its pharmacological modulation can lead to off-target effects. Increased expression of LDLr and CD36 may lead to metabolic alteration and lipid accumulation in other tissues than the liver affecting different cellular compartments. One of the most affected organelles is the mitochondria where cholesterol accumulation may alter the both inner and outer membrane, increasing the rigidity, finally leading to the dysfunction of metabolic pathways and the consequent energy depletion. For this reason, a lot of interest is put on mitochondria and their role in tissues with high energy demand, such as the heart, or involved in hormone production, such as the pancreas. On this background, we want to investigate whether PCSK9, regulating its main targets, the LDLr and CD36, may affect lipid metabolism in other organs than the liver and how this can affect organs functionality and systemic metabolism. As PCSK9 may have a role in peripheral lipid metabolism we tested how PCSK9 can affect lipid accumulation in pancreatic and cardiac tissue, II) whether the absence of the LDLr rescues the cardiac or pancreatic phenotype by studying Pcsk9/LDLr Double KO mice and III) the role of circulating/liver-derived PCSK9 on tissues functionality.

Materials and Methods

1. Mice model

B6;129Sv-Pcsk9tm1Jdh/J male mice from the Jackson Laboratory (Bar Harbor, ME, USA) were backcrossed to C57Bl6J females for 10 generations. Heterozygous mutant mice from the F10 generation were intercrossed to generate littermates WT and KO mice. The mice were kept under controlled light/dark cycle (12 hours of light/12 hours of dark) and temperature-controlled conditions (21°C). They had free access to food and water, except when fasting (overnight for glucose tolerance test-GTT, 4h for insulin tolerance test-ITT) was required.

Starting at 8 weeks of age and for 20 weeks, mice were fed with a standard fat diet (SFD- 20% kcal Protein, 70% Carbohydrate, 10% kcal Fat, Research Diets, Inc) or a high fat diet (HFD- 20% kcal Protein, 35% Carbohydrate, 45% kcal Fat, Research Diets, Inc). The food intake and the body weights were measured weekly.

B6.129S7-LDLrtm1Her/J male mice from the Jackson Laboratory (Bar Harbor, ME, USA) were backcrossed to *Pcsk9 KO* females for 10 generations. Heterozygous mutant mice from the F10 generation were intercrossed to generate littermates *LDLr KO* and *Pcsk9/LDLr* DKO mice and treated as described before.

B6.Cg-Tg(Alb-cre)21Mgn/J male mice from the Jackson Laboratory (Bar Harbor, ME, USA) were backcrossed to *Pcsk9^{LoxP/LoxP}* females (provided by Merck Research Laboratories) for 10 generations. Heterozygous mutant mice from the F10 generation were intercrossed to generate littermates *AlbCre-/Pcsk9^{LoxP/LoxP}* and *AlbCre+/Pcsk9^{LoxP/LoxP}* which were treated as described before.

1.1 Diets

The standard fat diet (SFD) formula (Product #D12450H) is:

Ingredients	Gm %	Kcal %
Protein	119	20
Carbohydrate	68	70
Fat	4,3	10
Total	4,73	100
Ingredients	Gm %	Kcal %

Casein, 30 Mesh	200	800
L-Cystine	3	12
Corn Starch	452	18080,8
Maltodextrin 10	75	300
Sucrose	174	691,2
Cellulose, BW200	50	0
Soybean Oil	25	225
Lard	20	180
Mineral Mix S10026	10	0
Dicalcium Phosphate	13	0
Calcium Carbonate	5,5	0
Potassium Citrate, H ₂ O	16,5	0
Vitamin Mix V10001	10	40
Choline Bitartrate	2	0
FD&C Red Dye #40	0,04	0
Total	4,73	100

1.2 DNA isolation and genotyping

1.2.1 Mouse ear biopsy digest protocol

An ear biopsy was placed in a labelled 1,5 mL autoclaved Eppendorf tube. 0,5 mL of previously prepared Lysis Buffer [0,5% SDS (Bio-Rad), 0,2 M NaCl (Sigma), 0,5 mM Tris HCl pH 8 (Applichem), 4 mM EDTA (Sigma)] and 25 µL of Proteinase K (10 mg/mL – Roche) were added. The tubes were incubated at 56°C for 18 hours, then DNA was extracted and precipitated.

1.2.2 DNA extraction and precipitation

Tubes were spun at 13000 rpm for 5 minutes, and the solution was transferred in another 1,5 mL Eppendorf autoclaved tube. 500 µL of Phenol/Chloroform/Isoamyl alcohol 25:24:1 were added to the solution. Tubes were inverted and spun again at 13000 rpm for 5 minutes. The supernatants were transferred in other 1,5 mL autoclaved Eppendorf tubes. Subsequently, 800 µL of 95% ethanol were added. Tubes were inverted and spun at 13000 rpm for 5

minutes. The ethanol was discarded and the tubes were left to dry at room temperature for about 3-4 hours with the pellet inside. Finally, the pellet was resuspended in 25 μL of de-ionized water. Samples were stored at 4°C.

1.2.3 PCR protocol

The following mix was prepared in a 0,5 mL autoclaved Eppendorf tube, compatible with GeneAmp-PCR system 9700 machinery. The composition of the mix per each sample is:

- 26,75 μL of autoclaved water
- 10 μL of 5X Flexi Buffer
- 6 μL of MgCl_2 50 mM (Promega)
- 1 μL of dNTPs 2,5 mM
- 0,75 μL of olMR5170 Primer 20 μM
- 1,25 μL of olMR5171 Primer 20 μM
- 1,75 μL of olMR5172 Primer 20 μM
- 0,5 μL of Taq DNA Polymerase
- 3 μL of template DNA

Primer sequences used:

PCSK9	0: GATTGGGAAGACAATAGCAGGCATGC 1: ATTGTTGGAGGGAGAAGTACAGGGGT 2: GGGCGAGCATCAGCTCTTCATAATCT
PCSK9 Flox	FW: GGATAGTTCAGGGTTCAAAGCATGGG RW: GGTCTCCTCCATCAGCACCACAATG
LDLr	FW: AATCCATCTTGTTC AATGGCCGATC RW1: CCATATGCATCCCCAGTCTT RW2: GCGATGGATACTCACTGC
AlbCRE	FW: AGGTGTAGAGAAGGCACTCAGC RW: CTAATCGCCATCTTCCAGCAGG

The tubes were placed in the PCR machinery using this set cycling conditions:

- 94°C for 3 minutes → 1 cycle
 - 94°C for 30 seconds
 - 68°C for 1 minute
- } 40 cycles

- 72°C for 1 minute
- 72°C for 2 minutes → 1 cycle
- Keep at 10°C

Once the PCR is done, agarose gel electrophoresis was performed to evaluate the product of the amplification.

1.2.4 Agarose gel electrophoresis protocol

Agarose (SeanKem LE Agarosio, Lonza) was measured and dissolved in TAE Buffer 1X (TAE 50X: 500 mL of distilled water, 121 g of Tris (Applichem), 28 mL of Acetic acid, 50 mL EDTA 0,5 M) to obtain an 2,5% agarose gel for PCSK9 KO and 1,5% for other PCR.

The gel was poured into a gel tray with the well comb in place. The gel was let sit at room temperature for 20-30 minutes, until it was completely solidified. Then, the agarose gel was placed into the gel box (electrophoresis unit), which was filled with TAE 1X until the gel was entirely covered. The DNA solution was carefully loaded into the wells. The gel run at 90 V until the dye line was approximately 80-85% of the way down the gel. After the electrodes were disconnected from the power source, the gel was carefully removed from the gel box. The DNA fragments were visualised through UV light.

2. Gene expression

2.1 RNA extraction

To perform the quantification of gene expression, a heart biopsy was collected and for RNA extraction was used RNeasy Fibrous Tissue Mini Kit (Qiagen, Cat.No. 74704).

First at all, tissue ($\leq 30\text{mg}$) is disrupt and homogenize in 500 μL of RIPA Buffer using the TissueRuptor (Qiagen) and then transferred to a marked 1.5ml autoclaved Eppendorf. 590 μL RNase-free water and 10 μL proteinase K are added, mixed and incubated at 55°C for 10 minutes. After a centrifugation at 10000 g for 3 min, supernatant is transferred to new tube and 0,5 volumes of 96-100% ethanol is added and mixed. 700 μL of sample is transferred to RNeasy Mini column (in a 2 ml collection tube) and it is centrifuged for 15s at ≥ 8000 g. The eluate is discarded and the step is repeated until all the lysate has been used. 350 μL Buffer RW1 are added to RNeasy column, a centrifuge (15s at ≥ 8000 g) is made and the lysate is discarded. At this point, a mix of 10 μL of DNase stock solution with 70 μL of Buffer RDD per sample is prepared, added and incubated for 15 min at 20°-30°C. Subsequently, a series

of washes are made to clean the sample that has remained in the filter of the mini column. 350 μL Buffer RW1 are added to RNeasy column, centrifuged for 15s at ≥ 8000 g and the eluate is discarded. Two washes were then carried out with 500 μL of Buffer RPE (the second centrifuge is made for 2 minutes and not for 15 seconds). At the end, RNeasy column is placed in new 1,5 ml tube and 30 μL RNase—free water are added. After a centrifugation for 1 min at ≥ 8000 g and the eluate is conserved.

Isolated RNA was then quantified with Nanodrop through spectrophotometry and then stored at -80°C to maintain an efficient preservation.

2.2 RNA reverse transcription

RNA reverse transcription consists of an enzymatic reaction which aims in synthesizing complementary DNA (cDNA) starting from RNA in order to obtain a more stable nucleic acid. For each sample was prepared a 20 μL mix composed by 4 μL of Buffer 5X iScriptTM reaction mix (Bio-Rad) containing dNTPs, oligo[dT], random primers, buffer and MgCl_2 . The remaining 16 μL were composed by a mixture of RNA and Nuclease-free water, to add the same RNA volume even if the quantity of isolated RNA was different for each sample. The mix was inserted into a new 0,5 ml autoclaved Eppendorf tube and then inserted into the Mastercycler Nexus Gradient Eppendorf Thermocycler. Thermal protocol for retrotranscription was based on the following cycling conditions:

25°C	5 min
42°C	30 min
85°C	5 min
4°C	∞

2.3 Real-time PCR

Prepare the following mix per each gene that should be investigated (consider to plate samples in duplicate):

- 7,5 μL of Luna Universal qPCR Master Mix (New England BioLabs)
- 1,5 μL of forward primer
- 1,5 μL of reverse primer
- 2,5 μL of autoclaved water

Pipette 13 μL of mix per well and then add 2 μL of the appropriate sample.

The 96 wells-plate was placed in the Real-Time PCR machinery using this set cycling conditions:

- 95°C for 5 minutes → 1 cycle
- 95°C for 15 seconds
- 60°C for 30 seconds } 45 cycles
- 65°C for 10 seconds → 1 cycle
- 95°C

Mouse		Primer Sequence	Mouse		Primer Sequence
RPL13a	Fw:	GCGCCTCAAGGTGTTGGAT	ABCG1	Fw:	TTCATCGTCCTGGGCATCTT
	Rv:	GAGCAGCAGGGACCACCAT		Rv:	CGGATTTTGTATCTGAGGACGAA
LDLR	Fw:	GTGTGACCGTGAACATGACTGC	HADHB	Fw:	GCAGTTTTTCGCGGACTCTAA
	Rv:	CACTCCCACTGTGACACTTGA		Rv:	ATTCTGAAATCTGCCTGTGGG
HMG-CoA	Fw:	TGTGGTTTGTGAAGCCGTCAT	ACADVL	Fw:	GCTCTGCAAGGCTGTATGGA
	Rv:	TCAACCATAGCTTCCGTAGTTGTC		Rv:	CGATTCTGTCTCCGTCTC
SREBP2	Fw:	GCGGACAACACACAATATCATTG	ACADM	Fw:	GCTAGTGGAGACCAAGGAG
	Rv:	TGACTAAGTCCTTCAACTCTATGATTTG		Rv:	CCAGGCTGCTCTCTGGTAAC
ACAT1	Fw:	TGGCACGAATTGCAGCAT	ACADL	Fw:	TTTCCGGGAGAGTGTAAGGA
	Rv:	GCAGGCGCAAGTGGAAA		Rv:	ACTTCTCCAGCTTCTCCCA
PRKN	Fw:	ATGTCAGTCATCTTCTCTGTCA	ECHS1	Fw:	TTATGCTCTTGGTGGGGGTT
	Rv:	AGGTGACGACCTATTGCACA		Rv:	AGGAGGATTTCTGGCTGTCC
Pink1	Fw:	TGTGGAATATCTCGGCAGGTT	TFAM	Fw:	CGGGCCATCATTCGTCTG
	Rv:	GCTTGGGACCATCTCTGGAT		Rv:	AGACAAGACTGATAGACGAGGG
RHEB	Fw:	CTACCGGTCTGTGGGAAAGT	CPT1a	Fw:	CCGCCAATTCAAAAAGTACCT
	Rv:	CGCTGTGTCTACAAGCTGAA		Rv:	CATTTGGTTTGTACTACTAGAGTCCATT
ULK1	Fw:	CCTACACACCTTCTCCCAA	CPT1b	Fw:	ACCACATCCGCCAAGCA
	Rv:	GAGGAACCGGGTCGTGG		Rv:	TTCCTCAGGTGTCTGTCTTGGGA
P62	Fw:	AGATAGCCTTGGAGTCGGTG	PGC1a	Fw:	TGCCTTCATGCTGTGGTAAGTACT
	Rv:	TCAGCCTCTGTAGATGGGTC		Rv:	AAAACCCCGCATTCTAAAGC
ABCA1	Fw:	GGTTTGAGATGGTTATACAATAGTTGT	PGC1b	Fw:	CCTCTCCAGGCAGGTTCAAC
	Rv:	TTCCCGGAAACGCAAGTC		Rv:	GGCCAGAAGTTCCTTAGGATAG
LXR	Fw:	CGACAGAGCTTCGTCCACAA			
	Rv:	GCTCGTTCCCAGCATTTT			

3. Protein expression

3.1 Protein extraction

Place the organ in a 5 mL tube and add 500 µL of RIPA. Keep on ice.

Homogenize the tissue with the Tissue Ruptor (30 seconds) – rinse the Tissue Ruptor with water after each sample. Keep the samples on ice to avoid overheating. Leave the samples on ice for 15 minutes.

Then, transfer the sample in a 1,5 ml Eppendorf tube. Centrifuge at 13000 g for 5 minutes at 4°C and finally transfer the supernatant in another 1,5 Eppendorf tube.

3.2 Protein quantification (Lowry)

Prepare the standard curve using albumin (2 mg/ml).

- 0 → 200 µL water
- 5 → 2,5 µL albumin + 197,5 µL water
- 10 → 5 µL albumin + 195 µL water
- 20 → 10 µL albumin + 190 µL water
- 30 → 15 µL albumin + 185 µL water
- 40 → 20 µL albumin + 180 µL water

If samples come from tissues, dilute them 1:5 in water

Prepare the solution A+B (50:1). Add 1 mL to each sample. Vortex and incubate for 10 minutes at 37°C.

Prepare the solution Folin+water (1:1) and add 100 µL to each sample. Vortex and incubate for 30 minutes at 37°C (vortex again after 15 minutes).

Place 200 µL of sample per well in a 96 well-plate.

Read the plate at 550 nm.

3.3 Western blot

Place the pair of glasses on the appropriate supports and fill them with water to check the absence of leakages. Prepare the running and stacking gels, adding just before using TEMED and APS.

Running gel 10% (x 2 gels)

- 8 mL H₂O
- 5 mL Tris 1,5M
- 200 µL SDS 10%
- 6,7 mL Acrylamide
- 10 µL TEMED
- 100 µL APS

Stacking gel 12% (x 2 gels)

- 6,1 mL H₂O
- 2,5 mL Tris 0,5M
- 100 µL SDS 10%
- 1,3 mL Acrylamide
- 10 µL TEMED
- 50 µL APS

Stratify 7/8 mL of running gel and put on top some water to flatten the gel. Once the running gel is set, discard the water and pipette directly on top of it the stacking gel, ensuring there are no bubbles.

Prepare the samples in a final volume of 20 µL: the ratio between the sample and Laemmli 4X (4% SDS, 20% glycerol, 10% 2-mercaptoethanol, 0,004% bromophenol blue and 0,125M Tris HCl; pH approximately 6,8) should be 1:4.

Boil the samples for 3 minutes.

When also the stacking gel is set, load the samples and 5 μ L of molecular weight marker (Precision Plus Protein™ Standards; Cat #161-0374, Bio-rad). Place electrophoresis cassette into gel tank and place the entire set up into a plastic overflow tub. Fill the tank with Running Buffer [Running Buffer 10X: 130,3 g/L glycine, 30,3 g/L Tris, 0,1% SDS]. Connect electrophoresis cassette to power supply and run at 30-35 mA for stacking gel, then 50-60 mA for resolving gel. Allow to run until loading buffer reaches the base of the resolving gel. In the meantime, cut nitrocellulose to slightly larger than the gel and wet in ddH₂O to allow them to start to activate.

Separate gel from cassette, cutting off the stacking gel next to the edge of the marker. Slide the gel from the glass in a tank with Transfer Buffer [Transfer Buffer 10X: 144 g/L glycine, 30,3 g/L Tris, 20% MeOH]. Put all on the first sponge with the gel face up. Place on top of the gel the nitrocellulose membrane. Dampen the membrane with Transfer Buffer and roll over to ensure there are no bubbles. Put on top the second sponge and transfer the whole sandwich into the transfer equipment. Plug the Trans Blot Cell (Hoefer Scientific Instrument) into power supply and transfer at 200 mA for 2 hours.

Incubate nitrocellulose membrane in 5% non-fat dried milk in 0,1% PBS-Tween for 1 hour (or overnight at 4°C) to block non-specific antibody binding.

Incubate in primary antibody for 1 hour (or overnight at 4°C), under the conditions required by the antibody [Tubulin 1:2000, LDLr 1:400, CD36 1:2000 in 5% non-fat dried milk in 0,1% PBS-Tween].

Wash the membrane with PBS-Tween 0,1% (3 times, 10 minutes each).

Incubate in secondary antibody for 1 hour (or overnight at 4°C), under the conditions required by the antibody [anti-rabbit 1:2000 in 5% non-fat dried milk in 0,1% PBS-Tween].

Wash the membrane with PBS-Tween 0,1% (3 times, 10 minutes each).

Immunoreactive bands were detected by exposing the membranes to Clarity™ Western ECL chemiluminescent substrates (Bio-rad) for 5 minutes and images were acquired with ODYSSEY® Fc-Imaging system (LiCor).

The analysis was done using the Image Studio™ Software. Band density was analysed, and the results were expressed as relative intensity normalized to β -actin protein expression.

4. Glucose Tolerance (GTT) and Insulin Tolerance Tests (ITT)

GTT was performed after 12 and 20 weeks of SFD or HFD treatment. Mice were fasted overnight (12-16h), weighed and blood glucose was measured by snipping the tail and using

a glucose meter (ONE-TOUCH Ultra) before and after intraperitoneal injection of glucose solution or after a oral bolus of glucose solution (2g/kg body weight). At the end of the test all the tail wounds were cauterized and the mice were provided with food.

Fasting and refeeding experiments were performed at 20 weeks. Mice were fasted overnight, weighted, housed one for cage and refeed ad libitum for 4h (food was weighted at the beginning of the test and after the 4h). Blood glucose was measured by snipping the tail and using a glucose meter (ONE-TOUCH Ultra). Blood was collected at sacrifice in Eppendorf tubes containing EDTA 0.5%. Blood samples were centrifuged for 14 min at 7000 rpm at 4°C and plasma was collected and immediately stored at -20°C for ELISA assay.

Insulin Tolerance Test (ITT) was performed after 12 and 20 weeks of SFD or HFD treatment. Mice were fasted for 4h, weighed and blood glucose was measured by snipping the tail and using a glucose meter (ONE-TOUCH Ultra). Insulin solution (0.2IU/kg body weight) was injected in the intraperitoneal cavity and mice were bled as described above after 20, 40, 60, 120 min. Insulin solution was prepared from stock of 100 UI insulin solution (Humuline R 100 UI/mL) and was diluted in a physiological solution (NaCl 0.9%) with 3% of bovine serum albumin (BSA Sigma-Aldrich). At the end of the test the tail wounds were cauterized and the mice were provided with food.

5. Cholesterol, triglycerides, insulin, C-Peptide and PCSK9 measurement.

Plasma cholesterol and triglycerides levels were measured as previously described (Bonacina et al., 2016). Insulin levels were measured in plasma with Mercodia Ultrasensitive Mouse Insulin ELISA and according to manufacturer instructions. For insulin detection in pancreas Mercodia Mouse Insulin ELISA was used. Pancreas were processed in 350 µl of Tissue Protein Extraction Reagents (Thermo Fisher Scientific) containing a cocktail of protease and phosphatase inhibitors (Roche Diagnostics). PCSK9 was measured on plasma aliquots collected after overnight fasting and stored at -80°C for up to three weeks by a commercial enzyme-linked immunosorbent assay (ELISA) kit (R&D Systems, Minneapolis, MN). Plasma samples were diluted 50 times and then processed as per manufacturer instructions.

6. Metabolomics analysis

For metabolomic analyses, heart has been homogenized in methanol/acetonitrile 1:1 with a tissue-lyser and internal standards for metabolites quantification has been added. Our team

developed different methods to quantify several metabolites (almost 1000 different species) in different pathways as Glycolysis, Pentose phosphate, Krebs cycle, Fatty Acid synthesis and Oxidation (acylcarnitines), Aminoacids, biogenic amines and several phospholipid families. Briefly, quantitative analyses of different metabolites have been performed either by Liquid Chromatography tandem Mass Spectrometry (LC-MS/MS) or Flow Injection Analyses (FIA-MS/MS) depending on the nature of metabolites to be quantified. Metabolomic data have been obtained on an API-4000 triple quadrupole mass spectrometer (AB SCIEX) coupled with a HPLC system (Agilent) and CTC PAL HTS autosampler (PAL System). Standard curves for each metabolite was used to determine the absolute levels of different metabolites.

7. Oxygen Consumption Rate (OCR)

Heart samples have been transferred to the DW1 chamber and permeabilized with 0.16 ng/ml digitonin. After analyzing basal respiration rate, maximal coupled respiration was recorded by adding 20 mM ADP. Uncoupled respiration was obtained with 12.5 M oligomycin and maximal uncoupled respiration was evaluated in the presence of 60 μ M carbonyl-cyanide-m-chlorophenyl-hydrazine (CCCP).

8. Mitochondrial DNA quantification

10 mg of cardiac tissue were placed in a labelled 1,5 mL autoclaved Eppendorf tube. 0,5 mL of previously prepared Lysis Buffer [0,5% SDS (Bio-Rad), 0,2 M NaCl (Sigma), 0,5 mM Tris HCl pH 8 (Applichem), 4 mM EDTA (Sigma)] and 25 μ L of Proteinase K (10 mg/mL – Roche) were added. The tubes were incubated at 56°C for 18 hours, then DNA was extracted and precipitated. Tubes were spun at 13000 rpm for 5 minutes, and the solution was transferred in another 1,5 mL Eppendorf autoclaved tube. 500 μ L of Phenol/Cloroform/Isoamyl alcohol 25:24:1 were added to the solution. Tubes were inverted and spun again at 13000 rpm for 5 minutes. The supernatants were transferred in other 1,5 mL autoclaved Eppendorf tubes. Subsequently, 800 μ L of 95% ethanol were added. Tubes were inverted and spun at 13000 rpm for 5 minutes. The ethanol was discarded and the tubes were left to dry at room temperature for about 3-4 hours with the pellet inside. Finally, the pellet was resuspended in 25 μ L of de-ionized water. Samples were stored at 4°C.

DNA content was quantified measuring $A_{260\text{ nm}}$ with a NanoDrop (Thermo Fisher Scientific). 15 ng of DNA were used for amplification by real-time quantitative with Luna® Universal.

1 μ M of each primer were used to a final volume of 15 μ l of reaction mix with 7,5 μ l of master MIX.

36B4 (genomic DNA)

Fw: AGATGCAGCAGATCCGCAT Rv: GTTCTTGCCCATCAGCACC

ND1 (mt DNA)

Fw: CCTACCAATACCACACCCAT Rv: CGTAAAGCTCCGAATAGTGAG

COX II (mt DNA)

Fw: TGGTGAACACTACGACTGCT Rv: CTGGGATGGCATCAGTTT

The threshold cycle number (Ct) values for each reaction were calculated mtDNA content was determined as $2^{\Delta C_t}$ or fold difference of mtDNA from nDNA.

9. Exhaustion test

A week before the experiment the animals were accustomed to both the operator and the treadmill. For three continuous days the animals were acclimatized to treadmill exercise and let run on the treadmill with 20° of inclination (Ugo Basile Instruments) at the speed of 5 m/min for 10 min. The first day the mouse are allowed to explore the treadmill without electric shock. The second day the mice were let run on the treadmill and keep in contact for a few second with the electric stimulus. The day of the experiment all experimental group were warm up for 4 min at the speed of 5m/min after which the treadmill velocity was increased to 14 m/min for 2 min. Every 2 min the treadmill speed was increased by 2 m/min until the animals were considerate exhausted. Exhaustion was expressed as the inability of the mouse to return to run within 10 s of direct contact with an electric grid (2Hz, 1,22 mA) or the permanence in the fatigue zone, considered as the minimum distance from the grid to contain the entire animal. Running time was measured and running distance calculated.

10. Forelimb grip test

Muscle strength of all mouse line was tested using a grip-strength test performed using the grip strength meter Ugo Basile, Gemonio, Italy, model 47106. The animals were kept from the tail and are approached longitudinally to the grid attached to the grip-strength meter. The mice immediately grasp the grid just with the forelimb and holds on until the gently force of the experimenter exceeded its strength. At this point the peak force (g) was recorded. The test was considered complete when three consecutive tests were repeated for 5 times. After each test the animal were let rest for 1 min. The highest three values were considered and

the average were normalized on animal body weight. All measurements were performed by the operator in a blinded fashion.

11. Proteomics

11.1 Sample preparation and protein extraction

Heart from PCSK9 KO mice (n=6 WT mice and n=6 PCSK9 KO) were pooled up to 20 mg and lysed in the presence of RIPA buffer (Tris-HCl 50 mM pH 7.2, EDTA 5 Mm, SDS 0.1%) and protease inhibitors (Cell Signaling, Cat# 5872S) at a ratio of 1:100. Samples were homogenized and incubated for 30 min at 4°C, followed by 30 min under agitation at 4°C. Subsequently, samples were centrifuged at 13000 g for 5 min, the supernatant was collected. Samples were added with acetone (4:1 vol/vol), incubated for 15 min in ice, centrifuged for 10 min at 12000g at 4°C, supernatants were discarded. Pellets resuspended buffered urea (8M, Tris-HCl 100mM pH 8.5. Lowry protein assay was performed to measure the total protein content.

11.2 Peptide preparation and purification in solution digestion

Samples were then dried using a vacuum concentrator (45°C for 45 min) and the dried residues resuspended in 10 µl of Ambic 50 mM (pH 8.5). Protein disulphide bonds were reduced by addition of dithioerithreitol (DTT) to a final concentration of 5 mM (30 min incubation at 55°C). Samples were cooled down to room temperature and the alkylation was performed by addition of iodoacetamide to a final concentration of 15 mM, followed by 30 min of incubation in the dark. Proteins were then digested overnight with trypsin (Sigma, Cat# T2601) at an enzyme-to-protein ratio of 1:20, at 37°C. After digestion, the reaction was stopped by acidification with 50% trifluoroacetic acid (TFA) to have 1% TFA as final concentration.

11.3 LC-MS/MS

All samples were analyzed at UNITECH OMICs (University of Milan, Italy) using a Dionex Ultimate 3000 nano- LC system (Sunnyvale CA, USA) connected to an orbitrap Fusion™ Tribrid™ Mass Spectrometer (Thermo Scientific, Bremen, Germany) equipped with a nanoelectrospray ion source operating in positive ion mode. Three technical replicates per

group were injected and the peptide mixtures were pre-concentrated onto an Acclaim PepMap C18 5 μm , 100 \AA , 100 μm ID x 2cm (Thermo Scientific) and separated at 35°C on an EASY- Spray PepMap RSLC C18 column: 3 μm , 100 \AA , 75 μm ID x 15 cm (Thermo Scientific). Peptides were eluted with gradient runs from 96% buffer A (0.1% aqueous formic acid) to 40% buffer B (0.1% aqueous formic acid /acetonitrile (2:8)). Run total length: 110 min. Flow rate: 300 nL min⁻¹. MS spectra were collected over an m/z range of 375 – 1500 Da at resolution 120.000 in data dependent mode, cycle time 3 sec between master scans. Fragmentation was induced by higher energy collisional dissociation (HCD) with collision energy set at 35 eV.

Peptides were separated on a reverse phase column (50 cm length, 75 μm inner diameter) packed in-house with ReproSil-Pur C18-AQ 1.9 μm resin (Dr. Maisch GmbH, Ammerbuch, Germany). Reverse-phase chromatography was performed with an EASY-nLC 1000 ultrahigh pressure system, coupled to a Fusion Mass Spectrometer (Thermo Scientific). Peptides were loaded with buffer A (0.1% (v/v) formic acid) and eluted with a nonlinear 120 min gradient of 5–60% buffer B (0.1% v/v formic acid, 80% v/v acetonitrile) at a flow rate of 250 nl/min. After each gradient, the column was washed with 95% buffer B and re-equilibrated with buffer A. Column temperature was kept at 50°C by an in-house designed oven with a Peltier element, and operational parameters were monitored in real time by the Spray Qc software. MS data were acquired with a shotgun proteomics method, in which every full scan is followed by up to 15 data-dependent MS/MS scans. Target value for the full scan MS spectra was 3 106 charges in the 300–1650 m/z range with a maximum injection time of 20 ms and a resolution of 60000. Isolation of precursors was performed with the quadrupole at window of 1.4 m/z. Precursors were fragmented by higher-energy collisional dissociation (HCD) with normalized collision energy (NCE)/stepped NCE of 27. MS/MS scans were acquired at a resolution of 15000 with an ion target value of 1 105, a maximum injection time of 25 ms, and an underfill ratio of 10%. Repeated sequencing of peptides was minimized by a dynamic exclusion time of 20 s.

11.4 Analysis of Proteomic Data

Prior to data analysis, each MS raw file was converted from the ThermoFisher raw format to mzML format (centroid mode) using the MSconvert tool of the software ProteoWizard (version 3.0.1957). mzML files were then processed using a proteomic pipeline built using

OpenMS ver. 2.4 (Röst et al., 2016) nodes operating within the open source software platform KNIME® ver. 4.0 (Konstanz Information Miner). Peptides identification was done using an approach based on the combination of the search engines XTandem (Craig and Beavis, 2004), MS-GF+ (Kim et al., 2008), Novor (Ma et al., 2015) and SpectraST (Lam et al. 2007), against a mouse Uniprot FASTA database (uniprot-mus+musculus.fasta, downloaded at www.uniprot.org in September 2019), and a common contaminant proteins database (Lam et al. 2007). The spectral library required by the SpectraST search engine was downloaded from the website www.peptideatlas.org (file NIST_mouse_IT_2012-04-21_7AA.splib). Cysteine carbamidomethylation was set as fixed modification and methionine oxidation as variable modification. Where applicable, fragment mass tolerance was set at 0.02 Da and precursor mass tolerance at 5.0 ppm. Peptide sequences were indexed through the OpenMS PeptideIndexer node, setting leucine/isoleucine equivalence. Protein inference was then carried out using the Protein Inference Analysis (PIA) algorithm, using the default parameters set by the developers (Uszkoreit et al., 2015, 2019). Protein abundance estimates were calculated with prior generation of spectral features by the node FeatureFinderMultiplex (Nilse et al., 2016) followed by PIA-assisted false discovery rate (FDR)- multiple scores estimation and filtering (combined FDR score<0.01), their ID mapping and combination with peptide IDs, their subsequent alignment, grouping and normalization (e.g. FeatureUnlabeledQT and ConsensusMapNormalizer nodes) (Nilse et al., 2016). Proteins and peptides label free quantification (LFQ) was then computed with the OpenMS ProteinQuantifier node based on intensities of the n=3 most abundant identified peptides. The relative output files were read as tables of the CSVreader node output and exported into Microsoft Office Excel 2016 for further formatting and statistical elaboration.

12. Echocardiographic

Echocardiographic views are performed with a high-resolution echocardiography system suitable for small animals: Vevo 2100, VisualSonics, Toronto, Canada, which is equipped with a 30 MHz linear matrix transducer (MS400). To perform echocardiographic analyzes, the animal will initially be placed in an induction chamber where it is anesthetized with a gaseous mixture of O₂ (1 L / min) and 1.5-3% isoflurane. An ocular lubricant will be applied to the animal in order to keep the eye normally hydrated during anesthesia. The animal is then placed, in a supine position, on a heated platform (37 ° C) equipped with an integrated

system of electrodes, which allow the monitoring of heart rate and obtaining electrocardiographic signals. During transthoracic echocardiography the animals will be subjected to a low anesthesia regimen, 1% isoflurane, blown through a special mask, in order to keep the heart rate higher than or equal to 450 beats per minute. To optimize the visibility of the heart chambers, a heated ultrasound gel is applied to the shaved chest of the mouse. At the end of the experiment, the animals are removed from the bed and placed in a heated cage, where they are observed until awakening. Any abnormalities in the respiratory or heart rate, however, result in the immediate suspension of the echocardiographic session. The echocardiographic session is about 30 minutes.

13. PLIC study

The Progressione della Lesione Intimale Carotidea (PLIC) study is a large survey of the general population followed at the Center for the Study of Atherosclerosis, Bassini Hospital (Cinisello Balsamo, Milan, Italy). The study was approved by the Scientific Committee of the Università degli Studi di Milano (Cholesterol and Health: Education, Control and Knowledge – Studio CHECK ((SEFAP/Pr.0003) – reference number Fa-04-Feb-01). Each subject signed the informed consent and the study was conducted in accordance with the Declaration of Helsinki.

Of the 2141 of the PLIC study, PCSK9 genotype for p.Arg46Leu was available on 1919; of them 302 were selected for this analysis because free from statin and/or fibrates treatments and glucose lowering drugs. Of them 16 were carriers of the PCSK9 p.Arg46Leu mutation. The studied sub-population was representative of the entire cohort in term of clinical, pathological and pharmacological history (Kolmogorov-Smirnov non-parametric test, not shown).

Blood samples were collected for the determination of lipid profile and glucose level; CVD risk and the presence of the metabolic syndrome were assessed, as previously described.

Homeostasis Model Assessment of insulin resistance (HOMA-IR) as well as Homeostasis Model Assessment of insulin resistance of Beta cells function (HOMA-BC) indexes were derived from fasting insulin and glucose sera levels. HOMA-IR was calculated as follows: $= [(\text{fasting glucose (mmol/l)} \times \text{fasting insulin (pmol/l)}) / 405]$. HOMA-BC was calculated as follows: $= [(360 - \text{fasting insulin (pmol/l)}) / (\text{fasting glucose (mmol/l)} - 63)]$. HOMA Calculator (<https://www.dtu.ox.ac.uk/homacalculator/>) was used.

14. Statistical analysis

Data are expressed as mean + SEM. Comparisons within groups were made by using t-test for paired samples. Comparisons between groups were made by using t-test for independent samples. Analysis were made with Excel and Graphpad. For this study * $p < 0.05$, ** $p < 0.01$ and *** $p < 0.001$ were considered significant.

Results

Pcsk9 KO mice display an impaired glucose tolerance excluding insulin resistance

The effect of PCSK9 lack was initially evaluated on plasma glucose, mice were fed a SFD or a HFD diet for 20 weeks. Plasmatic glucose levels were exactly superimposable at baseline, following GTT, *Pcsk9 KO* mice have a significant delay of glucose clearance and higher glucose AUC, in both the SFD (Figure 1A and 1C) or the HFD (Figure 7B and 7D) groups after 20 weeks of diet. The observation that *Pcsk9 KO* mice presented glucose intolerance following GTT despite similar baseline glucose levels (following overnight fasting), prompted us to perform a fast and refeeding experiment to better understand possible differences in plasma glucose levels under physiological conditions. ITT was performed to exclude insulin resistance in WT and *Pcsk9 KO* mice, after a 4h fast. The animals were injected with insulin (0.2IU/kg body weight) intraperitoneally, the decrease in plasma glucose levels was similar in WT and *Pcsk9 KO* mice fed SFD (Figure 7E) or HFD (Figure 7F) for 20 weeks, thus excluding the presence of insulin resistance in the *Pcsk9* deficient state.

Pcsk9 deficiency affects pancreatic islet morphology and insulin secretion.

We then investigated whether *Pcsk9* deficiency affects insulin production and pancreatic β -cells function. Plasma insulin and C-peptide levels were significantly decreased in *Pcsk9 KO* mice compared to WT littermates (Figure 8A). After overnight fasting animals were at libitum refeed for 4h, a reduced increment in plasma insulin levels in *Pcsk9 KO* mice was observed versus WT mice (Figure 8B). We next evaluated whether the phenotype observed in *Pcsk9 KO* mice could also be the consequence of altered incretins production even if the effect was observed after both refeeding and intraperitoneal 0-5 min experiment. GLP1 and GIP plasma levels in fasted and refeed conditions were similar in WT and *Pcsk9 KO* mice (Figure 8C and 8D). We then wonder if the effect was due to decrease insulin production or release, indeed, in contrast to reduced circulating levels, we observed a significant increase of pancreatic insulin content in *Pcsk9 KO* mice compared to WT mice (Figure 9A and 9B). These data suggest that *Pcsk9* mutant *KO* mice might have a defective insulin secretion, which could lead to an increased accumulation in beta cells. We, therefore, studied pancreatic islet morphology and observed that islets from *Pcsk9 KO* mice showed larger islet size (Figure 9C). These findings were paralleled by a different islet size distribution between *Pcsk9 KO* and WT mice (Figure 9D).

The reduced LDLr degradation mediates cholesterol accumulation and pancreatic islet dysfunction

Cholesterol is really important for pancreatic functionality, particularly for membrane formation and insulin vesicle trafficking. For this reason, the LDLr is expressed on high levels also on the surface of pancreatic β cells where it plays a key role in the uptake of LDL. Increased beta-cell cholesterol levels were associated with decreased insulin secretion. The analysis of pancreatic sections from WT and *Pcsk9 KO* mice showed that LDLr is present mainly in β cells (Figure 10A) and, as detected by Western Blot analysis (Figure 10B and 10C) its expression is increased in pancreatic islets isolated from *Pcsk9 KO* animals compared to WT mice.

We then investigated how the increased expression of LDLr might trigger changes in pancreatic islets lipid content. As expected, *Pcsk9 KO* mice islets presented higher cholesterol esters levels compared to WT islets, together with significant changes in fatty acid lipid profile (Figure 10D). Lipid accumulation was paralleled by the downregulation of genes involved in cholesterol biosynthesis and uptake, including HMGCoA-R and LDLR, the increase of the expression of ACAT1, which promotes cholesterol esterification (Figure 10E).

To further test the hypothesis that the observed phenotype in *Pcsk9 KO* mice could be dependent on the impact on LDLr, GTT and ITT were evaluated in *Pcsk9/LDLr* DKO mice and *LDLr* KO animals. The delayed glucose response observed in *Pcsk9* deficient conditions was not observed in SFD fed *Pcsk9/LDLr* DKO mice and, indeed, GTT and ITT curves were superimposable between the two animal groups (Figure 11A and 11B) and similar to those observed in WT animals.

Moreover, DKO mice and *LDLr* KO littermates have a similar pancreatic islets histology (Figure 11C and 11D). Indicating that the PCSK9/LDLr axis could explain the phenotype observed in *Pcsk9* deficient animals.

Beta-cell functionality is not affected in Pcsk9 liver selective KO mice

PCSK9 is mostly produced by the liver but is also produced by a broad range of organs including the brain, the intestine, the lung, and the pancreas (Figure 12A). To investigate the role of circulating, liver-derived PCSK9 (Seidah et al., 2003), from that of locally produced

protein, we tested glucose metabolism in SFD fed liver-specific *Pcsk9* KO mice. PCSK9 mRNA expression was almost abolished in the liver from *AlbCre⁺/Pcsk9LoxP/LoxP* while mRNA and protein expression in the pancreas was similar between *AlbCre⁺/Pcsk9LoxP/LoxP* and *AlbCre⁻/Pcsk9LoxP/LoxP* mice (Figure 12B), confirming the liver specificity of the KO model. *AlbCre⁻/Pcsk9LoxP/LoxP* mice presented similar GTT and ITT curves (Figure 12C and 12D). Pancreatic β cells morphology (Figure 12E) and pancreatic insulin levels were similar in the two animal models (133.6 ± 47.16 ng/mg of tissue vs 119.1 ± 43.2 ng/mg of tissue for *AlbCre⁺/Pcsk9LoxP/LoxP* and *AlbCre⁻/Pcsk9LoxP/LoxP* mice; $p=0.629$). These data suggest that circulating, liver-derived PCSK9 does not impact LDLR expression in the pancreas.

Impact of genetic polymorphism of PCSK9 in systemic metabolism and cardiac phenotype

To further extend these data in humans, we focus our attention on the impact of the *PCSK9* 46L loss of function (LOF) polymorphism on circulating lipid levels, cardiac parameters the homeostasis model assessment: insulin resistance (HOMA-IR) and beta-cell function (HOMA-BC). HOMA-BC but not HOMA-IR was significantly lower in carriers of the *PCSK9* 46L variant compared to carriers of the wild type allele (Fig 13A and 13B) indicating that under PCSK9 deficient conditions impaired β cells functionality occurs also in man. These data suggest confirm a relationship between PCSK9 deficiency and insulin secretion. To fully characterize the cardiovascular impact of the LOF on these subjects a cardiac characterization has been performed. The left ventricular mass has been investigated and the subject bringing a loss of function polymorphism for PCSK9 displays an increase LVM index compared to controls (Figure 13C). No differences were observed in the ejection fraction between groups (Figure 13D). These data suggest a compensatory mechanism to support cardiac functionality in tissue with a metabolic alteration.

Mice model KO for Pcsk9 display a heart failure with a preserved ejection fraction

To investigate whether PCSK9 impacts lipid and lipoprotein heart metabolism and cardiac function, we wonder if cardiac morphology in *Pcsk9* KO was somehow affected compared to wild-type (WT) male mice fed for 20 weeks with a standard fat diet (SFD). Electrocardiographic analysis (Figure 14A) was performed and showed that the heart of *Pcsk9* KO mice was presented increased thickness of the left ventricular posterior wall

(LVPW) under systole and diastole as compared to WT mice (Figure 14B and 14C). This observation was coupled to increased relative wall thickness (Figure 14D) despite heart to body weight ratio (Figure 14E) and ejection fraction (Figure 14F) similar to that of WT mice. To evaluate whether this profile results in impaired cardiac functionality in *Pcsk9* KO mice, exercise intolerance and running resistance in fatigue tests were performed. *Pcsk9* KO mice presented a significant reduction compared to WT mice in the running distance and the running time observed in the exhaustion test (Figure 15A and 15B).

This was not the consequence of muscle impairment as a similar performance between *Pcsk9* KO and WT mice were observed in the forelimb grip test (Figure 15C). These data indicate that *Pcsk9* KO mice present a profile suggestive of heart failure with preserved ejection fraction (HFpEF).

Mitochondrial impairment and altered cardiac metabolism in PCSK9 deficient mice.

The cardiac phenotype presented above and previous observation showing that *Pcsk9* KO mice present lipid accumulation in peripheral tissues, prompted us to further evaluate the impact of PCSK9 deficiency on cardiac lipid metabolism and its relevance for heart energetic demand.

We first evaluated tissue oxygen consumption as an index of oxidative phosphorylation (which, in contractile cells, is mainly dependent on fatty acid oxidation) on freshly isolated hearts from *Pcsk9* KO mice and WT littermates. *Pcsk9* KO hearts exhibited a significant reduction in oxygen consumption rate (OCR) compared to control mice under maximal coupled and uncoupled respiration (Figure 16A). This finding prompted to test whether ATP production is affected. Both ATP levels (Figure 16B) and the total energy charge (Figure 16C) were reduced in the heart of *Pcsk9* KO mice compared to WT littermates. Moreover, a detailed proteomic analysis showed that the expression of several mitochondrial proteins is affected in *Pcsk9* KO (Figure 17A), including that of key structural components of the electron transport chain complexes (Figure 17B). This finding was further confirmed by western blot analysis of a set of proteins representative of each mitochondrial complex, including NADH Ubiquinone Oxidoreductase Subunit B8 (Ndufb8 - Complex I), Succinate Dehydrogenase Complex Iron-Sulfur Subunit B (Sdhb - Complex II), and Ubiquinol-Cytochrome C Reductase Core Protein 2 (Uqcrc2 - Complex IV) that were significant were reduced in the heart of *Pcsk9* KO mice (Figure 17C and Figure 17D) compared to WT littermates. No significant differences were observed in the expression of Mitochondrially

Encoded Cytochrome C Oxidase I (mtCO1 - complex III) and ATP synthase F1 subunit alpha (Atp5a1 - Complex V). In parallel with this finding, also, mitochondrial DNA copy number for COX2 and ND1 was reduced (Figure 17E) suggesting that mitochondrial function and content are affected in the heart of *Pcsk9* KO mice. We next asked whether this profile reflects into altered cardiac metabolism; combined metabolomic, proteomic, and lipidomic profile analysis in the heart of *Pcsk9* KO and wild type mice (Figure 18A) revealed that impaired mitochondrial activity results from impaired fatty acid oxidation, as indicated by FAO proteome pathway analysis (Figure 18A), reduced protein expression of Sterol Carrier Protein 2 (SCP2), Enoyl-CoA Hydratase, Short Chain 1 (ECHS1) (Figure 18A) coupled to the accumulation of intermediate chain C8 and C10 fatty acids (Figure 18A) and decreased TCA cycle flux (Figure 18A) as indicated by the reduced levels of TCA metabolites and enzymes catabolizing key enzymatic reactions. This metabolic deficient status is partly compensated by increased anaerobic glycolysis as suggested by a reduced level of Glucose-6P (Figure 18A) coupled to increased glycogen degradation (Figure 18A) and increased lactate release in the bloodstream (Figure 18A). Augmented glycolytic flux, not only supports energetic demand but also contributes to the PP pathway which could be relevant for anabolic reactions involved in left ventricular wall thickening. Still, as shown in Figure 18A this is not enough to support heart energy demand thus resulting in reduced energy charge. Ingenuity Pathway analysis supports the reduction of the main mitochondrial metabolic pathways with increased activity of pathway for glucose supply as glycogen degradation (Figure 18B). To further investigate mitochondrial dysfunction a gene expression was performed and a significant reduction of Hydroxyacyl-CoA Dehydrogenase Trifunctional Multienzyme Complex Subunit Beta (HADHB) and Acyl-CoA Dehydrogenase Long Chain (ACADL), genes involved in beta-oxidation, (Figure 18C) and an increased expression of Parkin, gene involved in mitochondrial fission, (Figure 18D) was observed.

PCSK9 deficiency leads to lipid accumulation through LDLr and CD36.

To get further insights on molecular mechanisms explaining the phenotype observed, we investigated the expression of key PCSK9 targets in the heart. Both the expression of LDLr and CD36 were increased in *Pcsk9* KO mice compared to WT littermates (Fig 19A to 19D). This profile is associated with increased total cholesterol (Fig 19E) with total triglycerides content being similar (Fig 19F). The observation of increased cholesterol levels coupled to

increased LDLr receptor expression in the heart of *Pcsk9* KO mice points to a possible role of LDLr in driving increased cardiac lipid accumulation. To test this hypothesis, we characterized heart function, morphology, and metabolism and in mice lacking both *Pcsk9* and *LDLr* (DKO).

DKO mice presented a significant reduction compared to *LDLr* KO mice in the running distance and the running time observed in the exhaustion test (fig 20A to 20B) which was independent of muscular dysfunction as the forelimb grip test was not different (fig 20C). The echocardiographic analysis showed that DKO mice presented a significant increase in left ventricular thickening during systole (Fig 20D) without alterations in Ejection Fraction (Fig 20E) and the Relative Wall Thickness (RWT) was slightly increased. The metabolic analysis showed that ATP levels and energy charge were still significantly reduced in DKO mice as compared to *LDLr* KO mice (Fig 21A) This profile is in agreement with the reduced flux of TCA coupled to mitochondrial metabolic pathway dysfunction (Fig 22A) in the heart and increased anaerobic glycolysis (Figure 22B) with higher plasmatic levels of lactate (Figure 22C), as side metabolites observed in DKO compared to *LDLr* KO mice.

Circulating PCSK9 does not impact heart metabolism.

In both humans and mice, the circulating part of PCSK9 is almost entirely produced by the liver and then released into the bloodstream. This observation justifies the use of mice models *AlbCre⁺/Pcsk9LoxP/LoxP* as a model to mimic the effect of the pharmacological treatment obtained with the use of monoclonal antibodies. PCSK9 is produced by different tissue but is very low expressed in the heart both Atrial Appendage and Left Ventricles (Figure 12A). The model is then used to test whether the cardiac impact of PCSK9 lack was a consequence of the circulating part of the protein rather than the paracrine effect of PCSK9 produced by cardiomyocytes, aorta, endothelial cells, or epicardial fat. Indeed, epicardial fat, as PCSK9 producer, is accumulating more in human subjects bringing a loss of function polymorphism for PCSK9. The initial characterization of functional impairment due to cardiac dysfunction suggests that *AlbCre⁺/Pcsk9LoxP/LoxP* mice don't have any difference in running distance (Figure 23A) and time (Figure 23B) compared to *AlbCre⁻/Pcsk9LoxP/LoxP*. The observed phenotype was independent of muscular inefficiency as supported by the forelimb grip test results (Figure 23C). This functional experiment partially excludes the development of the cardiac phenotype observed in the full KO. To confirm this observation, the cardiac morphology was investigated by echocardiographic analysis. As

expected no differences were highlighted in left ventricular thickness during systole (Figure 23D) and ejection fraction (Figure 23E).

Discussion

Several trials showed that PCSK9 inhibition reduces LDL-C levels and CVD, by a mechanism involving increased hepatic LDLr expression. Mendelian randomization studies have confirmed that PCSK9 loss of function variants associate with lower LDL-C but also with higher plasma glucose levels and increased risk of developing type 2 diabetes (Ference et al., 2016; Schmidt et al., 2017). The latter observation suggests that PCSK9 might affect the physiology of other pathways other than those involved in LDL uptake in the liver. Indeed, although the liver is the major producer of PCSK9 and its main target, PCSK9 is produced also by other tissues and therefore affects other biological responses.

On this premise, we investigated how PCSK9, by regulating its main targets, including LDLr and CD36 expression, might affect lipid metabolism in organs other than the liver and how this could affect tissue physiology and systemic metabolism. we described in experimental models the PCSK9 targets LDLr in pancreatic islets and LDLr and CD36 cardiac tissue thus modulating their function. We initially focused our attention on pancreatic functionality. Intracellular cholesterol accumulation in pancreatic beta cells was associated with increased cellular toxicity with the consequent glucose intolerance and reduced insulin secretion. Cholesterol uptake in β cells mainly occurs following LDL-LDLr interaction. We showed here that *Pcsk9* KO mice present with impaired glucose tolerance, independent of the type of diet used (high fat or standard fat) but preserved insulin response. To further explain this observation, we measured insulin and c-peptide levels under fasting conditions and after a 4h of ad libitum refeeding, showing that they were both significantly reduced in *Pcsk9* KO mice. Moreover, PCSK9 KO mice presented major alterations in pancreatic morphology with larger pancreatic islets accumulating insulin and cholesterol esters paralleled by increased LDLr expression. Furthermore, the expression of genes involved in cholesterol metabolism suggests that pancreatic beta cells are activating machinery to esterify, detoxify, and removing free cholesterol promoting cholesterol efflux. The presence of impaired β cell function in *Pcsk9* KO mice was further confirmed in humans, where subjects with a PCSK9 LOF variant presented decreased HOMA-BC but not HOMA-IR compared to age and sex-matched carriers of the common allele. We then aimed to confirm that this phenotype was dependent on LDL-r expression and therefore characterized glucose and insulin response in *Pcsk9/LDLr* Double KO mice. No differences were observed in GTT and ITT response compared to control mice, thus indicating that the phenotype previously observed was a consequence of the regulation of PCSK9 on LDLr expression. To further confirm this observation a detailed analysis on pancreatic islet morphology was performed a

morphological analysis and indicated no major differences between WT islets and islets of both *LDLr* KO and *Pcsk9/LDLr* Double KO.

Next, we aimed at investigating whether liver-derived circulating PCSK9 is involved in the control of beta-cell physiology. To this aim we used a liver selective KO model, which presents undetectable PCSK9 in the circulating while maintains PCSK9 production in other tissues including the pancreas. Liver selective *Pcsk9* KO mice presented plasma and pancreatic insulin levels, LDLr expression as well as pancreatic islets cholesterol esters levels similar to those of control mice; accordingly, also glucose tolerance and insulin tolerance did not differ. These data indicate that circulating PCSK9 does not affect LDLr expression in the pancreas. This observation points to the role of locally produced PCSK9 in the pancreas as the main cause of glucose intolerance phenotype. As this model mimics the phenotype of patients treated with anti-PCSK9 antibodies, where PCSK9 is sequestered from the circulation but is still produced in extrahepatic tissues, our findings reassure about the safety of monoclonal antibodies being neutral in affecting the risk of new-onset diabetes. We next focused on investigating a potential role for PCSK9 in regulating heart lipid demand. Unlike the liver, the heart is not able to synthesize a high amount of fatty acids (FA), and therefore lipids demand is primarily supported by the uptake from the circulation. We first characterized the cardiac functionality of *Pcsk9* mice compared to WT littermates and following echocardiographic analysis showed that *Pcsk9* KO mice present an increased thickness of the left ventricular posterior wall with no differences in ejection fraction. This phenotype suggests that PCSK9 KO failing hearts can initially compensate for their failure to sustain the energetic demand. This phenotype is typical of heart failure with preserved ejection fraction where cardiomyocytes switch their metabolism from fatty acids, oxidation into mitochondria, to glycolysis and ketone bodies (Doenst et al., 2013). This, however, is not enough to support heart function and indeed *Pcsk9* KO mice presented a significant reduction in the running distance and the running time observed in the exhaustion test compared to WT mice; a finding which was not the consequence of muscle impairment. Of note, the heart as, contracting tissue, is normally highly dependent on fatty acid oxidation and oxygen consumption. For this reason, we evaluated tissue oxygen consumption on freshly isolated hearts from *Pcsk9* KO mice and WT littermates and observed that *Pcsk9* KO has a significant reduction of maximum coupled and uncoupled respiration. Together with this observation the total energy charge and ATP production were reduced probably as a consequence of major mitochondrial dysfunction. Indeed, following shotgun proteomic profiling, we observed a significant reduction of the ETC and the principal complexes

proteins. This mitochondrial impairment was confirmed also by the reduction in mitochondrial mass. We next asked whether this profile translates into altered cardiac metabolism; combined metabolomic, proteomic, and lipidomic analyses of the heart of *Pcsk9* KO and wild type mice revealed that impaired mitochondrial activity probably is the consequence of impaired fatty acid oxidation and decreased TCA cycle flux as indicated by the reduced levels of TCA metabolites and enzymes catabolizing key enzymatic reactions. This metabolic deficient status is partly compensated by increased anaerobic glycolysis coupled to increased glycogen degradation and anaerobic glycolysis. Augmented glycolytic flux, not only supports energetic demand but also contributes to the PP pathway which could be relevant for anabolic reactions involved in left ventricular wall thickening.

To get further insights on molecular mechanisms explaining the phenotype observed, we investigated the expression of key PCSK9 targets in the heart showing that both LDLR and CD36 expression is increased together with cholesterol accumulating in cardiomyocytes that might contribute to impair mitochondrial function, thus affecting heart morphology and contractile activity. The observation of increased cholesterol levels coupled to increased LDLr receptor expression in the heart of *Pcsk9* KO mice pointed to a possible role of LDLr in driving increased cardiac lipid accumulation. To test this hypothesis, we characterized heart function, morphology, and metabolism and in mice lacking both *Pcsk9* and *LDLr* (DKO).

On the contrary of what was observed at the pancreatic level DKO mice still presented a significant reduction compared to *LDLr* KO mice in the running distance and the running time observed in the exhaustion test which was independent of muscular dysfunction as the forelimb grip test was not different. These data indicate that the impact of PCSK9 on heart function is not related to the modulation of LDLr expression. Indeed, the echocardiographic analysis showed that DKO mice presented a significant increase in left ventricular thickening during systole without alterations in Ejection Fraction and the metabolic status was suggesting an energy depletion. This profile is in agreement with the reduced flux of TCA coupled to mitochondrial metabolic pathway dysfunction in the heart and increased plasma levels of lactate, as side metabolites of increase anaerobic glycolysis, observed in DKO compared to *LDLr* KO mice. Of note data obtained in the liver, selective PCSK9 KO mice excluded a role for circulating PCSK9 in the phenotype observed. Genetic data in humans suggested that lifelong reduction of both circulating and locally produced PCSK9 results in a deteriorated heart profile. Indeed, 46L subjects present increased left ventricular mass index with no changes in both Ejection Fraction and Skeletal Muscle Mass. These findings

support the impact of metabolic changes on cardiac function. Heart Failure is known to be the natural progression of the diabetic disease as a result of peripheral insulin resistance (Riehle et al., 2016), which however was previously ruled out in these subjects (Da Dalt et al., 2019), further confirming the role of lipid accumulation within the tissue thus contributing to cardiomyocyte impairment.

Taken together our results support the safety of anti-PCSK9 monoclonal Antibodies as well as that of liver selective PCSK9 gene silencing. Indeed, data from clinical trials didn't show any increased incidence of new-onset diabetes compared to the placebo group. Similarly, available data on monoclonal antibody treatment, did not affect Heart Failure progression (Sabatine et al., 2017). This observation should be interpreted with caution as LDL-C reduction translates into fewer ischemic heart events thus slowing down heart function deterioration. As such is it reasonable to separate the effects of global PCSK9 deficiency where HFpEF is observed versus those of circulating PCSK9 deficiency that excludes any impact of heart function. This further reinforces the safety of anti-PCSK9 therapies which target circulating (monoclonal antibodies) or liver selectively produced (siRNA) PCSK9.

Figures

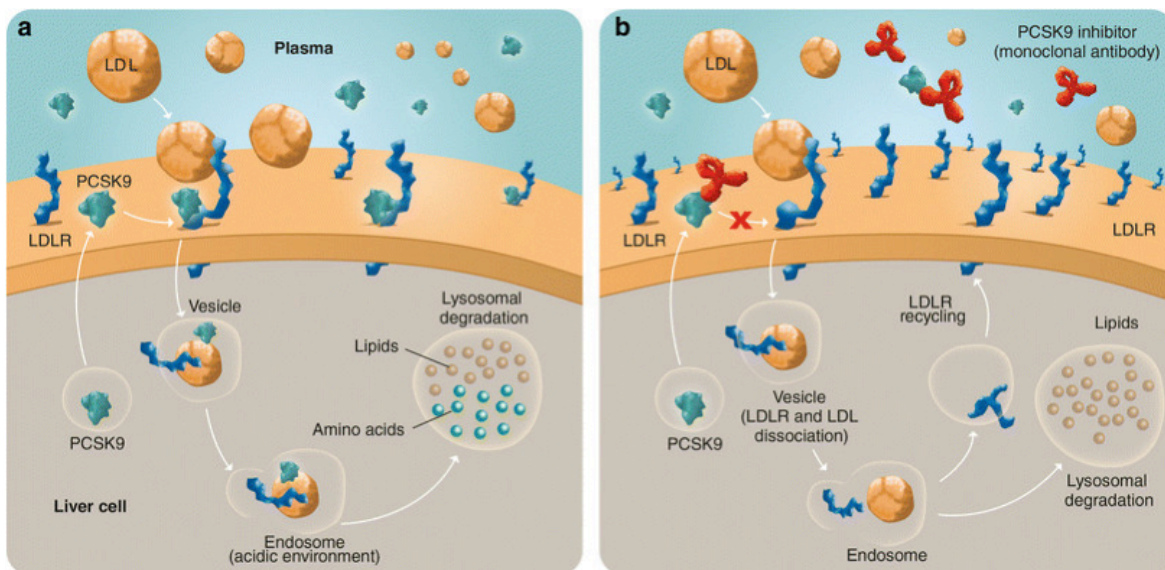


Figure 1 LDLr turnover. (A) PCSK9 binds LDLr-LDL complex, promoting the LDLr internalization in the endosome, thus leading to its degradation. (B) Monoclonal Antibodies takes away PCSK9 and permits the recycle of LDLr to the cell surface (Krahenbuhl et al., 2016).

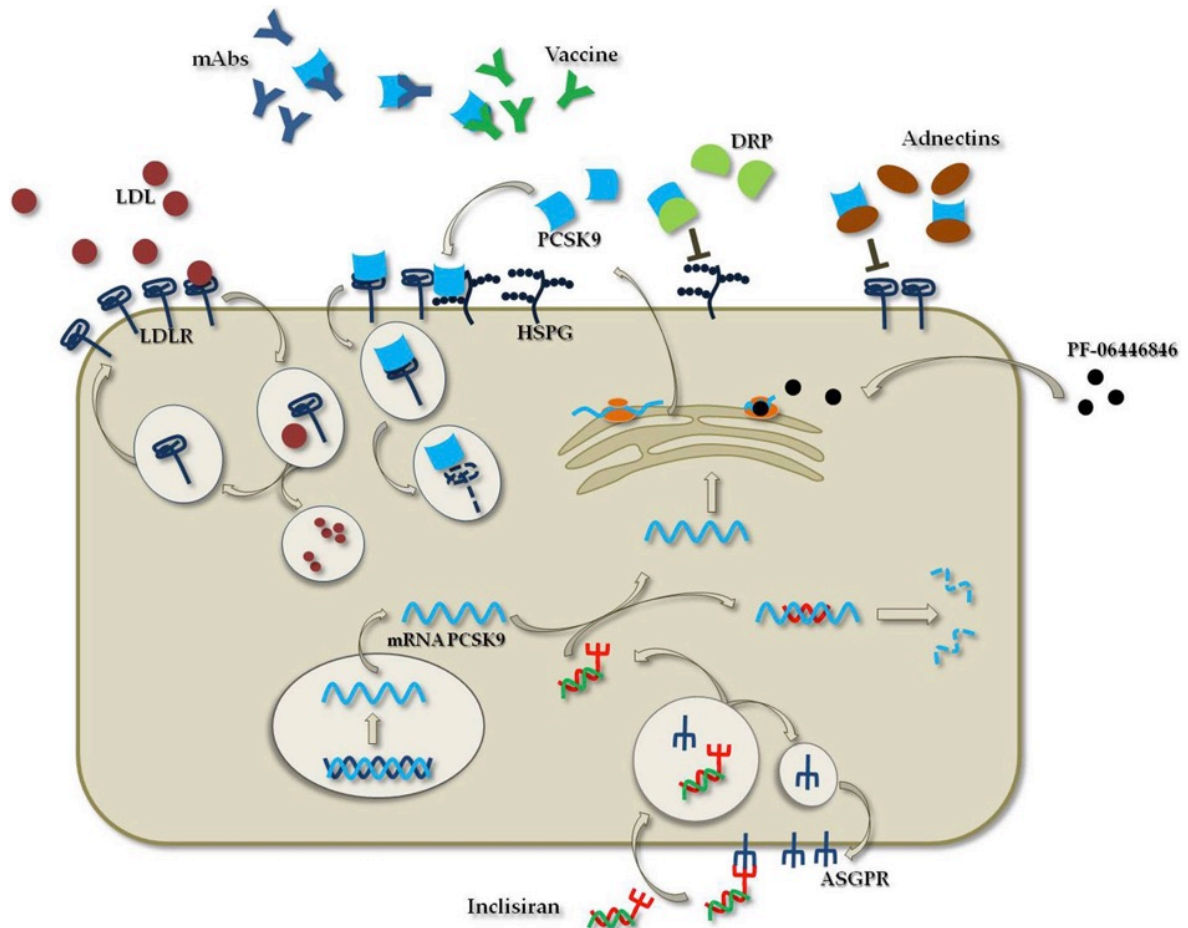


Figure 2 Anti-PCSK9 pharmacological treatment. (A) the LDLr-LDL complex is normally internalized and the LDLr is recycled on the cell membrane (B) mAb takes away PCSK9 (C) Vaccine stimulates Ab production against PCSK9 (D and E) DRP and Adnectines prevent the binding of PCSK9 to the LDLr (F) PF-06446846 binding the RNA-ribosome complex prevent PCSK9 production (G) Inclisiran, targeted to the liver through the sialic acids bind the RNA inhibiting PCSK9 production (Catapano et al., 2020).

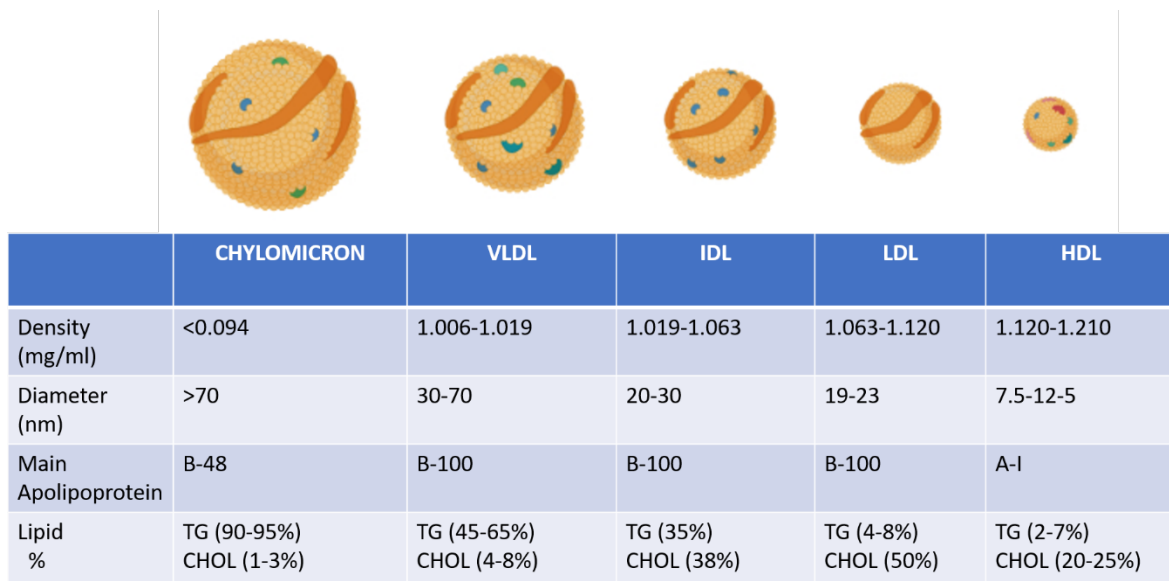


Figure 3 Lipoprotein composition and classes. Lipoproteins can be classified based on their density, diameter or lipid composition. Chylomicrons have the higher dimensions and they are composed predominantly by TGs, as for VLDL particles, at the hepatic level. The extraction of TGs from VLDLs leads to the production of IDLs, lipoproteins enriched in cholesterol. HDLs are the smaller lipoproteins and they are particularly enriched of proteins, that represent the 45-55% of the molecule. [Created with Biorender]

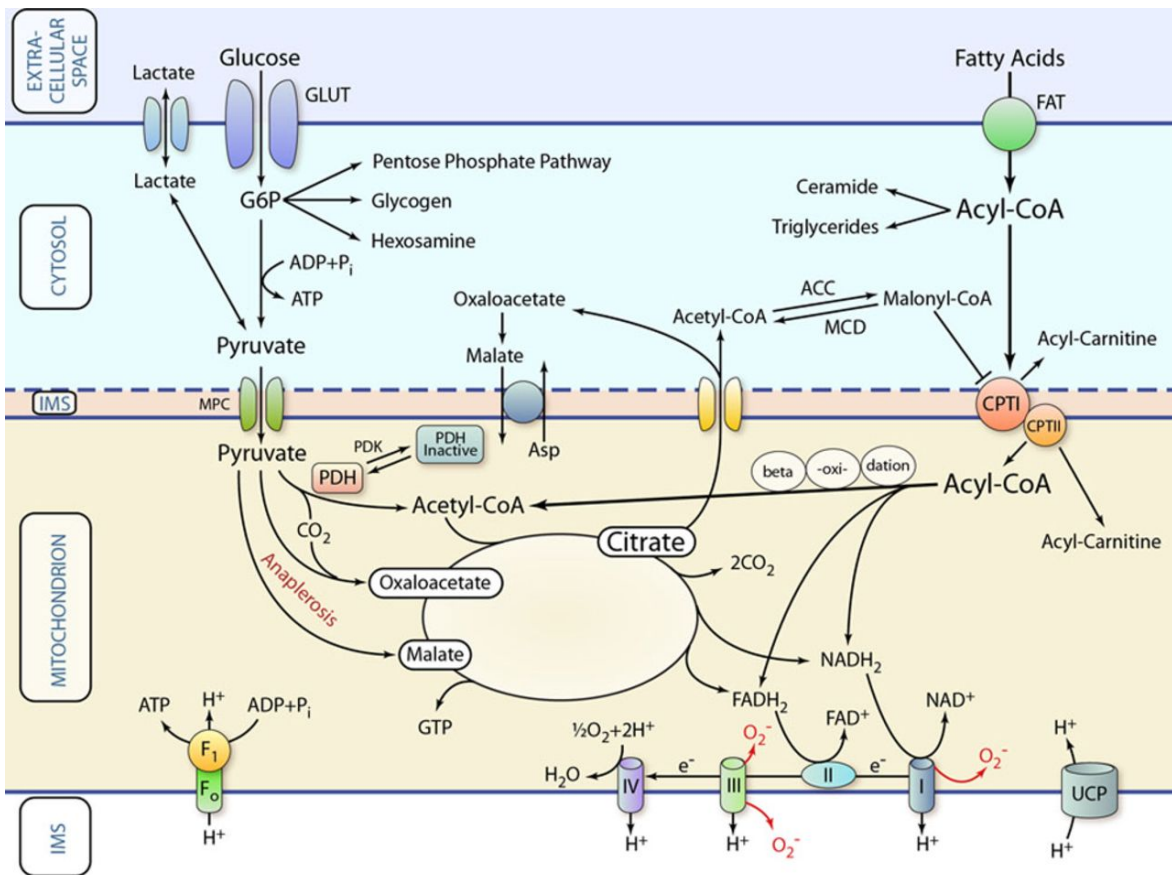


Figure 4 Cellular metabolic pathways. Aerobic metabolic pathways are schematized to highlight the 3 principal pathways as glycolysis, fatty acids oxidation and Krebs cycle. Glycolysis use glucose to produce pyruvate that is internalized in the mitochondria as Acetyl-CoA to be used as substrate for Krebs Cycle. Every cycle of fatty acid oxidation removes 2 carbon atoms from a Acyl-CoA to supply the Krebs cycle. All the NADH₂ and FADH₂ produced from metabolic pathways is used from ETC for ATP production (Doenst et al., 2013).

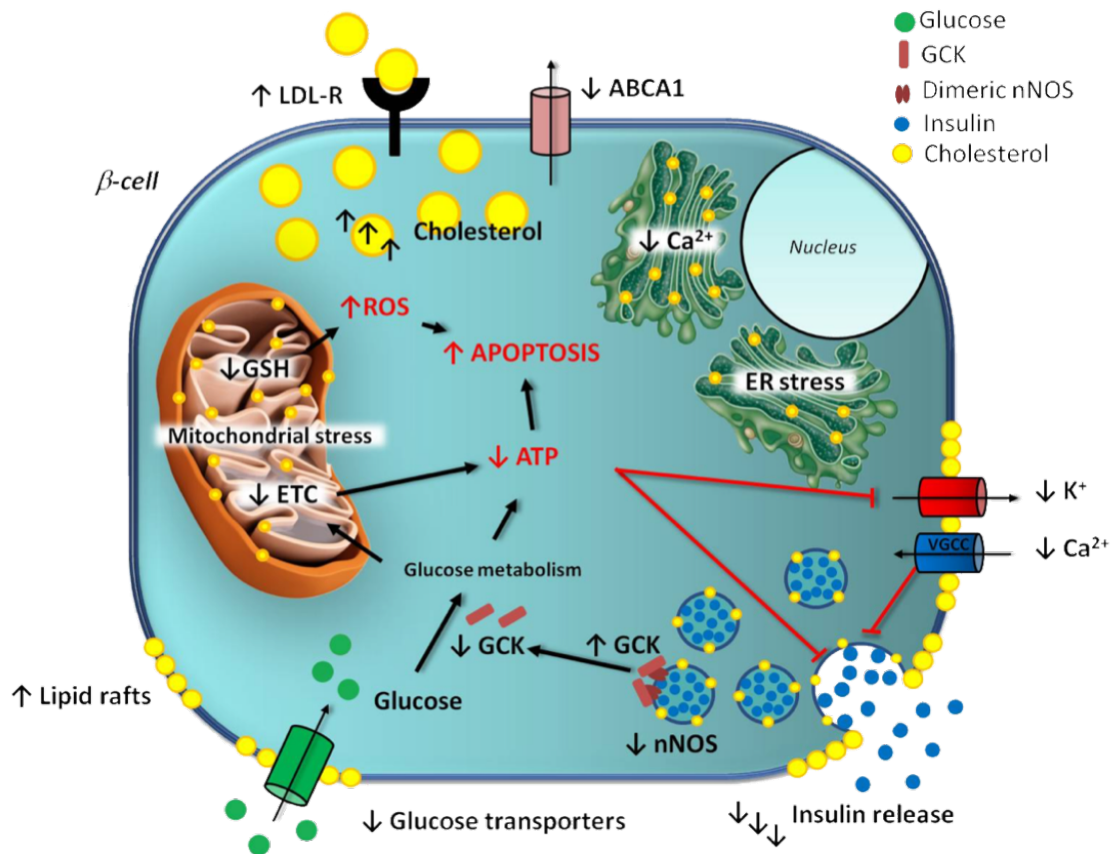


Figure 5 Cholesterol and pancreatic beta-cell functionality. Cholesterol accumulating in lipid droplets and as free-cholesterol in cellular membrane can alter membrane fluidity; this results in reduced glucose transporter membrane levels, increased glucokinase (GCK) retention in insulin granules and alteration of spatial organization of L-type voltage-gated Ca²⁺ channels (VGCC) and K⁺ ATP channels. As a consequence, insulin secretion decreases. Cholesterol can affect ER functionality leading to depletion of calcium store, thus increasing ER stress (Perego et al., 2019).

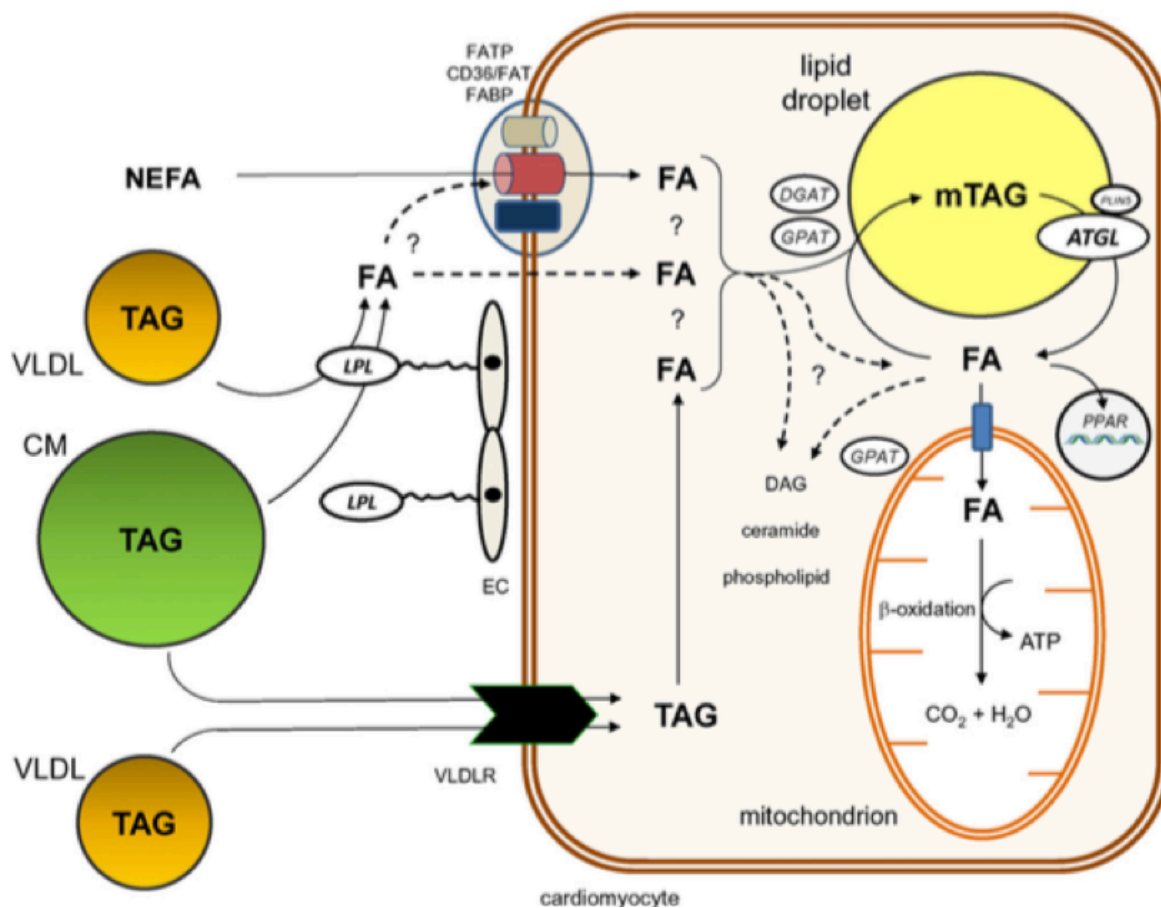


Figure 6 Cardiac lipotoxicity. Fatty acids are internalized via VLDLR or CD36 and are stored into lipid droplets as Diacylglycerol, Triacylglycerol and ceramides. The accumulation of this lipotoxic mediators may affect cardiomyocytes functionality leading to cell death (Evans et al., 2016).

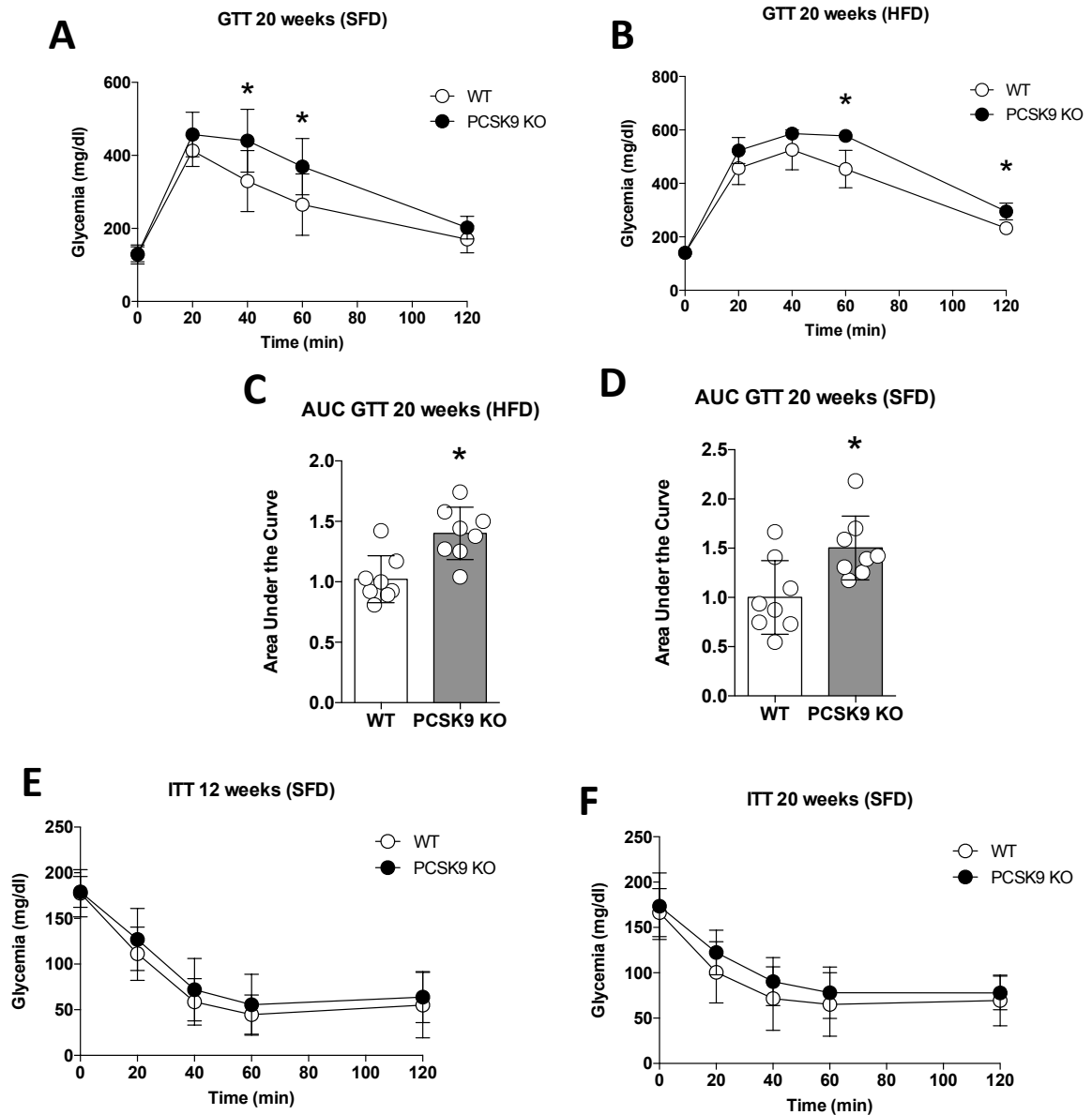


Figure 7 *Pcsk9* KO Glycaemic profile. Glucose tolerance test were performed at 20 weeks of diet for both animal at SFD (A) and HFD (B). The glycaemic profile is expressed as Area Under the Curve (C and D). Insulin Tolerance test were performed for KO and WT mice at 20 weeks of diet for both diets SFD (E) and HFD (F). (* $p < 0.05$) (8 animals for each group)

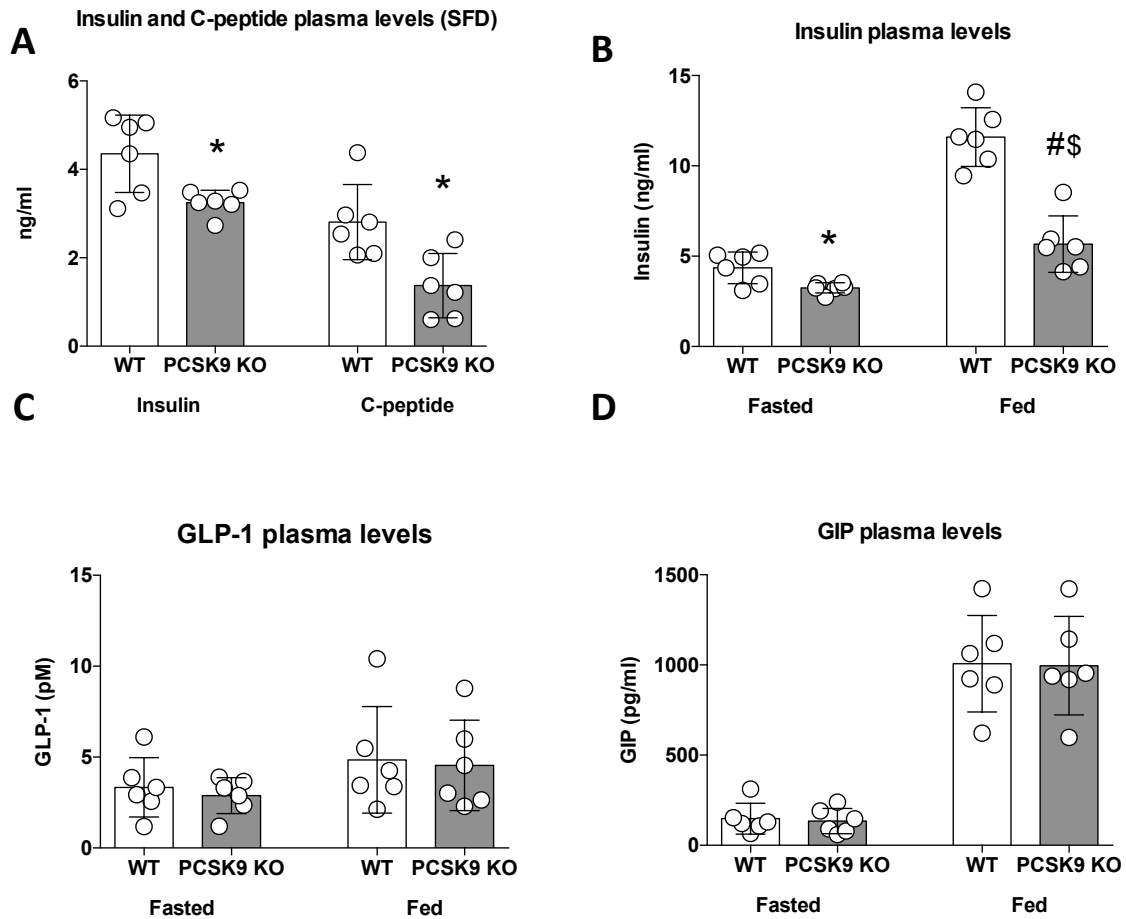


Figure 8 Insulin and Incretins production. Plasmatic levels of both insulin and C-peptide were measured at fasting condition for both *Pcsk9* KO mice and WT (A). A fast and refeed test were performed and insulin levels were measured (B). Incretins levels GLP-1 and GIP were measured at basal condition and after 4h of refeed (C and D). (* $p < 0.05$ wt vs KO, # vs. WT fed, and \$vs. *Pcsk9* KO fasted) (6 animals for each group).

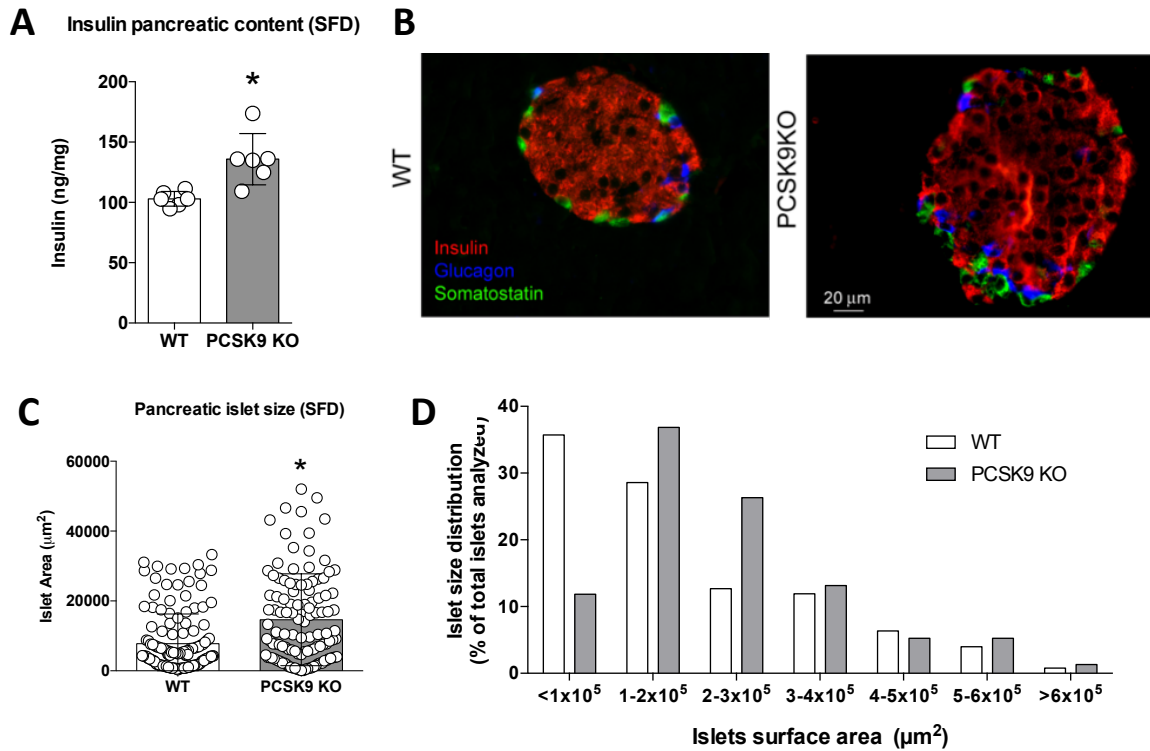


Figure 9 Pancreatic insulin and morphology. Insulin was dosed in the pancreas of both *Pcsk9* KO mice and WT (A). A confocal microscopy was performed to study islet morphology and insulin content (B). Pancreatic islet size was measured (C) and stratified according their dimension (D) (* $p < 0.05$ wt vs KO) (6 animals for each group).

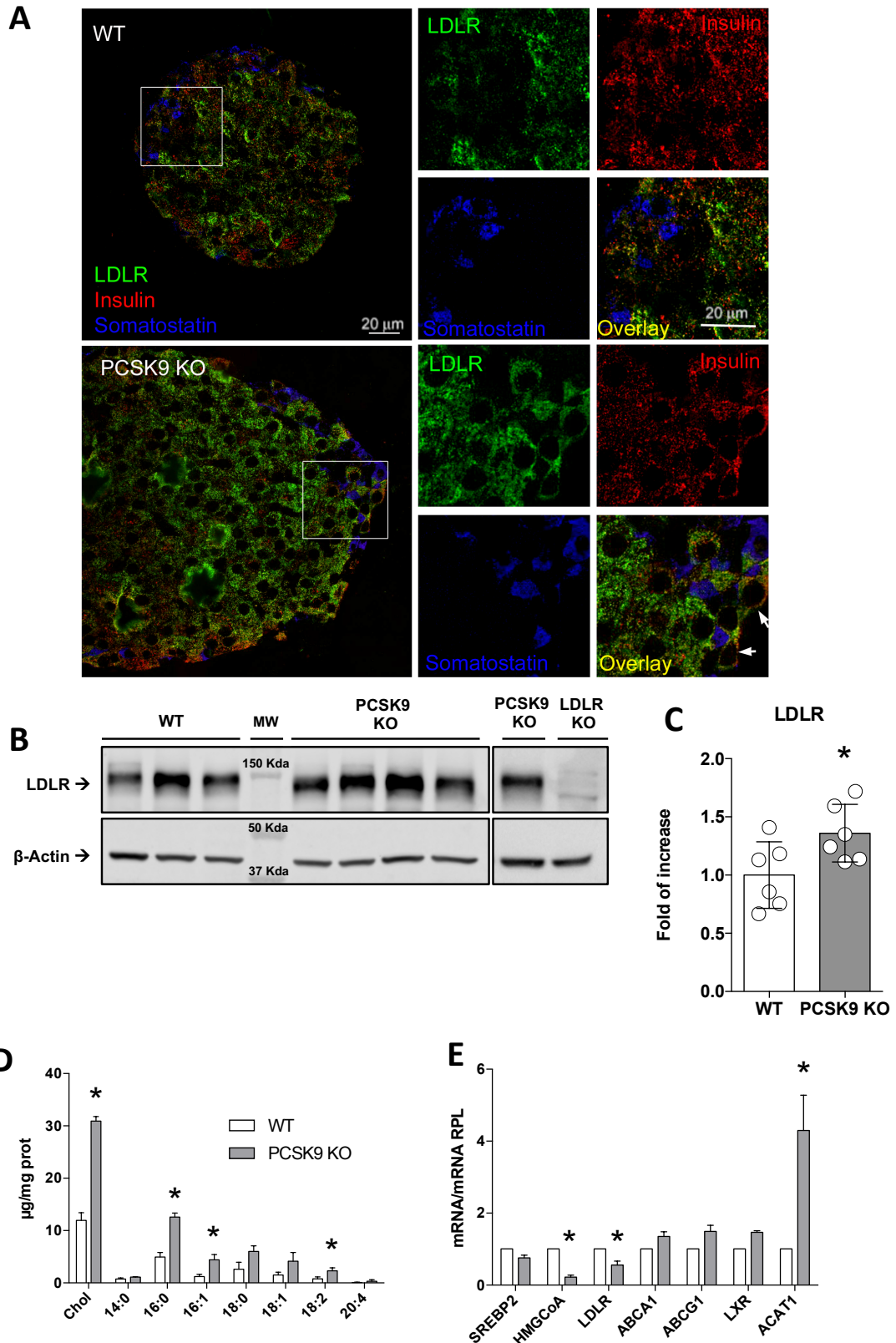


Figure 10 *LDLr expression and cholesterol metabolism.* A confocal microscopy was performed to study islet morphology and LDLr expression (A). Pancreatic islets were isolated and LDLr expression was assessed with Western Blot analysis (B and C). Lipid profiles were performed (D) and gene expression of cholesterol metabolic genes was investigated (E) (* $p < 0.05$ wt vs KO) (6 animals for each group).

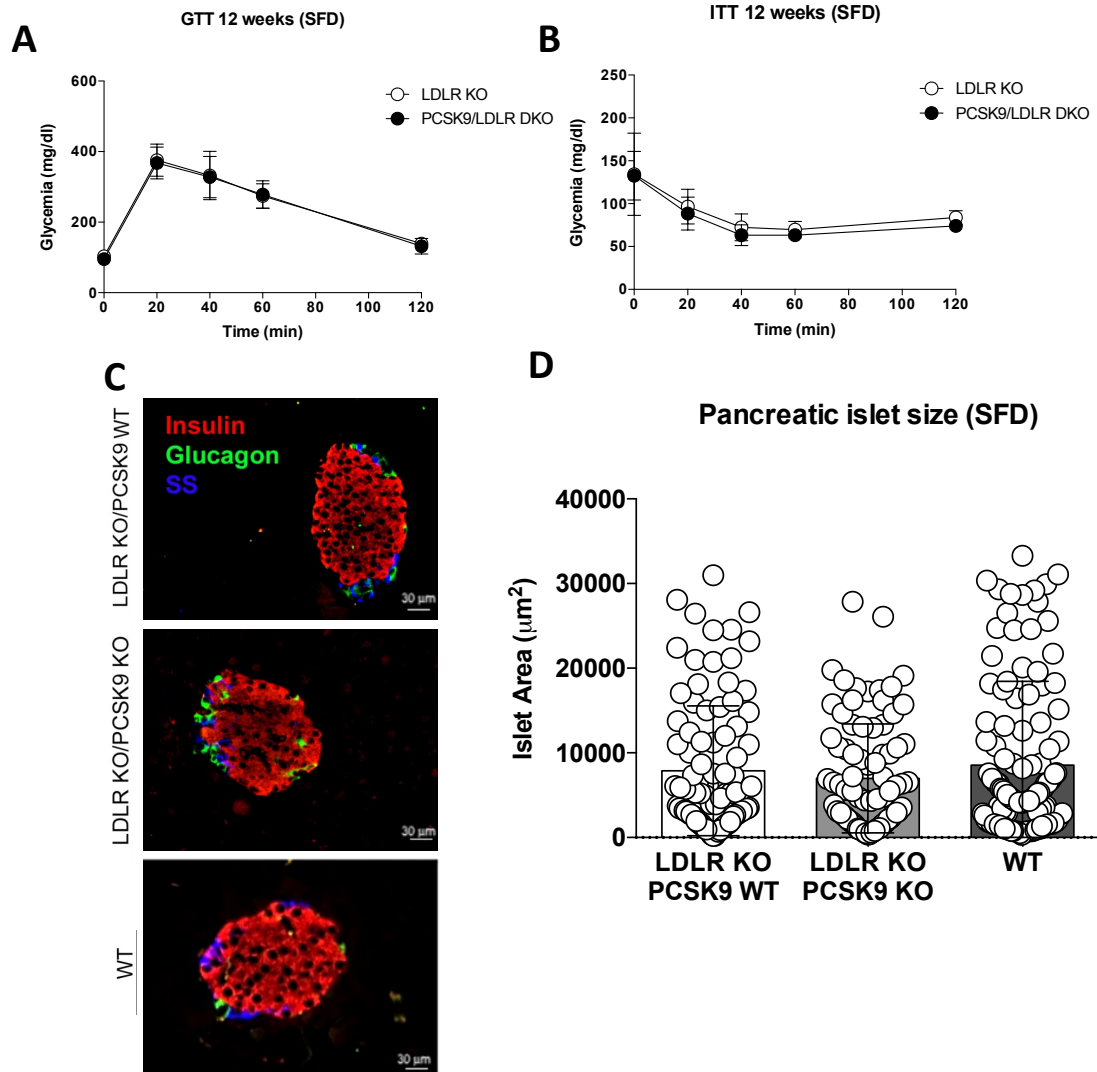


Figure 11 *LDLr* double *KO* animals glucose metabolism. Glucose tolerance test (A) and Insulin Tolerance Test (B) were performed in *LDLr* *KO* mice and *LDLr* *KO/ Pcsk9* *KO* mice. Islet morphology (C) and size were investigated (D) (5 animals for each group).

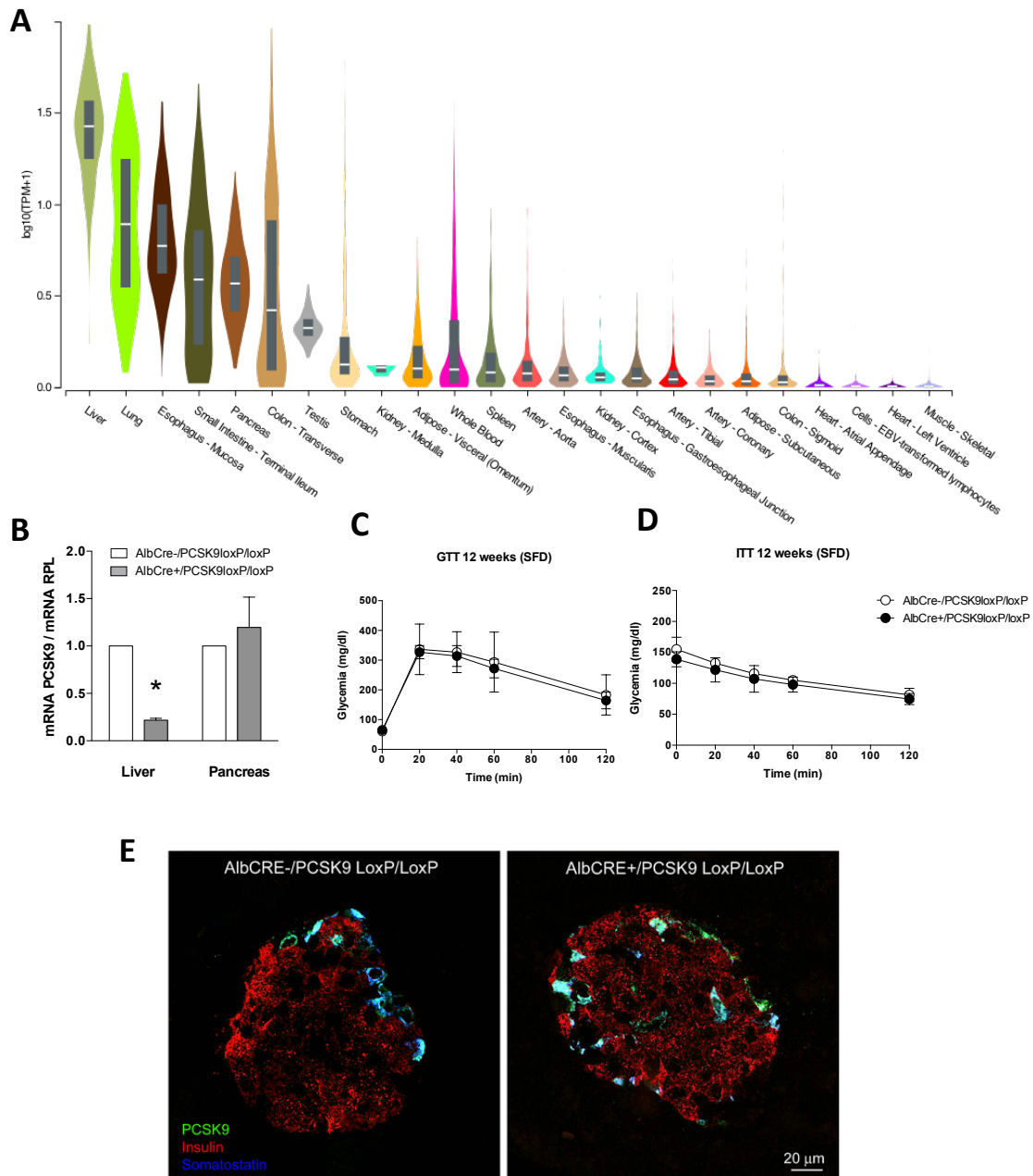


Figure 12 Circulating PCSK9 levels does not impact glycaemic profile. PCSK9 gene expression in human tissues according to the Genotype–Tissue Expression (GTEx) portal are shown. Data are reported as RPKM (Reads per Kilobase per Million mapped reads) (A). PCSK9 mRNA expression in the liver or in the pancreas (B). Glucose tolerance test (C) and Insulin Tolerance Test (D) were performed in liver selective KO animals compared to PCSK9 loxP/loxP mice. A representative image of pancreatic islet is showed (E). (* $p < 0.05$) (5 animals for each group).

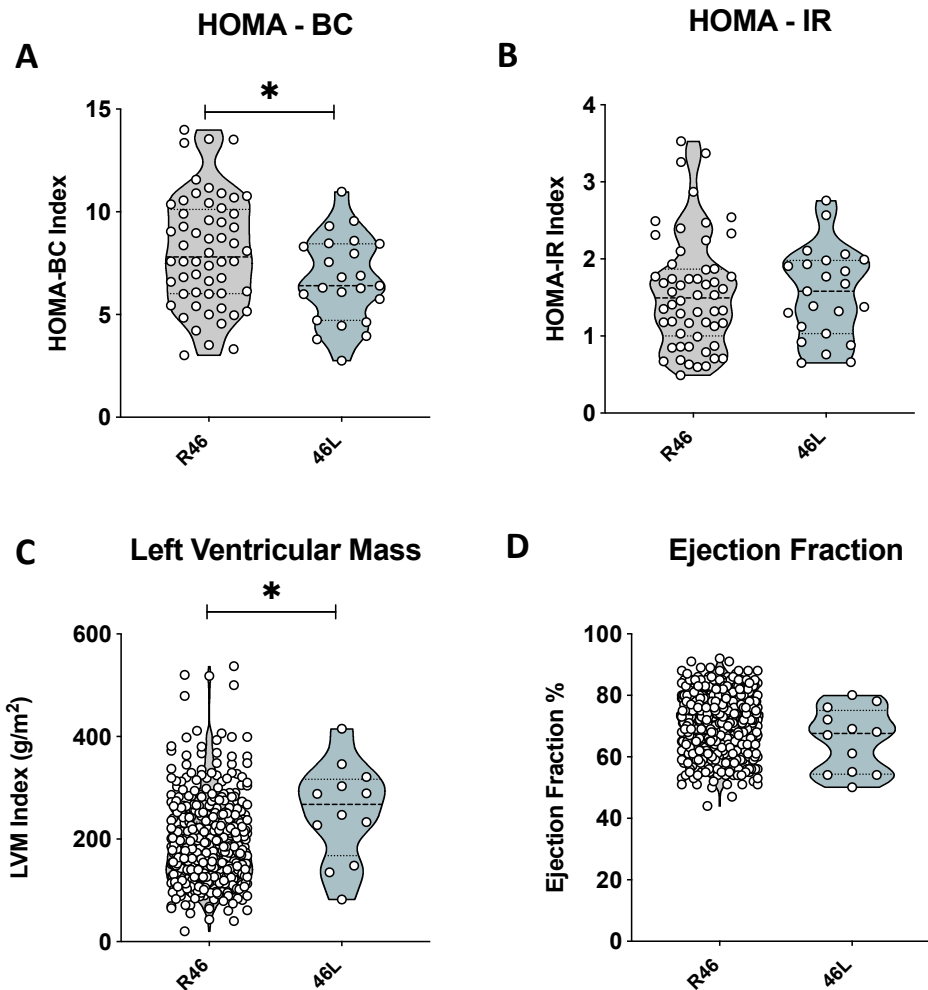


Figure 13 Human loss of function polymorphism for PCSK9. Homeostasis Model of Assessment Beta-Cells (HOMA-BC) Index according to R46L genotype in the PLIC Study. HOMA-BC Index is calculated as: $(360 \times \text{Fasting Insulin (mg/dL)}) / (\text{Fasting Glucose (mg/dL)} - 63)$. P derived from U-Mann Whitney test for comparison (A). Homeostasis Model of Assessment Insulin-Resistance (HOMA-IR) Index according to R46L genotype in the PLIC Study. HOMA-IR Index is calculated as: $(\text{Fasting Insulin (mg/dL)} \times \text{Fasting Glucose (mg/dL)}) / 405$. P derived from U-Mann Whitney test for comparison (B). Cardiac parameters were investigated with echocardiographic analysis and Left Ventricular Mass (C) and Ejection fraction (D) are displayed (* $p < 0.05$).

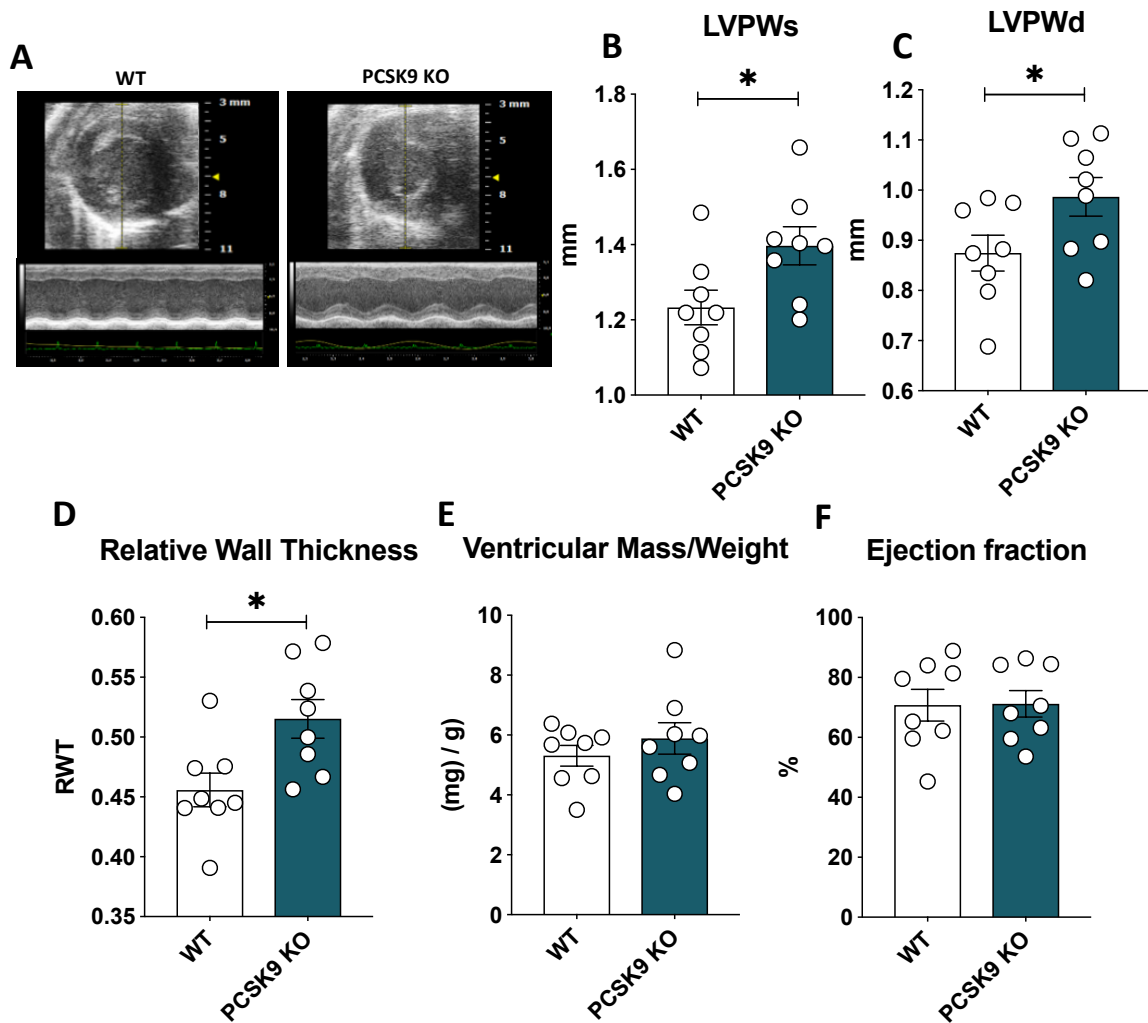


Figure 14 *Pcsk9* KO mice echocardiographic analysis. A representative image is displayed for both WT and *Pcsk9* KO mice(A). Left Ventricular Posterior Wall Thickness during Systole (B) and Diastole (C) were investigated. Relative Wall Thickness (C), Ventricular mass (D) and Ejection fraction were considered (* $p < 0.05$) (8 animals for each group).

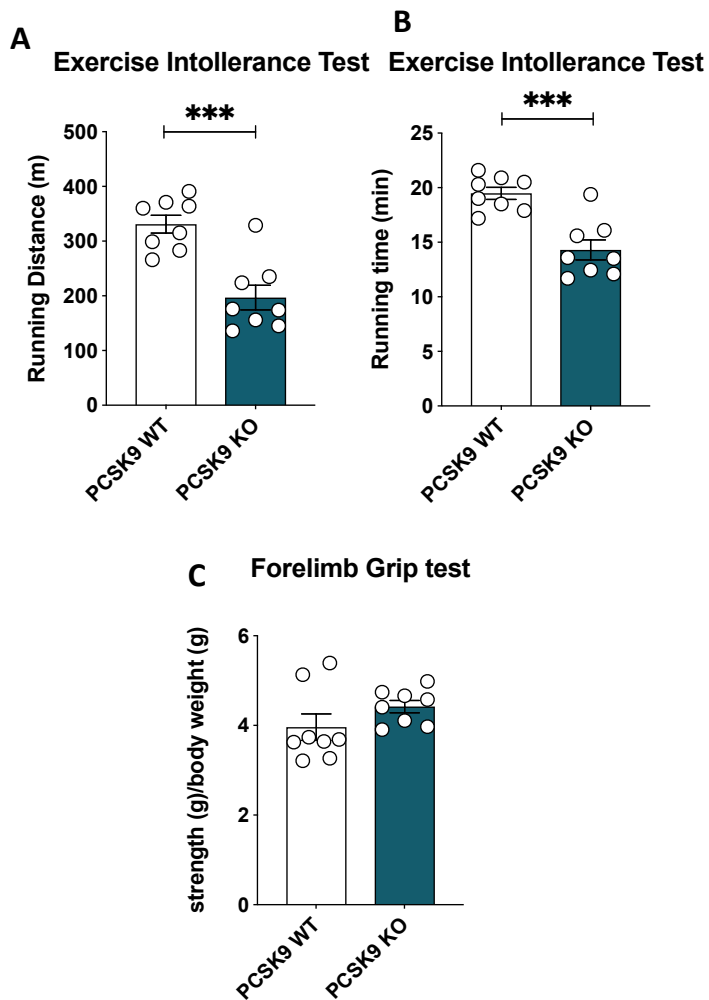


Figure 15 Functional tests. Exercise intolerance test were performed and Running distance (A) and time (B) were investigated. Mouse strength were investigated with forelimb grip test (C). (***) $p < 0.001$ (8 animals for each group).

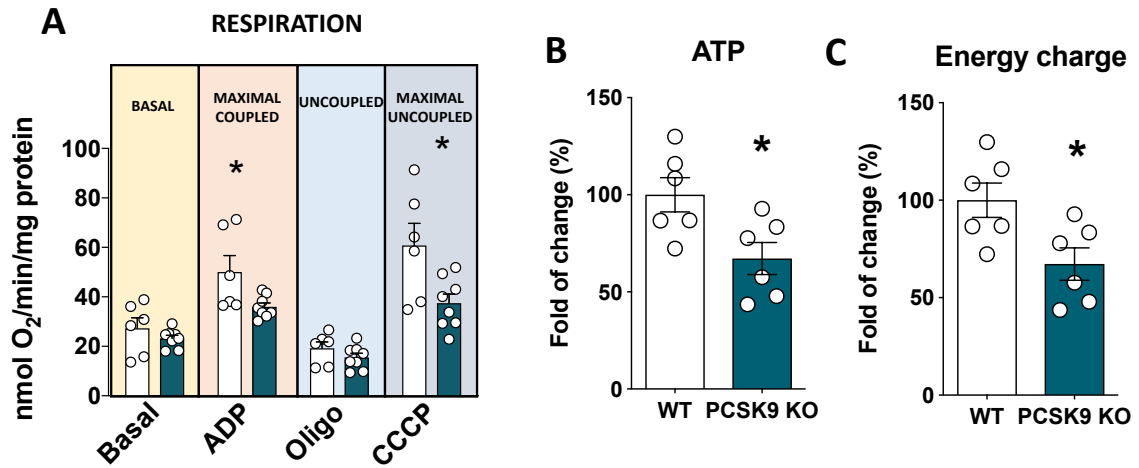


Figure 16 Mitochondrial metabolism. Heart oxygen consumption were investigated (A) (8 *Pcsk9* KO vs 6 WT). ATP levels (B) and Energy charge (C) were calculated. (* $p < 0.05$) (6 animals for each group).

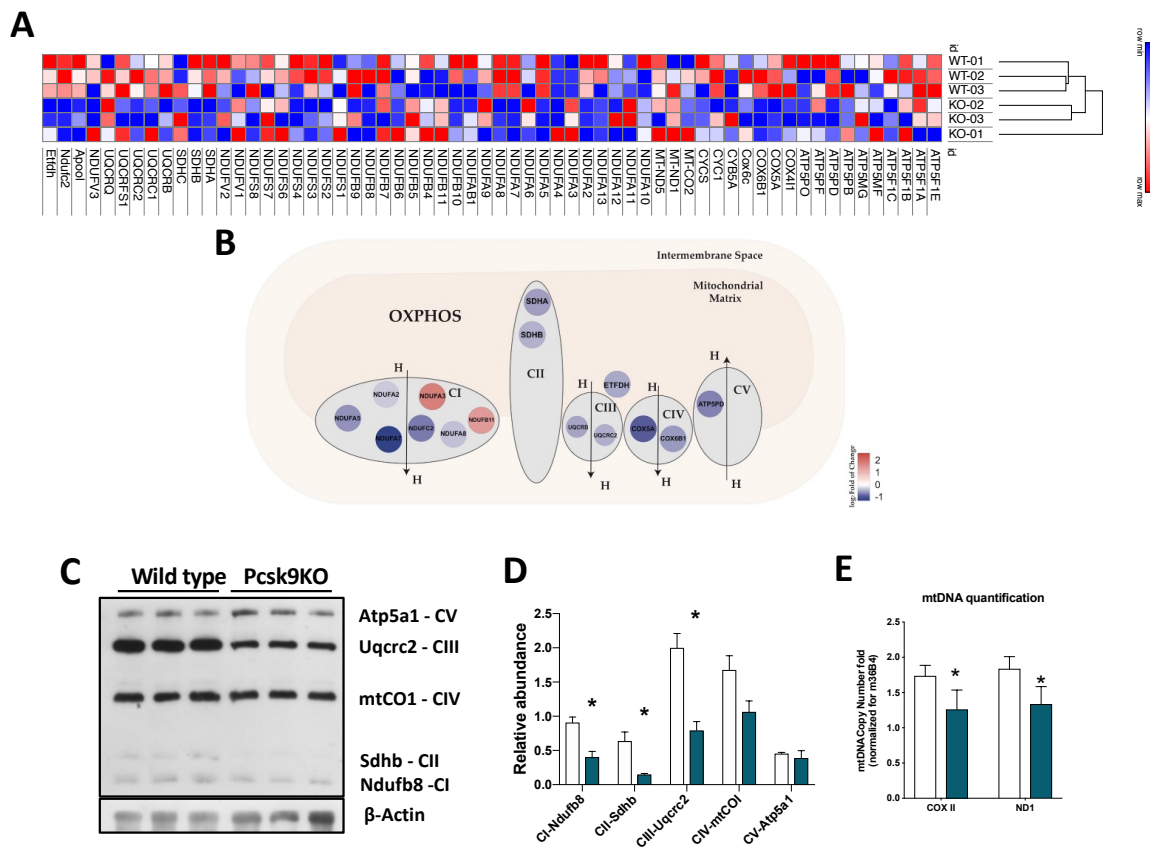


Figure 17 Electron Transport Chain (ETC) dysfunction. A proteomic analysis on heart were used to investigate ETC complexes (A and B). Western blot analysis on ETC complexes were performed (D) and the mitochondrial DNA quantified with 2 genes COXII and ND1 (E). (* $p < 0.05$) (3 animals for each group).

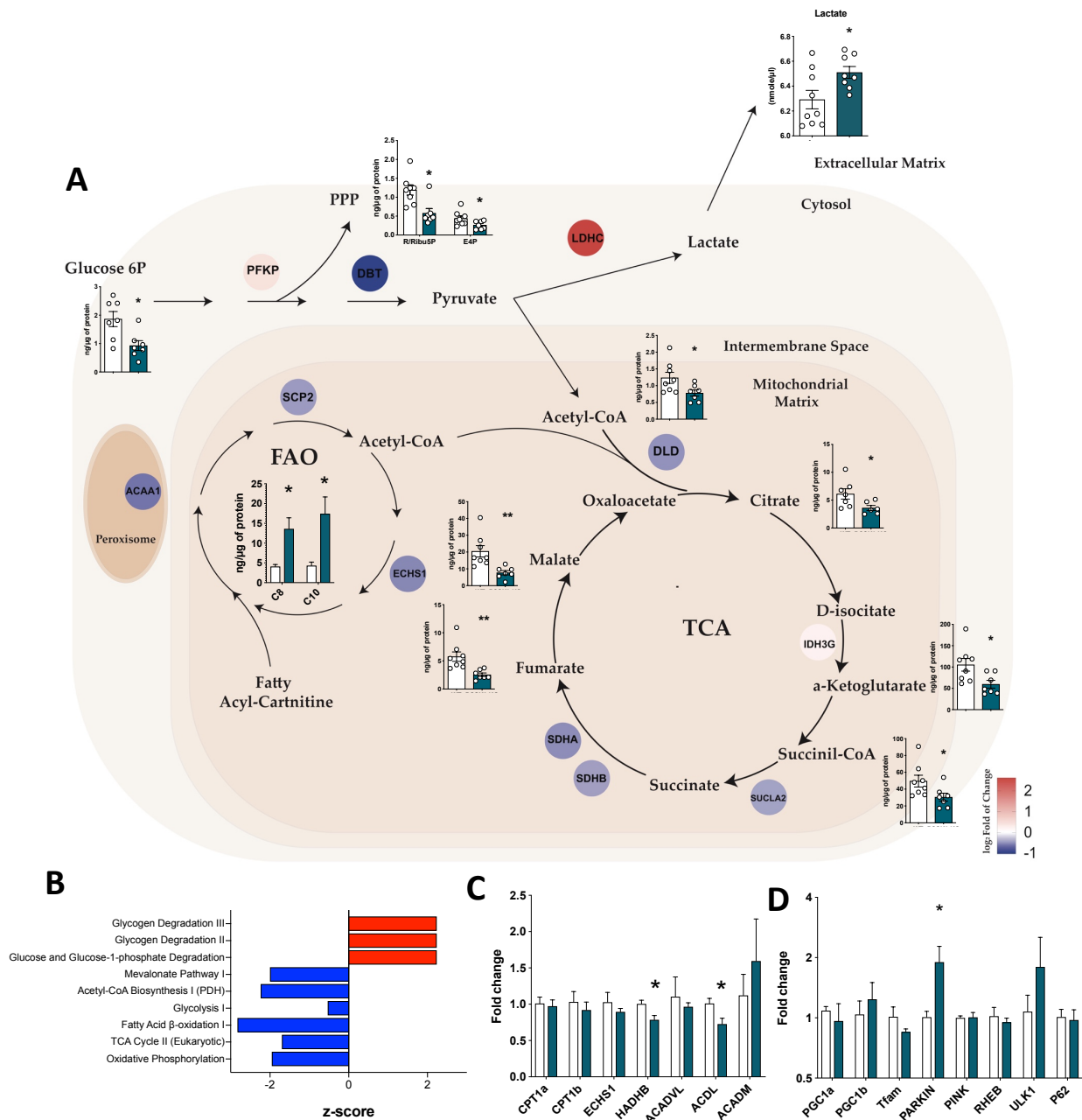


Figure 18 Cellular metabolic pathways. Proteomic (3 animals for each group). and metabolomic (7 animals for each group). data were used to investigate the principal metabolic pathways (A). An Ingenuity Pathway analysis IPA were performed to study the z-score of the principal metabolic pathways (B). Gene expression of genes involved in beta oxidation (C) and gene involved in mitochondrial homeostasis (D) were investigated. (*p<0.05) (5 animals for each group).

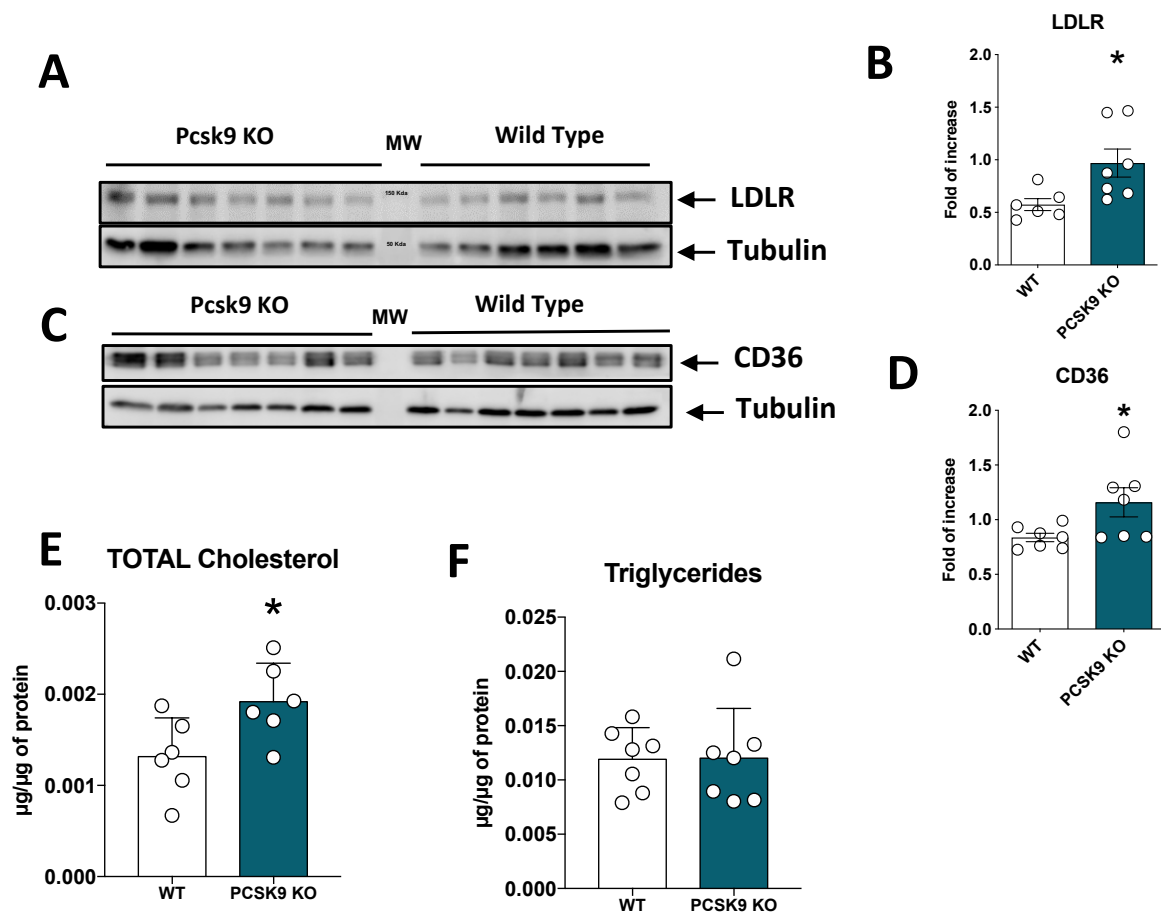


Figure 19 Lipid receptors and lipid heart content. Western blot analysis was performed to test LDLr (A and B) and CD36 (C and D) expression. Total cholesterol (E) and triglycerides were dosed from lipid heart extract (* $p < 0.05$) (7 animals for each group).

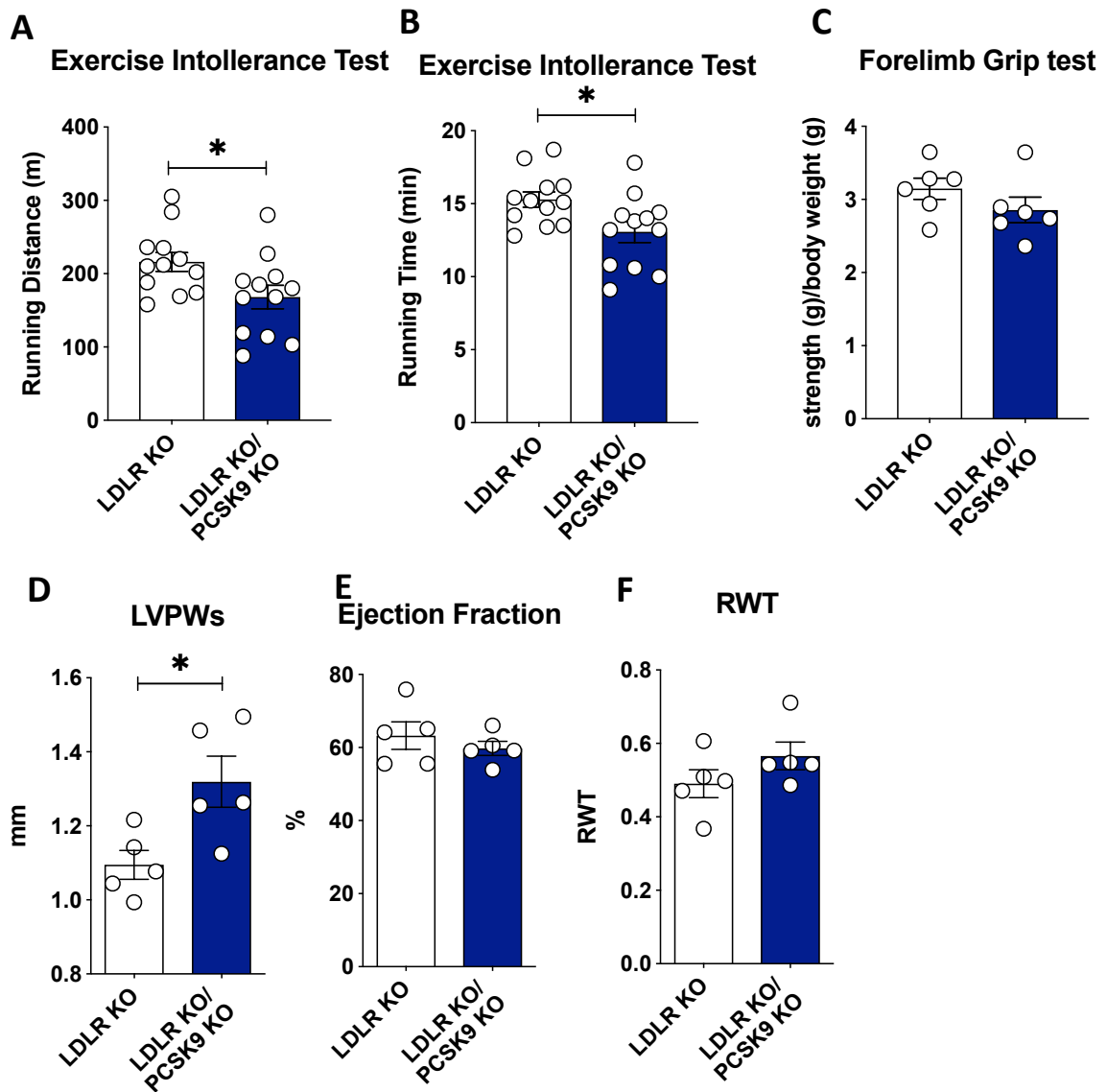


Figure 20 Functional and morphological analysis of PCSK9 and LDLr double KO. Exercise intolerance test were performed and Running distance (A) and time (B) were investigated (12 animals for each group). Mouse strength were investigated with forelimb grip test (C). Left Ventricular Posterior Wall Thickness during Systole (C) was investigated. Ejection fraction (E) and Relative Wall Thickness (G) were considered (**p<0.01) (5 animals for each group).

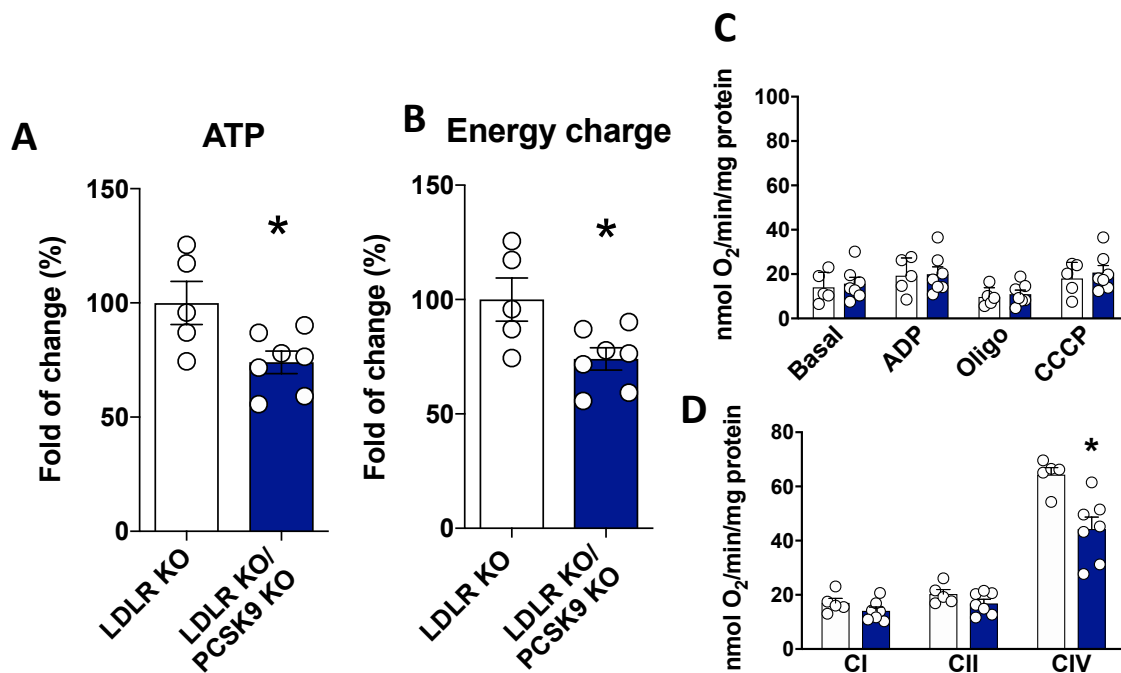


Figure 21 Double KO Mitochondrial metabolism. Heart ATP levels (A) and Energy charge(B) were calculated. Oxygen consumption (C) and ETC complexes activity (D) were investigated (* $p < 0.05$) (5 *LDLr* KO vs 7 Double KO animals for group).

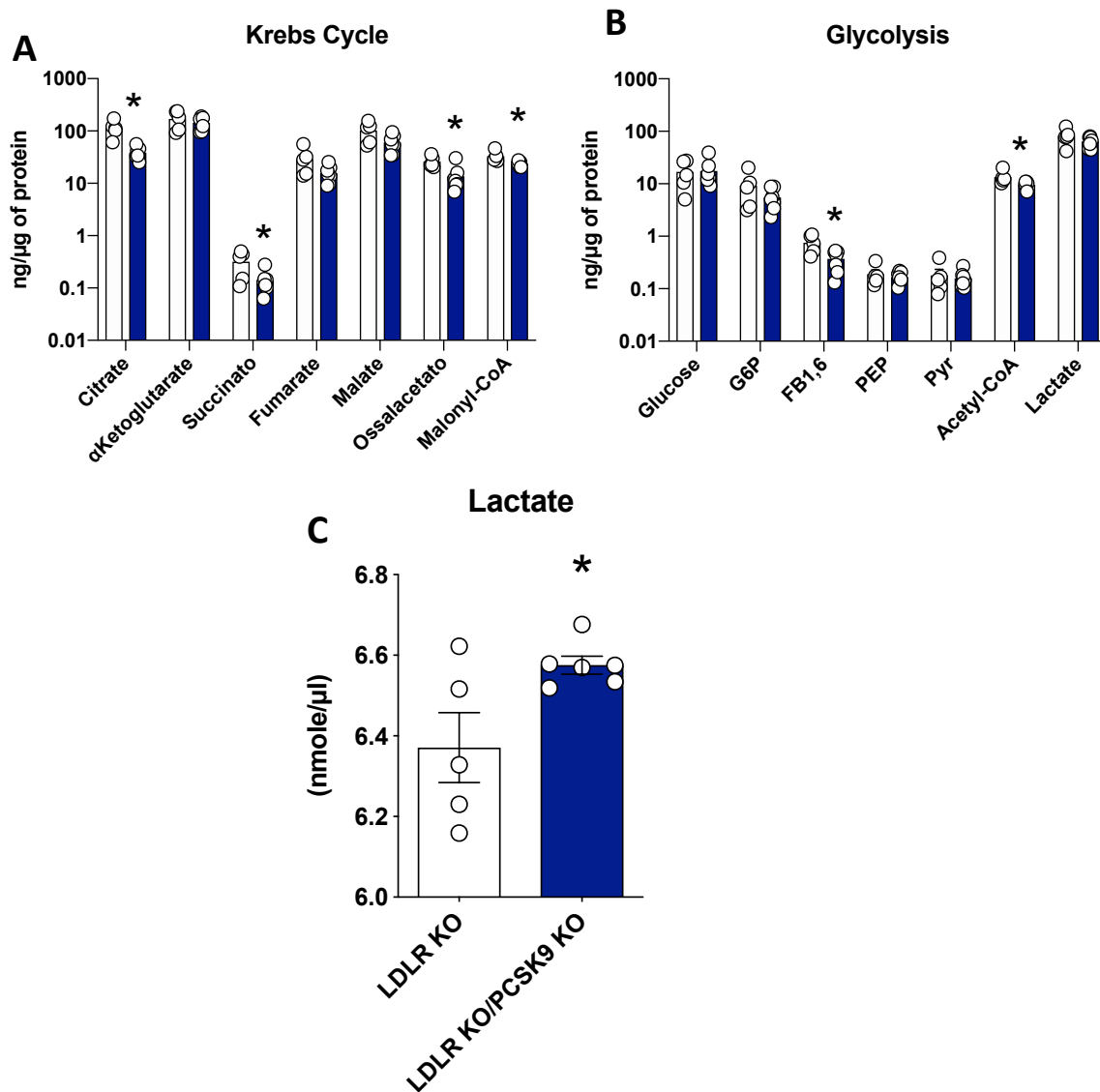
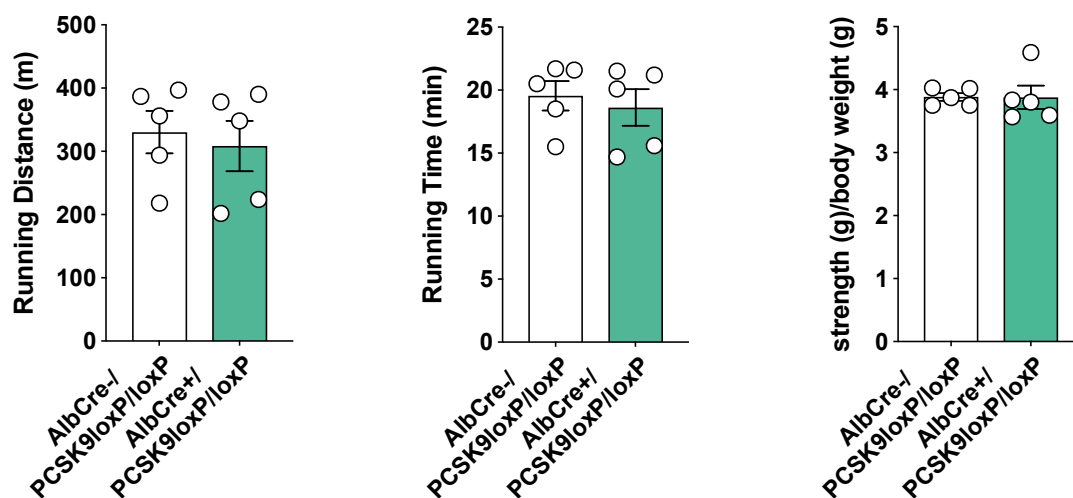


Figure 22 Double KO metabolic pathways. Metabolomics analysis were used to quantify krebs cycle (A) and glycolysis (B) metabolites. Lactate were quantified in the plasma of both groups (C) (* $p < 0.05$) (5 LDLr KO vs 6 Double KO animals for group).

A Exercise Intolerance Test **B** Exercise Intolerance Test **C** Forelimb Grip test



D LVPWs **E** Ejection fraction **F** RWT

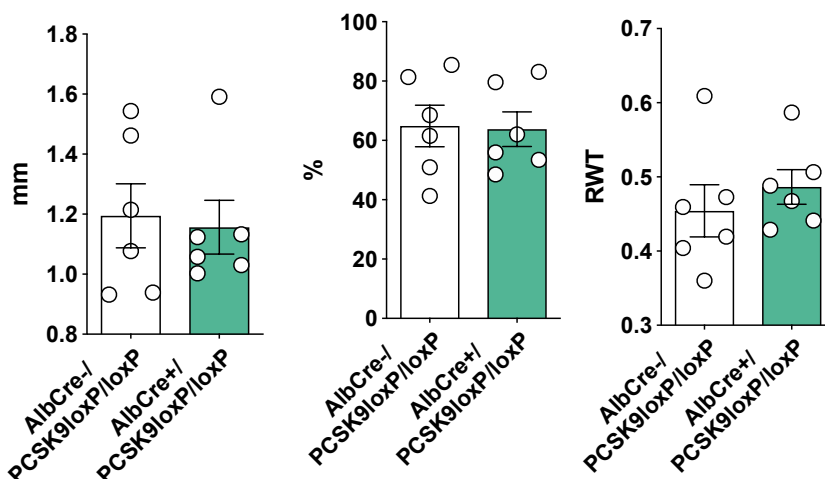


Figure 23 Functional and morphological analysis of liver selective Pcsk9 KO mice. Exercise intolerance test were performed and Running distance (A) and time (B) were investigated (5 animals for each group). Mouse strength were investigated with forelimb grip test (C). Left Ventricular Posterior Wall Thickness during Systole (C) was investigated. Ejection fraction (E) and Relative Wall Thickness (G) were considered (5 animals for each group).

References

- Abifadel, M., Varret, M., Rabes, J. P., Allard, D., Ouguerram, K., Devillers, M., Boileau, C. (2003). Mutations in PCSK9 cause autosomal dominant hypercholesterolemia. *Nat Genet*, *34*(2), 154-156. doi:10.1038/ng1161
- Abozguia, K., Shivu, G. N., Ahmed, I., Phan, T. T., & Frenneaux, M. P. (2009). The heart metabolism: pathophysiological aspects in ischaemia and heart failure. *Curr Pharm Des*, *15*(8), 827-835. doi:10.2174/138161209787582101
- Argaves, W. S. (2001). Members of the low density lipoprotein receptor family control diverse physiological processes. *Front Biosci*, *6*, D406-416. doi:10.2741/argaves
- Benjannet, S., Rhainds, D., Hamelin, J., Nassoury, N., & Seidah, N. G. (2006). The proprotein convertase (PC) PCSK9 is inactivated by furin and/or PC5/6A: functional consequences of natural mutations and post-translational modifications. *J Biol Chem*, *281*(41), 30561-30572. doi:10.1074/jbc.M606495200
- Bonacina, F., Barbieri, S. S., Cutuli, L., Amadio, P., Doni, A., Sironi, M., . . . Norata, G. D. (2016). Vascular pentraxin 3 controls arterial thrombosis by targeting collagen and fibrinogen induced platelets aggregation. *Biochim Biophys Acta*, *1862*(6), 1182-1190. doi:10.1016/j.bbadis.2016.03.007
- Brand, M. D., & Nicholls, D. G. (2011). Assessing mitochondrial dysfunction in cells. *Biochem J*, *435*(2), 297-312. doi:10.1042/BJ20110162
- Brown, M. S., & Goldstein, J. L. (1976). Receptor-mediated control of cholesterol metabolism. *Science*, *191*(4223), 150-154. doi:10.1126/science.174194
- Calvo, D., Dopazo, J., & Vega, M. A. (1995). The CD36, CLA-1 (CD36L1), and LIMPII (CD36L2) gene family: cellular distribution, chromosomal location, and genetic evolution. *Genomics*, *25*(1), 100-106. doi:10.1016/0888-7543(95)80114-2
- Careskey, H. E., Davis, R. A., Alborn, W. E., Troutt, J. S., Cao, G., & Konrad, R. J. (2008). Atorvastatin increases human serum levels of proprotein convertase subtilisin/kexin type 9. *J Lipid Res*, *49*(2), 394-398. doi:10.1194/jlr.M700437-JLR200
- Catapano, A. L., Pirillo, A., & Norata, G. D. (2020). New Pharmacological Approaches to Target PCSK9. *Curr Atheroscler Rep*, *22*(7), 24. doi:10.1007/s11883-020-00847-7
- Chaudhary, R., Garg, J., Shah, N., & Sumner, A. (2017). PCSK9 inhibitors: A new era of lipid lowering therapy. *World J Cardiol*, *9*(2), 76-91. doi:10.4330/wjc.v9.i2.76
- Chaurasia, B., & Summers, S. A. (2015). Ceramides - Lipotoxic Inducers of Metabolic Disorders. *Trends Endocrinol Metab*, *26*(10), 538-550. doi:10.1016/j.tem.2015.07.006
- Cilia, L., Saeed, A., Ganga, H. V., & Wu, W. C. (2019). Heart Failure With Preserved Ejection Fraction: Prevention and Management. *Am J Lifestyle Med*, *13*(2), 182-189. doi:10.1177/1559827617695219
- Cnop, M., Hannaert, J. C., Gruppings, A. Y., & Pipeleers, D. G. (2002). Low density lipoprotein can cause death of islet beta-cells by its cellular uptake and oxidative modification. *Endocrinology*, *143*(9), 3449-3453. doi:10.1210/en.2002-220273
- Cohen, J. C., Boerwinkle, E., Mosley, T. H., Jr., & Hobbs, H. H. (2006). Sequence variations in PCSK9, low LDL, and protection against coronary heart disease. *N Engl J Med*, *354*(12), 1264-1272. doi:10.1056/NEJMoa054013
- Da Dalt, L., Ruscica, M., Bonacina, F., Balzarotti, G., Dhyani, A., Di Cairano, E., . . . Norata, G. D. (2019). PCSK9 deficiency reduces insulin secretion and promotes glucose intolerance: the role of the low-density lipoprotein receptor. *Eur Heart J*, *40*(4), 357-368. doi:10.1093/eurheartj/ehy357
- Dadu, R. T., & Ballantyne, C. M. (2014). Lipid lowering with PCSK9 inhibitors. *Nat Rev Cardiol*, *11*(10), 563-575. doi:10.1038/nrcardio.2014.84
- Davis, C. G., Elhammer, A., Russell, D. W., Schneider, W. J., Kornfeld, S., Brown, M. S., & Goldstein, J. L. (1986). Deletion of clustered O-linked carbohydrates does not

- impair function of low density lipoprotein receptor in transfected fibroblasts. *J Biol Chem*, 261(6), 2828-2838.
- Davis, C. G., Goldstein, J. L., Sudhof, T. C., Anderson, R. G., Russell, D. W., & Brown, M. S. (1987). Acid-dependent ligand dissociation and recycling of LDL receptor mediated by growth factor homology region. *Nature*, 326(6115), 760-765. doi:10.1038/326760a0
- Davis, C. G., van Driel, I. R., Russell, D. W., Brown, M. S., & Goldstein, J. L. (1987). The low density lipoprotein receptor. Identification of amino acids in cytoplasmic domain required for rapid endocytosis. *J Biol Chem*, 262(9), 4075-4082.
- de Carvalho, C., & Caramujo, M. J. (2018). The Various Roles of Fatty Acids. *Molecules*, 23(10). doi:10.3390/molecules23102583
- DeBose-Boyd, R. A. (2008). Feedback regulation of cholesterol synthesis: sterol-accelerated ubiquitination and degradation of HMG CoA reductase. *Cell Res*, 18(6), 609-621. doi:10.1038/cr.2008.61
- Demers, A., Samami, S., Lauzier, B., Des Rosiers, C., Ngo Sock, E. T., Ong, H., & Mayer, G. (2015). PCSK9 Induces CD36 Degradation and Affects Long-Chain Fatty Acid Uptake and Triglyceride Metabolism in Adipocytes and in Mouse Liver. *Arterioscler Thromb Vasc Biol*, 35(12), 2517-2525. doi:10.1161/ATVBAHA.115.306032
- Dlugosz, P., & Nimpf, J. (2018). The Reelin Receptors Apolipoprotein E receptor 2 (ApoER2) and VLDL Receptor. *Int J Mol Sci*, 19(10). doi:10.3390/ijms19103090
- Doehner, W., von Haehling, S., & Anker, S. D. (2008). Insulin resistance in chronic heart failure. *J Am Coll Cardiol*, 52(3), 239; author reply 239-240. doi:10.1016/j.jacc.2008.03.044
- Doenst, T., Nguyen, T. D., & Abel, E. D. (2013). Cardiac metabolism in heart failure: implications beyond ATP production. *Circ Res*, 113(6), 709-724. doi:10.1161/CIRCRESAHA.113.300376
- Dong, B., Singh, A. B., Shende, V. R., & Liu, J. (2017). Hepatic HNF1 transcription factors control the induction of PCSK9 mediated by rosuvastatin in normolipidemic hamsters. *Int J Mol Med*, 39(3), 749-756. doi:10.3892/ijmm.2017.2879
- Drosatos, K., & Schulze, P. C. (2013). Cardiac lipotoxicity: molecular pathways and therapeutic implications. *Curr Heart Fail Rep*, 10(2), 109-121. doi:10.1007/s11897-013-0133-0
- Evans, R. D., & Hauton, D. (2016). The role of triacylglycerol in cardiac energy provision. *Biochim Biophys Acta*, 1861(10), 1481-1491. doi:10.1016/j.bbali.2016.03.010
- Fears, R. (1981). The contribution of the cholesterol biosynthetic pathway to intermediary metabolism and cell function. *Biochem J*, 199(1), 1-7. doi:10.1042/bj1990001
- Febbraio, M., Hajjar, D. P., & Silverstein, R. L. (2001). CD36: a class B scavenger receptor involved in angiogenesis, atherosclerosis, inflammation, and lipid metabolism. *J Clin Invest*, 108(6), 785-791. doi:10.1172/JCI14006
- Feingold, K. R., & Grunfeld, C. (2000). Introduction to Lipids and Lipoproteins. In K. R. Feingold, B. Anawalt, A. Boyce, G. Chrousos, W. W. de Herder, K. Dungan, A. Grossman, J. M. Hershman, H. J. Hofland, G. Kaltsas, C. Koch, P. Kopp, M. Korbonits, R. McLachlan, J. E. Morley, M. New, J. Purnell, F. Singer, C. A. Stratakis, D. L. Trencze, & D. P. Wilson (Eds.), *Endotext*. South Dartmouth (MA).
- Ference, B. A., Robinson, J. G., Brook, R. D., Catapano, A. L., Chapman, M. J., Neff, D. R., . . . Sabatine, M. S. (2016). Variation in PCSK9 and HMGCR and Risk of Cardiovascular Disease and Diabetes. *N Engl J Med*, 375(22), 2144-2153. doi:10.1056/NEJMoa1604304
- Finck, B. N., Han, X., Courtois, M., Aimond, F., Nerbonne, J. M., Kovacs, A., . . . Kelly, D. P. (2003). A critical role for PPARalpha-mediated lipotoxicity in the pathogenesis of

- diabetic cardiomyopathy: modulation by dietary fat content. *Proc Natl Acad Sci U S A*, 100(3), 1226-1231. doi:10.1073/pnas.0336724100
- Fitzgerald, K., White, S., Borodovsky, A., Bettencourt, B. R., Strahs, A., Clausen, V., . . . Simon, A. (2017). A Highly Durable RNAi Therapeutic Inhibitor of PCSK9. *N Engl J Med*, 376(1), 41-51. doi:10.1056/NEJMoa1609243
- Glatz, J. F., Angin, Y., Steinbusch, L. K., Schwenk, R. W., & Luiken, J. J. (2013). CD36 as a target to prevent cardiac lipotoxicity and insulin resistance. *Prostaglandins Leukot Essent Fatty Acids*, 88(1), 71-77. doi:10.1016/j.plefa.2012.04.009
- Goldberg, I. J., Reue, K., Abumrad, N. A., Bickel, P. E., Cohen, S., Fisher, E. A., . . . Chen, J. (2018). Deciphering the Role of Lipid Droplets in Cardiovascular Disease: A Report From the 2017 National Heart, Lung, and Blood Institute Workshop. *Circulation*, 138(3), 305-315. doi:10.1161/CIRCULATIONAHA.118.033704
- Goldberg, I. J., Trent, C. M., & Schulze, P. C. (2012). Lipid metabolism and toxicity in the heart. *Cell Metab*, 15(6), 805-812. doi:10.1016/j.cmet.2012.04.006
- Haemmerle, G., Lass, A., Zimmermann, R., Gorkiewicz, G., Meyer, C., Rozman, J., . . . Zechner, R. (2006). Defective lipolysis and altered energy metabolism in mice lacking adipose triglyceride lipase. *Science*, 312(5774), 734-737. doi:10.1126/science.1123965
- Haemmerle, G., Zimmermann, R., Hayn, M., Theussl, C., Waeg, G., Wagner, E., . . . Zechner, R. (2002). Hormone-sensitive lipase deficiency in mice causes diglyceride accumulation in adipose tissue, muscle, and testis. *J Biol Chem*, 277(7), 4806-4815. doi:10.1074/jbc.M110355200
- Hoosdally, S. J., Andress, E. J., Wooding, C., Martin, C. A., & Linton, K. J. (2009). The Human Scavenger Receptor CD36: glycosylation status and its role in trafficking and function. *J Biol Chem*, 284(24), 16277-16288. doi:10.1074/jbc.M109.007849
- Horton, J. D., Goldstein, J. L., & Brown, M. S. (2002). SREBPs: activators of the complete program of cholesterol and fatty acid synthesis in the liver. *J Clin Invest*, 109(9), 1125-1131. doi:10.1172/JCI15593
- Hur, J. H., Park, S. Y., Dall'Armi, C., Lee, J. S., Di Paolo, G., Lee, H. Y., . . . Choi, C. S. (2016). Phospholipase D1 deficiency in mice causes nonalcoholic fatty liver disease via an autophagy defect. *Sci Rep*, 6, 39170. doi:10.1038/srep39170
- Ibrahimi, A., Bonen, A., Blinn, W. D., Hajri, T., Li, X., Zhong, K., . . . Abumrad, N. A. (1999). Muscle-specific overexpression of FAT/CD36 enhances fatty acid oxidation by contracting muscle, reduces plasma triglycerides and fatty acids, and increases plasma glucose and insulin. *J Biol Chem*, 274(38), 26761-26766. doi:10.1074/jbc.274.38.26761
- Judge, A., & Dodd, M. S. (2020). Metabolism. *Essays Biochem*, 64(4), 607-647. doi:10.1042/EBC20190041
- Kasner, M., Westermann, D., Lopez, B., Gaub, R., Escher, F., Kuhl, U., . . . Tschope, C. (2011). Diastolic tissue Doppler indexes correlate with the degree of collagen expression and cross-linking in heart failure and normal ejection fraction. *J Am Coll Cardiol*, 57(8), 977-985. doi:10.1016/j.jacc.2010.10.024
- Kassan, A., Herms, A., Fernandez-Vidal, A., Bosch, M., Schieber, N. L., Reddy, B. J., . . . Pol, A. (2013). Acyl-CoA synthetase 3 promotes lipid droplet biogenesis in ER microdomains. *J Cell Biol*, 203(6), 985-1001. doi:10.1083/jcb.201305142
- Kerner, J., & Hoppel, C. (2000). Fatty acid import into mitochondria. *Biochim Biophys Acta*, 1486(1), 1-17. doi:10.1016/s1388-1981(00)00044-5
- Kosenko, T., Golder, M., Leblond, G., Weng, W., & Lagace, T. A. (2013). Low density lipoprotein binds to proprotein convertase subtilisin/kexin type-9 (PCSK9) in human

- plasma and inhibits PCSK9-mediated low density lipoprotein receptor degradation. *J Biol Chem*, 288(12), 8279-8288. doi:10.1074/jbc.M112.421370
- Krahenbuhl, S., Pavik-Mezzour, I., & von Eckardstein, A. (2016). Unmet Needs in LDL-C Lowering: When Statins Won't Do! *Drugs*, 76(12), 1175-1190. doi:10.1007/s40265-016-0613-0
- Kwiterovich, P. O., Jr. (2000). The metabolic pathways of high-density lipoprotein, low-density lipoprotein, and triglycerides: a current review. *Am J Cardiol*, 86(12A), 5L-10L. doi:10.1016/s0002-9149(00)01461-2
- Kwok, S., Singh-Bist, A., Natu, V., & Kraemer, F. B. (1997). Dietary regulation of the very low density lipoprotein receptor in mouse heart and fat. *Horm Metab Res*, 29(10), 524-529. doi:10.1055/s-2007-979094
- Lagace, T. A. (2014). PCSK9 and LDLR degradation: regulatory mechanisms in circulation and in cells. *Curr Opin Lipidol*, 25(5), 387-393. doi:10.1097/MOL.0000000000000114
- Lei, B., Lionetti, V., Young, M. E., Chandler, M. P., d'Agostino, C., Kang, E., . . . Recchia, F. A. (2004). Paradoxical downregulation of the glucose oxidation pathway despite enhanced flux in severe heart failure. *J Mol Cell Cardiol*, 36(4), 567-576. doi:10.1016/j.yjmcc.2004.02.004
- Li, H., & Liu, J. (2012). The novel function of HINFP as a co-activator in sterol-regulated transcription of PCSK9 in HepG2 cells. *Biochem J*, 443(3), 757-768. doi:10.1042/BJ20111645
- Lipari, M. T., Li, W., Moran, P., Kong-Beltran, M., Sai, T., Lai, J., . . . Kirchhofer, D. (2012). Furin-cleaved proprotein convertase subtilisin/kexin type 9 (PCSK9) is active and modulates low density lipoprotein receptor and serum cholesterol levels. *J Biol Chem*, 287(52), 43482-43491. doi:10.1074/jbc.M112.380618
- Lopaschuk, G. D., Ussher, J. R., Folmes, C. D., Jaswal, J. S., & Stanley, W. C. (2010). Myocardial fatty acid metabolism in health and disease. *Physiol Rev*, 90(1), 207-258. doi:10.1152/physrev.00015.2009
- Lu, X., Liu, J., Hou, F., Liu, Z., Cao, X., Seo, H., & Gao, B. (2011). Cholesterol induces pancreatic beta cell apoptosis through oxidative stress pathway. *Cell Stress Chaperones*, 16(5), 539-548. doi:10.1007/s12192-011-0265-7
- Maranzana, E., Barbero, G., Falasca, A. I., Lenaz, G., & Genova, M. L. (2013). Mitochondrial respiratory supercomplex association limits production of reactive oxygen species from complex I. *Antioxid Redox Signal*, 19(13), 1469-1480. doi:10.1089/ars.2012.4845
- Marques, L. R., Diniz, T. A., Antunes, B. M., Rossi, F. E., Caperuto, E. C., Lira, F. S., & Goncalves, D. C. (2018). Reverse Cholesterol Transport: Molecular Mechanisms and the Non-medical Approach to Enhance HDL Cholesterol. *Front Physiol*, 9, 526. doi:10.3389/fphys.2018.00526
- Morales, A., Lee, H., Goni, F. M., Kolesnick, R., & Fernandez-Checa, J. C. (2007). Sphingolipids and cell death. *Apoptosis*, 12(5), 923-939. doi:10.1007/s10495-007-0721-0
- Moro, C., Bajpeyi, S., & Smith, S. R. (2008). Determinants of intramyocellular triglyceride turnover: implications for insulin sensitivity. *Am J Physiol Endocrinol Metab*, 294(2), E203-213. doi:10.1152/ajpendo.00624.2007
- Neubauer, S. (2007). The failing heart--an engine out of fuel. *N Engl J Med*, 356(11), 1140-1151. doi:10.1056/NEJMra063052
- Nishi, H., Higashihara, T., & Inagi, R. (2019). Lipotoxicity in Kidney, Heart, and Skeletal Muscle Dysfunction. *Nutrients*, 11(7). doi:10.3390/nu11071664

- Nohammer, C., Brunner, F., Wolkart, G., Staber, P. B., Steyrer, E., Gonzalez, F. J., . . . Hoefler, G. (2003). Myocardial dysfunction and male mortality in peroxisome proliferator-activated receptor alpha knockout mice overexpressing lipoprotein lipase in muscle. *Lab Invest*, 83(2), 259-269. doi:10.1097/01.lab.0000053916.61772.ca
- Norata, G. D., Garlaschelli, K., Grigore, L., Raselli, S., Tramontana, S., Meneghetti, F., . . . Catapano, A. L. (2010). Effects of PCSK9 variants on common carotid artery intima media thickness and relation to ApoE alleles. *Atherosclerosis*, 208(1), 177-182. doi:10.1016/j.atherosclerosis.2009.06.023
- Olivecrona, G. (2016). Role of lipoprotein lipase in lipid metabolism. *Curr Opin Lipidol*, 27(3), 233-241. doi:10.1097/MOL.0000000000000297
- Onal, G., Kutlu, O., Gozuacik, D., & Dokmeci Emre, S. (2017). Lipid Droplets in Health and Disease. *Lipids Health Dis*, 16(1), 128. doi:10.1186/s12944-017-0521-7
- Ossoli, A., Simonelli, S., Vitali, C., Franceschini, G., & Calabresi, L. (2016). Role of LCAT in Atherosclerosis. *J Atheroscler Thromb*, 23(2), 119-127. doi:10.5551/jat.32854
- Pagler, T. A., Rhode, S., Neuhofer, A., Laggner, H., Strobl, W., Hinterndorfer, C., . . . Stangl, H. (2006). SR-BI-mediated high density lipoprotein (HDL) endocytosis leads to HDL resecretion facilitating cholesterol efflux. *J Biol Chem*, 281(16), 11193-11204. doi:10.1074/jbc.M510261200
- Pan, Y., Zhou, Y., Wu, H., Chen, X., Hu, X., Zhang, H., . . . Liao, Y. (2017). A Therapeutic Peptide Vaccine Against PCSK9. *Sci Rep*, 7(1), 12534. doi:10.1038/s41598-017-13069-w
- Perego, C., Da Dalt, L., Pirillo, A., Galli, A., Catapano, A. L., & Norata, G. D. (2019). Cholesterol metabolism, pancreatic beta-cell function and diabetes. *Biochim Biophys Acta Mol Basis Dis*, 1865(9), 2149-2156. doi:10.1016/j.bbadis.2019.04.012
- Perman, J. C., Bostrom, P., Lindbom, M., Lidberg, U., StAhlman, M., Hagg, D., . . . Boren, J. (2011). The VLDL receptor promotes lipotoxicity and increases mortality in mice following an acute myocardial infarction. *J Clin Invest*, 121(7), 2625-2640. doi:10.1172/JCI43068
- Peters, D. T., Henderson, C. A., Warren, C. R., Friesen, M., Xia, F., Becker, C. E., . . . Cowan, C. A. (2016). Asialoglycoprotein receptor 1 is a specific cell-surface marker for isolating hepatocytes derived from human pluripotent stem cells. *Development*, 143(9), 1475-1481. doi:10.1242/dev.132209
- Pfeiffer, K., Gohil, V., Stuart, R. A., Hunte, C., Brandt, U., Greenberg, M. L., & Schagger, H. (2003). Cardiolipin stabilizes respiratory chain supercomplexes. *J Biol Chem*, 278(52), 52873-52880. doi:10.1074/jbc.M308366200
- Pinti, M. V., Fink, G. K., Hathaway, Q. A., Durr, A. J., Kunovac, A., & Hollander, J. M. (2019). Mitochondrial dysfunction in type 2 diabetes mellitus: an organ-based analysis. *Am J Physiol Endocrinol Metab*, 316(2), E268-E285. doi:10.1152/ajpendo.00314.2018
- Poirier, S., Mayer, G., Poupon, V., McPherson, P. S., Desjardins, R., Ly, K., . . . Seidah, N. G. (2009). Dissection of the endogenous cellular pathways of PCSK9-induced low density lipoprotein receptor degradation: evidence for an intracellular route. *J Biol Chem*, 284(42), 28856-28864. doi:10.1074/jbc.M109.037085
- Ray, K. K., Landmesser, U., Leiter, L. A., Kallend, D., Dufour, R., Karakas, M., . . . Kastelein, J. J. (2017). Inclisiran in Patients at High Cardiovascular Risk with Elevated LDL Cholesterol. *N Engl J Med*, 376(15), 1430-1440. doi:10.1056/NEJMoa1615758
- Ray, K. K., Stoekenbroek, R. M., Kallend, D., Leiter, L. A., Landmesser, U., Wright, R. S., . . . Kastelein, J. J. P. (2018). Effect of an siRNA Therapeutic Targeting PCSK9 on

- Atherogenic Lipoproteins: Prespecified Secondary End Points in ORION 1. *Circulation*, 138(13), 1304-1316. doi:10.1161/CIRCULATIONAHA.118.034710
- Riehle, C., & Abel, E. D. (2016). Insulin Signaling and Heart Failure. *Circ Res*, 118(7), 1151-1169. doi:10.1161/CIRCRESAHA.116.306206
- Rosca, M. G., Tandler, B., & Hoppel, C. L. (2013). Mitochondria in cardiac hypertrophy and heart failure. *J Mol Cell Cardiol*, 55, 31-41. doi:10.1016/j.yjmcc.2012.09.002
- Russell, D. W., Brown, M. S., & Goldstein, J. L. (1989). Different combinations of cysteine-rich repeats mediate binding of low density lipoprotein receptor to two different proteins. *J Biol Chem*, 264(36), 21682-21688.
- Sabatine, M. S., Giugliano, R. P., Keech, A. C., Honarpour, N., Wiviott, S. D., Murphy, S. A., . . . Investigators. (2017). Evolocumab and Clinical Outcomes in Patients with Cardiovascular Disease. *N Engl J Med*, 376(18), 1713-1722. doi:10.1056/NEJMoa1615664
- Saini-Chohan, H. K., Holmes, M. G., Chicco, A. J., Taylor, W. A., Moore, R. L., McCune, S. A., . . . Sparagna, G. C. (2009). Cardiolipin biosynthesis and remodeling enzymes are altered during development of heart failure. *J Lipid Res*, 50(8), 1600-1608. doi:10.1194/jlr.M800561-JLR200
- Schmidt, A. F., Swerdlow, D. I., Holmes, M. V., Patel, R. S., Fairhurst-Hunter, Z., Lyall, D. M., . . . Sattar, N. (2017). PCSK9 genetic variants and risk of type 2 diabetes: a mendelian randomisation study. *Lancet Diabetes Endocrinol*, 5(2), 97-105. doi:10.1016/S2213-8587(16)30396-5
- Schwartz, G. G., Steg, P. G., Szarek, M., Bhatt, D. L., Bittner, V. A., Diaz, R., . . . Investigators. (2018). Alirocumab and Cardiovascular Outcomes after Acute Coronary Syndrome. *N Engl J Med*, 379(22), 2097-2107. doi:10.1056/NEJMoa1801174
- Seferovic, P. M., & Paulus, W. J. (2015). Clinical diabetic cardiomyopathy: a two-faced disease with restrictive and dilated phenotypes. *Eur Heart J*, 36(27), 1718-1727, 1727a-1727c. doi:10.1093/eurheartj/ehv134
- Seidah, N. G., Benjannet, S., Wickham, L., Marcinkiewicz, J., Jasmin, S. B., Stifani, S., . . . Chretien, M. (2003). The secretory proprotein convertase neural apoptosis-regulated convertase 1 (NARC-1): liver regeneration and neuronal differentiation. *Proc Natl Acad Sci U S A*, 100(3), 928-933. doi:10.1073/pnas.0335507100
- Shapiro, M. D., Tavori, H., & Fazio, S. (2018). PCSK9: From Basic Science Discoveries to Clinical Trials. *Circ Res*, 122(10), 1420-1438. doi:10.1161/CIRCRESAHA.118.311227
- Sharma, P., & Sampath, H. (2019). Mitochondrial DNA Integrity: Role in Health and Disease. *Cells*, 8(2). doi:10.3390/cells8020100
- Shimabukuro, M., Higa, M., Zhou, Y. T., Wang, M. Y., Newgard, C. B., & Unger, R. H. (1998). Lipoapoptosis in beta-cells of obese prediabetic fa/fa rats. Role of serine palmitoyltransferase overexpression. *J Biol Chem*, 273(49), 32487-32490. doi:10.1074/jbc.273.49.32487
- Silverstein, R. L., & Febbraio, M. (2009). CD36, a scavenger receptor involved in immunity, metabolism, angiogenesis, and behavior. *Sci Signal*, 2(72), re3. doi:10.1126/scisignal.272re3
- Stanley, W. C., Recchia, F. A., & Lopaschuk, G. D. (2005). Myocardial substrate metabolism in the normal and failing heart. *Physiol Rev*, 85(3), 1093-1129. doi:10.1152/physrev.00006.2004
- Summers, S. A. (2006). Ceramides in insulin resistance and lipotoxicity. *Prog Lipid Res*, 45(1), 42-72. doi:10.1016/j.plipres.2005.11.002

- Takahashi, S., Kawarabayasi, Y., Nakai, T., Sakai, J., & Yamamoto, T. (1992). Rabbit very low density lipoprotein receptor: a low density lipoprotein receptor-like protein with distinct ligand specificity. *Proc Natl Acad Sci U S A*, 89(19), 9252-9256. doi:10.1073/pnas.89.19.9252
- Tall, A. R. (1998). An overview of reverse cholesterol transport. *Eur Heart J*, 19 Suppl A, A31-35.
- Tao, R., Xiong, X., DePinho, R. A., Deng, C. X., & Dong, X. C. (2013). FoxO3 transcription factor and Sirt6 deacetylase regulate low density lipoprotein (LDL)-cholesterol homeostasis via control of the proprotein convertase subtilisin/kexin type 9 (Pcsk9) gene expression. *J Biol Chem*, 288(41), 29252-29259. doi:10.1074/jbc.M113.481473
- Ussher, J. R., Jaswal, J. S., & Lopaschuk, G. D. (2012). Pyridine nucleotide regulation of cardiac intermediary metabolism. *Circ Res*, 111(5), 628-641. doi:10.1161/CIRCRESAHA.111.246371
- Ussher, J. R., Koves, T. R., Cadete, V. J., Zhang, L., Jaswal, J. S., Swyrd, S. J., . . . Lopaschuk, G. D. (2010). Inhibition of de novo ceramide synthesis reverses diet-induced insulin resistance and enhances whole-body oxygen consumption. *Diabetes*, 59(10), 2453-2464. doi:10.2337/db09-1293
- Wang, Y., Huang, Y., Hobbs, H. H., & Cohen, J. C. (2012). Molecular characterization of proprotein convertase subtilisin/kexin type 9-mediated degradation of the LDLR. *J Lipid Res*, 53(9), 1932-1943. doi:10.1194/jlr.M028563
- Watts, J. K., & Corey, D. R. (2012). Silencing disease genes in the laboratory and the clinic. *J Pathol*, 226(2), 365-379. doi:10.1002/path.2993
- Xia, F., Gao, X., Kwan, E., Lam, P. P., Chan, L., Sy, K., . . . Tsushima, R. G. (2004). Disruption of pancreatic beta-cell lipid rafts modifies Kv2.1 channel gating and insulin exocytosis. *J Biol Chem*, 279(23), 24685-24691. doi:10.1074/jbc.M314314200
- Yamamoto, T., Takahashi, S., Sakai, J., & Kawarabayasi, Y. (1993). The very low density lipoprotein receptor A second lipoprotein receptor that may mediate uptake of fatty acids into muscle and fat cells. *Trends Cardiovasc Med*, 3(4), 144-148. doi:10.1016/1050-1738(93)90015-X
- Zelcer, N., Hong, C., Boyadjian, R., & Tontonoz, P. (2009). LXR regulates cholesterol uptake through Idol-dependent ubiquitination of the LDL receptor. *Science*, 325(5936), 100-104. doi:10.1126/science.1168974

Activity Report Lorenzo Da Dalt

PhD in Experimental and Clinical Pharmacological Sciences

| Date of Birth: 25/10/1989 Melzo (MI) | Nationality: Italian | email: lorenzo.dadalt@unimi.it

WoS Researcher ID: [L-6919-2019](#)

Orcid ID: orcid.org/0000-0002-6298-8689

Scopus Author ID: [57203306791](#)

<https://publons.com/researcher/1712849/lorenzo-da-dalt/>

<https://scholar.google.com/citations?user=wpHG2IwAAAAJ&hl=it&oi=ao>

Publications

Bonacina F, **Da Dalt L**, Catapano AL, Norata GD. Metabolic adaptations of cells at the vascular-immune interface during atherosclerosis. *Mol Aspects Med.* 2020 Oct 5:100918. doi: 10.1016/j.mam.2020.100918. Epub ahead of print. PMID: 33032828; PMCID: PMC7534736. (IF 10.238)

Da Dalt L, et al., PCSK9 deficiency reduces insulin secretion and promotes glucose intolerance: the role of the low-density lipoprotein receptor. *Eur Heart J*, 2019. 40(4): p. 357-368. (IF 22.673)

Bonacina F, Coe D, Wang G, Longhi MP, Baragetti A, Moregola A, Garlaschelli K, Uboldi P, Pellegatta F, Grigore L, **Da Dalt L**, Annoni A, Gregori S, Xiao Q, Caruso D, Mitro N, Catapano AL, Marelli-Berg FM, Norata GD. Myeloid apolipoprotein E controls dendritic cell antigen presentation and T cell activation. *Nat Commun.* 2018 Aug 6;9(1):3083. doi: 10.1038/s41467-018-05322-1. PMID: 30082772; PMCID: PMC6079066. (IF 11.878)

Perego C, **Da Dalt L**, Pirillo A, Galli A, Catapano AL, Norata GD. Cholesterol metabolism, pancreatic β -cell function and diabetes. *Biochim Biophys Acta Mol Basis Dis.* 2019 Sep 1;1865(9):2149-2156. doi: 10.1016/j.bbdis.2019.04.012. Epub 2019 Apr 26. PMID: 31029825. (IF 4.328)

Gomaschi M, Fracanzani AL, Dongiovanni P, Pavanello C, Giorgio E, **Da Dalt L**, Norata GD, Calabresi L, Consonni D, Lombardi R, Branchi A, Fargion S. Lipid accumulation impairs lysosomal acid lipase activity in hepatocytes: Evidence in NAFLD patients and cell cultures. *Biochim Biophys Acta Mol Cell Biol Lipids.* 2019 Dec;1864(12):158523. doi: 10.1016/j.bbalip.2019.158523. Epub 2019 Sep 7. PMID: 31505261. (IF 4.519)

Congress and Presentation

15-17 October 2020 *SISA Regional and SITECS Congress. Milan, Italy.* Abstract title: “Ruolo di PCSK9 nel metabolismo cardiaco”.

04-07 October 2020 *88th, Congress of European atherosclerosis society. Virtual congress.* Abstract title for Science at a Glance: “Impact of PCSK9 on human-iPSC derived cardiomyocyte mitochondrial function and metabolism.”

25 September 2020 *PERGO meeting investigator.* Poster presentation: “THE PCSK9/LDLR AXIS IMPACTS INSULIN SECRETION AND GLUCOSE RESPONSE”.

6 December 2019 *EAS Advanced Course on Atherosclerosis – Rare Diseases in Lipoprotein Metabolism from Diagnosis to Treatment. Stockholm, Sweden*

24-27 November 2019 *33th, SISA National Congress. Rome, Italy.* Abstract title for oral presentation: “Pancreatic tissue selective Pcsk9 deficiency impacts Beta cells function and Insulin Release in mice models”.

20-23 November 2019 *39th, National Congress of Italian Society of Pharmacology. Florence, Italy.* Abstract title for oral presentation: “Proprotein convertase subtilisin/kexin type 9 (pcsk9) deficiency is associated with altered glucose metabolism, pancreatic function and insulin release.”

- 9-13 September 2019 **42th, Annual Scientific Meeting of European Lipoprotein Club (ELC). Tutzing, Germany. Abstract title for Oral presentation and winner of BEST ORAL PRESENTATION: “Tissue selective pcsk9-ko mice present altered glucose metabolism pancreatic function and insulin release “**
-
- 25-29 May 2019 **87th, Congress of European atherosclerosis society. Maastricht, The Netherland. Abstract title for Science at a Glance: “The PCSK9/LDLR axis impacts insulin secretion and glucose response**
-
- 28 february-2 march 2019 **Spring meeting, young researcher SISA, SIIA and SIMI, Novità nello studio dell’aterosclerosi e delle sue complicanze, Rimini, Italy.**
-
- 4-7 December 2018 **EAS Advanced Course on Atherosclerosis - Dyslipidaemia and Inflammation, Vienna, Austria**
-
- 30 November-1 December 2018 **Hyperlipidemia Academy, AMGEN, Barcelona, Spain. Speaker for Young Investigator Journal club presentation.**
-
- 25-27 November 2018 **32nd, SISA National Congress. Bologna, Italy. Abstract title: “Role of PROPROTEIN CONVERTASE SUBTILISIN/KEXIN TYPE 9 (PCSK9) in the functionality of cardiac mitochondria.” L. Da Dalt, G. Balzarotti, M. Audano, N. Mitro, G.D. Norata, A.L. Catapano**
-
- 19 October 2018 **Advanced Course on Rare Dyslipidaemia and Atherosclerosis. Importance of Personalized Medicine and Differential Diagnosis., Bassini Hospital; Cinisello Balsamo, Milan.**
-
- 4-6 October 2018 **SISA Regional and SITECS Congress. Milan, Italy. Abstract title: “Valutazione dell’impatto di PROPROTEIN CONVERTASE SUBTILISIN/KEXIN TYPE 9 (PCSK9) sul metabolismo lipidico a livello cardiaco”; L. Da Dalt, G. Balzarotti, M. Audano, N. Mitro, G.D. Norata, A.L. Catapano**
-
- 3 July 2018 **Next Step 9. Department of Pharmacological and Biomolecular Sciences, University of Milan, Italy. Abstract title: “Proprotein Convertase Subtilisin/Kexin Type 9 (PCSK9) and heart metabolism”; L. Da Dalt, G. Balzarotti, M. Audano, N. Mitro, G.D. Norata, A.L. Catapano**
-
- 5-8 May 2018 **86th, Congress of European atherosclerosis society. Lisbon, Portugal. Abstract title for Science at a Glance: “The PCSK9/LDLR axis impacts insulin secretion and glucose response**
-
- 12-15 April 2018 **New perspectives in pharmacology: from genetic to real life. 2ndSpring School, Chiesa in Valmalenco, Italy**
-
- 6-7 April 2018 **Spring meeting, young researcher SISA, SIIA and SIMI, Novità nello studio dell’aterosclerosi e delle sue complicanze, Rimini, Italy**
-
- 19, 20, 21 November 2017 **31st, SISA National Congress. Palermo, Italy. Abstract and best young presentation award, title: “Proprotein Convertase Subtilisin/Kexin Type 9 (PCSK9) and Heart metabolism” L. Da Dalt, G. Balzarotti, M. Audano, N. Mitro, G.D. Norata, A.L. Catapano**
-
- 19, 20, 21 October 2017 **SISA Regional and SITECS Congress. Milan, Italy. Abstract and best presentation award, title: “Proprotein Convertase Subtilisin/Kexin Type 9 (PCSK9) nel Metabolismo Cardiaco”; L. Da Dalt, G. Balzarotti, M. Audano, N. Mitro, G.D. Norata, A.L. Catapano**
-
- 20-25 August 2017 **iARS. Prague, Czech Republic**
-
- 29 June 2017 **Next Step 8. Department of Pharmacological and Biomolecular Sciences, University of Milan, Italy. Abstract title: “Role of Apolipoprotein E in the**

Immunometabolic regulation of dendritic cell function.” F. Bonacina, L. Da Dalt, A. Moregola, G.D. Norata, A.L. Catapano

Prize and Awards	
24-27 November 2019	33th, SISA National Congress. Rome, Italy. Abstract title for oral presentation and TRAVEL GRANT : “Pancreatic tissue selective Pcsk9 deficiency impacts Beta cells function and Insulin Release in mice models”.
9-13 September 2019	42th, Annual Scientific Meeting of European Lipoprotein Club (ELC). Tutzing, Germany. Abstract title for Oral presentation and winner of BEST ORAL PRESENTATION : “Tissue selective pcsk9-ko mice present altered glucose metabolism pancreatic function and insulin release “
25-29 May 2019	87th, Congress of European atherosclerosis society. Maastricht, The Netherland. Abstract title and TRAVEL GRANT for Science at a Glance: “The PCSK9/LDLR axis impacts insulin secretion and glucose response
25-27 November 2018	32nd, SISA National Congress. Bologna, Italy. TRAVEL GRANT and Abstract title: “Role of PROPROTEIN CONVERTASE SUBTILISIN/KEXIN TYPE 9 (PCSK9) in the functionality of cardiac mitochondria.” L. Da Dalt, G. Balzarotti, M. Audano, N. Mitro, G.D. Norata, A.L. Catapano
19, 20, 21 October 2017	SISA Regional and SITECS Congress. Milan, Italy. Abstract and best presentation award , title: “Proprotein Convertase Subtilisin/Kexin Type 9 (PCSK9) nel Metabolismo Cardiaco”; L. Da Dalt, G. Balzarotti, M. Audano, N. Mitro, G.D. Norata, A.L. Catapano
19, 20, 21 November 2017	31st, SISA National Congress. Palermo, Italy. Abstract, Travel Grant and best young presentation award , title: “Proprotein Convertase Subtilisin/Kexin Type 9 (PCSK9) and Heart metabolism” L. Da Dalt, G. Balzarotti, M. Audano, N. Mitro, G.D. Norata, A.L. Catapano
19, 20, 21 October 2017	SISA Regional and SITECS Congress. Milan, Italy. Abstract and best presentation award , title: “Proprotein Convertase Subtilisin/Kexin Type 9 (PCSK9) nel Metabolismo Cardiaco”; L. Da Dalt, G. Balzarotti, M. Audano, N. Mitro, G.D. Norata, A.L. Catapano

Scientific Society

SISA, Società Italiana Per lo Studio dell’Aterosclerosi
 European Atherosclerosis Society
 SIF, Società italiana Farmacologia

Reviewer for

Cardiovascular Research (I.F. 8.168)
Atherosclerosis (I.F. 4.239)
Annals of Medicine (I.F. 3.886)
Journal of Pharmacy and Pharmacology (I.F. 2.405)
Medical Science Monitor (I.F. 1.433)